



**CHALMERS**  
UNIVERSITY OF TECHNOLOGY

---

# **Material properties affecting cutting forces**

Master's thesis in Materials Engineering

Alexander T. Bengtsson  
Daniel Johansson



MASTER'S THESIS 2019

# Material properties affecting cutting forces

ALEXANDER T. BENGTSSON  
DANIEL JOHANSSON



**CHALMERS**  
UNIVERSITY OF TECHNOLOGY

Department of Industrial and Materials Science  
CHALMERS UNIVERSITY OF TECHNOLOGY  
Gothenburg, Sweden 2019

Material properties affecting cutting forces  
ALEXANDER T. BENGTSSON, DANIEL JOHANSSON

© ALEXANDER T. BENGTSSON, DANIEL JOHANSSON, 2019.

Supervisor: Amir Malakizadi, Chalmers University of Technology  
Supervisor: Sören Hägglund, Seco Tools AB  
Examiner: Peter Krajnik, Chalmers University of Technology

Master's Thesis 2019  
Department of Industrial and Materials Science  
Chalmers University of Technology  
SE-412 96 Gothenburg  
Telephone +46 31 772 1000

Typeset in L<sup>A</sup>T<sub>E</sub>X  
Printed by Chalmers Reproservice  
Gothenburg, Sweden 2019

Material properties affecting cutting forces  
ALEXANDER T. BENGTSSON, DANIEL JOHANSSON  
Department of Industrial and Materials Science  
Chalmers University of Technology

## Abstract

The aim of this master thesis is to evaluate the feasibility of using readily available material properties to estimate the constants in the proposed models that describe cutting resistance and therefore cutting force. The study is carried out for two types of workpiece materials, each from a different ISO-group. The investigated materials are 316L, an austenitic stainless steel, and 100Cr6, a high carbon through hardening steel. 316L is delivered by two different suppliers while 100Cr6 is delivered in three different hardening conditions, where the latter significantly alters the material characteristics.

The study includes characterization of the workpiece materials with activities including grain size estimation, inclusion analysis, tensile testing and hardness testing. Machining experiments are performed using a CNC-lathe and the cutting resistance is calculated based on the measured force response for a certain theoretical chip thickness. The data is generated by using the *stepwise increased feed-rate test* method. The relation between properties such as hardness and tensile strength with the cutting resistance is presented for the 100Cr6 material. Since there is a connection between the cutting resistance and the cutting force, it is thus feasible to calculate the cutting forces under arbitrary cutting conditions and for different tool geometries. It is also observed that, while the hardening condition of 100Cr6 has a significant effect on its cutting resistance, only a slight difference exists between 316L produced by different suppliers.

Keywords: Cutting forces, cutting resistance, machining, cutting resistance modeling, main cutting force modeling, 316L, 100Cr6, material characterization.



## Acknowledgements

First of all we want to show appreciation to our supervisors *Amir Malakizadi* and *Sören Hägglund*, without whose support this project would not have been possible. We would also like to thank *Peter Krajnik* for being our examiner during this project.

We would also like to express our most sincere gratitude towards *Seco Tools AB* and the *Department of Industrial and Materials Science* at *Chalmers University of Technology* for trusting us with this project. The study included many activities that provided valuable hands-on experience for us that will be useful in our future careers.

Furthermore we want to thank *Seco Tools* with everyone involved for supplying all the necessary tooling and workpiece materials as well providing general support. We also want to thank the *Department of Industrial and Materials Science* for providing all the necessary lab equipment, including the CNC-machine itself. Special thanks to *Håkan Millqvist* from the department for helping us extracting samples for the material characterization.

Alexander T. Bengtsson, Gothenburg, June 2019  
Daniel Johansson, Gothenburg, June 2019



# Contents

<b>List of Figures</b>	<b>xiii</b>
<b>List of Tables</b>	<b>xvii</b>
<b>List of symbols and abbreviations</b>	<b>xxi</b>
<b>1 Introduction</b>	<b>1</b>
1.1 Background . . . . .	1
1.2 Aim . . . . .	1
1.3 Limitations . . . . .	2
1.4 Specification of issue under investigation . . . . .	2
<b>2 Theory</b>	<b>3</b>
2.1 Forces in metal cutting . . . . .	3
2.1.1 Analytical approach to forces . . . . .	5
2.1.2 Empirical approach to forces . . . . .	5
2.1.2.1 Empirical models describing cutting resistance . . . . .	7
2.2 Process recommendations . . . . .	8
2.3 Cutting tool geometry . . . . .	10
2.3.1 Orthogonal cutting . . . . .	11
2.3.2 Chip geometry . . . . .	12
2.3.2.1 Equivalent chip thickness . . . . .	12
2.4 Machinability . . . . .	13
2.5 Material properties related to metal cutting . . . . .	14
2.6 Material structure and composition related to metal cutting . . . . .	15
2.7 Workpiece materials . . . . .	17
2.7.1 Selected workpiece materials . . . . .	17
2.8 Previous studies on links between cutting force and materials . . . . .	18
<b>3 Methods</b>	<b>21</b>
3.1 Workpiece materials . . . . .	21
3.1.1 316L workpieces . . . . .	21
3.1.2 100Cr6 workpieces . . . . .	22
3.2 Sample preparation . . . . .	22
3.2.1 316L sample preparation . . . . .	23
3.2.2 100Cr6 sample preparation . . . . .	24
3.3 Microscopy . . . . .	25

3.3.1	Optical microscopy . . . . .	25
3.3.1.1	Grain size estimation . . . . .	26
3.3.2	Inclusion analysis . . . . .	27
3.3.2.1	Identifying inclusions . . . . .	27
3.3.2.2	Quantifying inclusions . . . . .	27
3.4	Monotonic testing . . . . .	29
3.5	Hardness testing . . . . .	29
3.6	Machining experiments . . . . .	30
3.6.1	Face turning 316L workpieces . . . . .	33
3.6.1.1	Face turning 316L workpieces with recommended feeds . . . . .	33
3.6.1.2	Face turning 316L workpieces without nose engagement . . . . .	33
3.6.1.3	Face turning 316L workpieces with special inserts . . . . .	34
3.6.2	Face turning 100Cr6 workpieces . . . . .	35
3.7	Data analysis . . . . .	36
3.7.1	Obtaining the average forces . . . . .	36
3.7.2	Force normalization . . . . .	36
3.7.3	Cutting resistance as a function of equivalent chip thickness . . . . .	38
3.7.4	Investigating connection between material properties and cutting resistance . . . . .	39
3.8	Verifying result . . . . .	40
3.8.1	Machining experiments at Seco Tools . . . . .	40
3.8.2	Approximating cutting resistance . . . . .	40
3.8.2.1	Approximating based on a previous model . . . . .	40
3.8.2.2	Approximating cutting resistance of 316L with empirical relation determined for 100Cr6 . . . . .	41
<b>4</b>	<b>Results</b>	<b>43</b>
4.1	Material characterization . . . . .	43
4.1.1	316L characterization . . . . .	43
4.1.1.1	Inclusions 316L . . . . .	43
4.1.1.2	Grain size estimation 316L . . . . .	44
4.1.1.3	Hardness testing 316L . . . . .	45
4.1.2	100Cr6 characterization . . . . .	46
4.1.2.1	Inclusions 100Cr6 . . . . .	46
4.1.2.2	Microstructure 100Cr6 . . . . .	47
4.1.2.3	Hardness testing 100Cr6 . . . . .	47
4.1.2.4	Monotonic testing 100Cr6 . . . . .	48
4.2	Machining result . . . . .	50
4.2.1	Face turning 316L result . . . . .	50
4.2.2	Face turning 100Cr6 result . . . . .	53
4.3	Verifying cutting resistance . . . . .	55
4.4	Empirical relations between material properties and cutting resistance . . . . .	57
4.5	Approximating cutting resistance . . . . .	59
4.5.1	Approximation of $Cr_1$ for 100Cr6 based on a previous model . . . . .	59

4.5.2	Approximation of $Cr_1$ for 316L with constants based on the relation with hardness obtained from 100Cr6 . . . . .	61
<b>5</b>	<b>Discussion</b>	<b>63</b>
5.1	Quality of the data . . . . .	63
5.1.1	Force measurements . . . . .	64
5.1.2	Force normalization . . . . .	64
5.2	Verification . . . . .	66
5.3	Modeling cutting resistance . . . . .	66
5.3.1	Approximation of the main cutting force . . . . .	67
5.3.1.1	Approximation based on existing model . . . . .	67
5.3.1.2	Approximation based on only the Vickers Hardness . . . . .	67
<b>6</b>	<b>Conclusion</b>	<b>69</b>
6.1	Conclusions for the initial research questions . . . . .	70
6.2	Emerging questions . . . . .	71
6.3	Further studies . . . . .	71
	<b>Bibliography</b>	<b>73</b>
<b>A</b>	<b>Microstructure 316L</b>	<b>I</b>
<b>B</b>	<b>Microstructure 100Cr6</b>	<b>V</b>
<b>C</b>	<b>Inclusion analysis</b>	<b>IX</b>
<b>D</b>	<b>Tensile testing 100Cr6</b>	<b>XI</b>
<b>E</b>	<b>Cutting forces 316L</b>	<b>XV</b>
<b>F</b>	<b>Cutting forces 100Cr6</b>	<b>XVII</b>
<b>G</b>	<b>Average normalized forces 316L</b>	<b>XIX</b>
<b>H</b>	<b>Average normalized forces 100Cr6</b>	<b>XXI</b>
<b>I</b>	<b>Scatter in force between repetitions</b>	<b>XXIII</b>
<b>J</b>	<b>Cutting resistance plots 316L</b>	<b>XXVII</b>
<b>K</b>	<b>Cutting resistance plots 100Cr6</b>	<b>XXXIII</b>



# List of Figures

2.1	Forces in turning. a) [2, pp. 105], Figure 3.4, b) [2, p. 56], Figure 3.2.	4
2.2	Example of a process window. This particular window generated by Seco's web page for a specific insert geometry combined with 316L as material choice. . . . .	9
2.3	Model of equivalent chip thickness as proposed by Woxén. [4, pp. 134], Figure 5-10. . . . .	13
2.4	Aspects that affects machinability. . . . .	14
3.1	The figure illustrates the radial cross section and how the 316L samples are cut from the workpiece. . . . .	24
3.2	The figure illustrates the radial cross section and how the 100Cr6 samples are cut from the workpiece. . . . .	25
3.3	The figure illustrates how the samples for ISO-M are divided into areas at different radial depths for the grain size characterization. . . . .	26
3.4	The figure illustrates the area investigated for inclusions on the 316L samples. . . . .	28
3.5	The figure illustrates the areas investigated for inclusions on the 100Cr6 sample. . . . .	29
3.6	All feeds and cutting speeds used for the respective machining experiment. ( <i>316L special inserts</i> refers to the machining of 316L with the special made ISO-P inserts). . . . .	31
3.7	Schematical representation of face turning operation. [4, pp. 124] . . . . .	32
3.8	The figure illustrates the experimental setup for the face turning of the 316L workpieces without the nose engaged. Note that the insert is censored. . . . .	34
3.9	The figure illustrates the experimental setup for the face turning of the 100Cr6 workpieces as well as the 316L. Note that the insert is censored. . . . .	35
3.10	Model of the plane definitions in turning. [2, p. 41], Figure 2.7. . . . .	38
3.11	Flow chart schematically representing how the data for the cutting forces are treated towards calculating the cutting resistance. Note that <i>Insert 3</i> is not included due to it not being considered. . . . .	39
4.1	Graph that shows how the grain size varies with radial depth for the 316L workpieces from the two different suppliers. The average standard deviation over all data points is $0,70\mu\text{m}$ for <i>Supplier A</i> and $0,69\mu\text{m}$ for <i>Supplier B</i> , respectively. . . . .	45

4.2	The hardness variation with radial depth for the 316L workpieces. The average standard deviation over all data points is 4,0HV for <i>Supplier A</i> and 3,0HV for <i>Supplier B</i> , respectively. . . . .	46
4.3	Comparison of the microstructure of the 100Cr6 samples in three conditions. . . . .	48
4.4	Engineering stress-strain curves for the 100Cr6 workpieces. . . . .	49
4.5	The cutting resistance for the 316L workpieces, according to the Woxén-Johansson model. Plotted for all machining scenarios against the equivalent chip thickness, in <i>Log-Log</i> . . . . .	51
4.6	The main cutting force, according to the Woxén-Johansson model, for the 316L workpieces. Plotted for all machining scenarios against the equivalent chip thickness, in <i>Log-Log</i> (derived from the cutting resistance). . . . .	53
4.7	The cutting resistance for the 100Cr6 workpieces plotted against equivalent chip thickness, in <i>Log-Log</i> . . . . .	54
4.8	The main cutting force for the 100Cr6 workpieces plotted against equivalent chip thickness, in <i>Log-Log</i> (derived from the cutting resistance). . . . .	55
4.9	The cutting resistance of the 100Cr6 workpieces obtained at Seco's facility plotted against equivalent chip thickness, in <i>Log-Log</i> . . . . .	56
4.10	The main cutting force plotted against equivalent chip thickness, in <i>Log-Log</i> . Based on data from measured at Seco's facility. . . . .	57
4.11	The empirical relations between selected mechanical properties and $Cr_1$ for 100Cr6. . . . .	58
4.12	The empirical relations between selected mechanical properties and $Cr_2$ for 100Cr6, no curve fitting is attempted. . . . .	60
A.1	Microscopy image showing microstructure of a 316L sample from <i>Supplier A</i> , captured on <i>Sample 1</i> from a random spot within the radial depth of 0,0 – 3,5mm. . . . .	I
A.2	Microscopy image showing microstructure of a 316L sample from <i>Supplier A</i> , captured on <i>Sample 2</i> from a random spot within the radial depth of 16,0 – 19,5mm. . . . .	II
A.3	Microscopy image showing microstructure of a 316L sample from <i>Supplier B</i> , captured on <i>Sample 1</i> from a random spot within the radial depth of 0,0 – 3,5mm. . . . .	III
A.4	Microscopy image showing microstructure of a 316L sample from <i>Supplier B</i> , captured on <i>Sample 2</i> from a random spot within the radial depth of 16,0 – 19,5mm. . . . .	IV
B.1	Microstructure of 100Cr6 in <i>Annealed</i> condition. . . . .	V
B.2	Microstructure of 100Cr6 in <i>Hardening 1</i> condition. . . . .	VI
B.3	Microstructure of 100Cr6 in <i>Hardening 2</i> condition. . . . .	VII
C.1	Example image showing inclusions on a 316L sample from <i>Supplier B</i> . Captured on <i>Sample 2</i> , closer to the center of the workpiece. . . . .	IX

C.2	Example image of the sample from the 100Cr6 sample in annealed condition, captured on <i>Area 2</i> close to the center of the tube wall. . . . .	X
D.1	Stress strain curve for 100Cr6 in <i>Annealed</i> condition. . . . .	XI
D.2	Stress strain curve for 100Cr6 in <i>Hardening 1</i> condition. . . . .	XII
D.3	Stress strain curve for 100Cr6 in <i>Hardening 2</i> condition. . . . .	XIII
J.1	Comparison between the models when machining the 316L workpieces from <i>Supplier A</i> within the recommended feed window, plotted in <i>Log-Log</i> . . . . .	XXVII
J.2	Comparison between the models when machining 316L workpieces from <i>Supplier B</i> within the recommended feed window, plotted in <i>Log-Log</i> . . . . .	XXVIII
J.3	Comparison between the models when machining 316L workpieces from <i>Supplier A</i> without nose contact within recommended feeds, plotted in <i>Log-Log</i> . . . . .	XXIX
J.4	Comparison between the models when machining 316L workpieces from <i>Supplier B</i> without nose contact within recommended feeds, plotted in <i>Log-Log</i> . . . . .	XXX
J.5	Comparison between the models when machining 316L workpieces from <i>Supplier A</i> based on two different types inserts (the same used for 100Cr6), plotted in <i>Log-Log</i> . . . . .	XXXI
J.6	Comparison between the models when machining 316L workpieces from <i>Supplier A</i> based on two different types inserts (the same used for 100Cr6), plotted in <i>Log-Log</i> . . . . .	XXXII
K.1	Comparison between the models when machining 100Cr6 <i>Annealed</i> workpieces, plotted in <i>Log-Log</i> . . . . .	XXXIII
K.2	Comparison between the models when machining 100Cr6 <i>Hardening 1</i> workpieces, plotted in <i>Log-Log</i> . The <i>W/J extended model</i> is not included here. . . . .	XXXIV
K.3	Comparison between the models when machining 100Cr6 <i>Hardening 2</i> workpieces, plotted in <i>Log-Log</i> . The <i>W/J extended model</i> is not included here. . . . .	XXXV



# List of Tables

3.1	Chemical composition in <i>wt%</i> from <i>Supplier A</i> of the 316L workpieces.	21
3.2	Chemical composition in <i>wt%</i> from <i>Supplier B</i> of the 316L workpieces.	22
3.3	Chemical composition in <i>wt%</i> for the 100Cr6 workpieces. . . . .	22
3.4	Table showing the selected feeds for the feed steps for both machining operations for the 316L workpieces using <i>Insert 4</i> , in the unit [ <i>mm/rev</i> ].	33
3.5	Table showing the selected feeds for the feed steps for both machining operations for the 316L workpieces with <i>Insert 1</i> , <i>Insert 2</i> and <i>Insert 3</i> , in the unit [ <i>mm/rev</i> ]. . . . .	34
3.6	Table showing the selected feeds for the feed steps used for the 100Cr6 workpieces, in the unit [ <i>mm/rev</i> ]. . . . .	36
3.7	Table containing the constants for the approximation. As presented in [11]. . . . .	41
4.1	Table showing the average area fraction of inclusions on the images within the respective area at different depths comparing the two suppliers. . . . .	43
4.2	Table showing the average area fraction of inclusions on the images within each area at different depths on the sample of the annealed 100Cr6 workpieces. . . . .	47
4.3	Table containing the average hardness for each material condition followed by the respective standard deviation. . . . .	48
4.4	Table over the different material parameters obtained through the tensile test for the 100Cr6 workpieces. . . . .	49
4.5	Table containing the model parameters, according to the Woxén-Johansson model, for the cutting resistance of the 316L workpieces for all different experiments. . . . .	52
4.6	Table containing the model parameters, according to the Woxén-Johansson model, for the cutting resistance of the 100Cr6 workpieces.	54
4.7	Table containing the model parameters for the cutting resistance of the 100Cr6 workpieces obtained at Seco's facility. . . . .	56
4.8	Table containing a comparison for the model parameters between those obtained at Chalmers and at Seco. . . . .	56
4.9	Table containing the constants for the empirical relations shown for 100Cr6. . . . .	59
4.10	Table containing the model parameters of 100Cr6 for the approximation of the cutting resistance. . . . .	60

4.11	Table containing the result of the approximation. The error is the comparison with the result obtained at Chalmers. . . . .	61
4.12	Table containing the result of the approximation based on experiments at Seco's facility. . . . .	61
E.1	The measured main cutting forces for the 316L workpieces when machining with recommended feeds and without nose contact respectively, using <i>Insert 4</i> , where each repetition is presented. $V_c = 230m/min, a_p = 2mm$ . . . . .	XV
E.2	The measured main cutting forces for the 316L when machining with special inserts where each repetition is presented. $V_c = 230m/min, a_p = 2mm$ . . . . .	XVI
F.1	The measured main cutting forces for the 100Cr6 <i>Annealed</i> workpieces where each repetition is presented. $V_c = 150m/min, a_p = 2mm$ . . . .	XVII
F.2	The measured main cutting forces for the 100Cr6 <i>Hardening 1</i> workpieces where each repetition is presented. $V_c = 90m/min, a_p = 2mm$ . . . . .	XVIII
F.3	The measured main cutting forces for the 100Cr6 <i>Hardening 2</i> workpieces where each repetition is presented. $V_c = 60m/min, a_p = 2mm$ . . . . .	XVIII
G.1	The normalized average cutting force for each feed level for 316L when machining with recommended feeds and without nose contact respectively, using <i>Insert 4</i> . $V_c = 230m/min, a_p = 2mm$ . . . . .	XIX
G.2	The normalized average cutting force for each feed level for 316L when machining with special inserts. $V_c = 230m/min, a_p = 2mm$ . . . . .	XIX
H.1	The normalized average main cutting forces for each feed level for the 100Cr6 <i>Annealed</i> workpieces. $V_c = 150m/min, a_p = 2mm$ . . . . .	XXI
H.2	The normalized average main cutting forces for each feed level for the 100Cr6 <i>Hardening 1</i> workpieces. $V_c = 90m/min, a_p = 2mm$ . . . . .	XXI
H.3	The normalized average main cutting forces for each feed level for the 100Cr6 <i>Hardening 2</i> workpieces. $V_c = 60m/min, a_p = 2mm$ . . . . .	XXII
I.1	The variation between repetitions divided by the average value presented in percent when machining the 316L workpieces with recommended feeds and without nose contact respectively, using <i>Insert 4</i> . $V_c = 230m/min, a_p = 2mm$ . . . . .	XXIII
I.2	The variation between repetitions divided by the average value presented in percent for machining the 316L workpieces with special inserts. $V_c = 230m/min, a_p = 2mm$ . . . . .	XXIV
I.3	The variation between repetitions divided by the average value presented in percent for the 100Cr6 <i>Annealed</i> workpieces. $V_c = 150m/min, a_p = 2mm$ . . . . .	XXIV
I.4	The variation between repetitions divided by the average value presented in percent for the 100Cr6 <i>Hardening 1</i> workpieces. $V_c = 90m/min, a_p = 2mm$ . . . . .	XXIV

I.5	The variation between repetitions divided by the average value presented in percent for the 100Cr6 <i>Hardening 2</i> workpieces. $V_c = 60m/min, a_p = 2mm$ . . . . .	XXV
-----	--	-----



# List of symbols and abbreviations

$a_p$	[ $mm$ ]	Depth of cut
$A$	[ $mm^2$ ]	Chip area
$b_1$	[ $mm$ ]	Theoretical chip width
$b_e$	[ $mm$ ]	Equivalent chip width
$b_{max}$	[ $mm$ ]	Maximum allowed chip width
$C_1$	-	Cutting force constant in $F_c = C_2 + C_1 \cdot h_1$
$C_2$	-	Cutting force constant in $F_c = C_2 + C_1 \cdot h_1$
$C_p$	[ $J/K$ ]	Specific heat capacity
$Cr$	[ $N/mm^2$ ]	Cutting resistance
$Cr_1$	-	Cutting resistance constant in $Cr = Cr_1 + \frac{Cr_2}{h_e}$ and $Cr = Cr_1 + Cr_2 \cdot h_e^{Cr_3}$
$Cr_2$	-	Cutting resistance constant in $Cr = Cr_1 + \frac{Cr_2}{h_e}$ and $Cr = Cr_1 + Cr_2 \cdot h_e^{Cr_3}$
$Cr_3$	-	Cutting resistance constant in $Cr = Cr_1 + Cr_2 \cdot h_e^{Cr_3}$
$E$	[ $GPa$ ]	Young's modulus
$e_f$	[%]	Elongation at rupture
$f$	[ $mm/rev$ ]	Cutting feed
$F_c$	[ $N$ ]	Main cutting force
$F_f$	[ $N$ ]	Feed force
$F_p$	[ $N$ ]	Passive force
$h_1$	[ $mm$ ]	Theoretical chip thickness
$h_2$	[ $mm$ ]	Mean chip thickness
$h_e$	[ $mm$ ]	Equivalent chip thickness
$h_{eW}$	[ $mm$ ]	Equivalent chip thickness proposed by Woxén
$h_{0min}$	[ $mm$ ]	Minimum orthogonal distance
$h_{emax}$	[ $mm$ ]	Maximum allowed equivalent chip thickness
$HV$	[ $HV$ ]	Vickers hardness
$k_c$	[ $N/mm^2$ ]	Specific cutting force
$k_{c1.1}$	-	Constant in $k_c = k_{c1.1} \cdot h_1^{m_c}$
$k$	[ $W/mK$ ]	Thermal conductivity
$l$	[ $mm$ ]	Contact length
$m_c$	-	Constant in $k_c = k_{c1.1} \cdot h_1^{m_c}$
$r_n$	[ $mm$ ]	Nose radius
$r_e$	[ $mm$ ]	Edge radius
$R_p$	[ $MPa$ ]	Yield strength
$R_{p0.2}$	[ $MPa$ ]	Yield strength, at 0,2% plastic deformation
$R_m$	[ $MPa$ ]	Tensile strength
$V_c$	[ $m/min$ ]	Cutting speed

## List of symbols and abbreviations

---

$\alpha$	[°]	Clearance angle
$\alpha'$	-	Constant in <i>Equation 2.10</i>
$\beta'$	-	Constant in <i>Equation 2.10</i>
$\delta'$	-	Constant in <i>Equation 2.10</i>
$\varepsilon_b$	[%]	Elongation at rupture, in <i>Equation 2.10</i>
$\eta'$	-	Constant in <i>Equation 2.10</i>
$\gamma$	[°]	Rake angle
$\gamma'$	-	Constant in <i>Equation 2.10</i>
$\kappa$	[°]	Major cutting edge angle
$\kappa_b$	[°]	Minor cutting edge angle
$\lambda$	[°]	Inclination angle
$\nu'$	-	Constant in <i>Equation 2.10</i>
$\omega'$	-	Constant in <i>Equation 2.10</i>
$\phi$	[°]	Shear plane angle
$\xi'$	-	Constant in <i>Equation 2.10</i>

# 1

## Introduction

This research project is intended to improve the models used when calculating recommendations for cutting data applied for different types of workpiece materials. The work include analyses of material properties/characteristics, force measurements during machining experiments, data analysis and modeling.

### 1.1 Background

This master's thesis is carried out on the behalf of Seco Tools AB, a world leading provider of cutting tools. Seco is part of Sandvik Machining Solutions and they have their main facility located in Fagersta, Sweden. They offer metal cutting solutions for milling, stationary tools, holmaking and tooling systems. In addition to this Seco also offer software applications that based on cutting data guides the user to the best possible results. If the available cutting data is more precise and adapted depending on the choice of material, the cutting process will be more efficient. A more efficient cutting process leads to longer tool life and better surface quality of the machined material.

### 1.2 Aim

The purpose of the master's thesis is to evaluate the feasibility of using readily available material properties to estimate the constants in order to fine tune a model that describes the cutting resistance. The aim is to be able to predict the cutting forces during arbitrary cutting conditions. With good feasibility it means that this approach should be valid for at least similar materials to those included in the study. The choice of materials are from two ISO groups, one material from ISO-P and the other from ISO-M. The intention for ISO-P is to isolate the effect of mechanical properties by performing experiments on the same material subjected to different heat treatments. For ISO-M the focus is to vary the material supplier in order to study the effects of batch-to-batch variations of the same material on the cutting forces.

The study is done by analyzing how specific material properties are connected to the cutting resistance during turning. The main intention for the work is to investigate if readily available material properties such as tensile strength, hardness, chemistry

and/or the physical microstructure can be used to calculate the constants in a proposed model describing the cutting resistance.

The analysis includes measurement of static forces during primarily face turning operation. The forces are measured while varying the feed rates and maintaining all other parameters constant. By this method the energy per cut volume of material can be plotted, *i.e.* the cutting resistance. The aim is to predict the cutting forces by analyzing the connection between material properties and the constants that describe the cutting resistance.

### 1.3 Limitations

The purpose of this master's thesis is limited to validate the feasibility of using readily available material properties to estimate the cutting resistance. The study is limited to only two different materials, each from a separate material group. From the ISO-P group the material is limited to a type of bearing steel, *100Cr6*, which is a high carbon through hardening steel. Meanwhile from the ISO-M group the material is limited to an austenitic stainless steel, *316L*.

Material characterization is limited to *Environmental scanning electron microscopy, ESEM, Light optical microscopy, LOM*, hardness testing and tensile testing. These are applicable methods to attain results regarding the material parameters that are believed to possibly affect the cutting resistance.

Only static forces are measured during machining since only they are relevant to the models intended to be used in this study. This means that the dynamic forces that occurs during machining are not measured or accounted for in any way. Forces during the cutting tool's entry and exit in the material are also not analyzed. The forces are measured using the unworn tools, thus the effect of tool wear on the forces are not investigated.

### 1.4 Specification of issue under investigation

In the list below the general research questions are formulated.

- How is the cutting resistance and consequently the main cutting force connected to the selected material properties?
- Can the cutting resistance and thereby the main cutting force be approximated based on material properties?
- Which material properties have sufficient impact on cutting resistance to be considered in the approximation?
- Which established model should be used as the base for approximation?

# 2

## Theory

In the following sections, theories of metal cutting and turning in particular are presented as well as theories regarding material properties/characteristics related to metal cutting and information about the materials included in this study.

### 2.1 Forces in metal cutting

Knowledge about the forces in metal cutting is relevant for several reasons. From a practical point of view it is for example used to estimate the power needed for the process. Cutting forces can also be used to estimate the machinability of a material and is the easiest and most well-established response to measure. The methods for measuring the forces have been developed and improved during the last century. All methods used for measurement are based on the deflection of the tool during machining with a dynamometer. In turning there is three force components in orthogonal directions. The direction of the force components in the case of longitudinal turning is illustrated in *Figure 2.1a*. The directions may change when changing the mode of turning, although they still remain orthogonal with each other. Furthermore in *Figure 2.1b* the force components in relation to the the cutting edge of the tool is presented.

The components are the *main cutting force* ( $F_c$ ), *feed force*, ( $F_f$ ) and the *passive force* ( $F_p$ ). The main cutting force is in most cases the largest component and is acting on the rake face of the tool, perpendicular to the cutting edge. The feed force is acting parallel to the direction of the cutting feed and is thus normal to the main cutting force. The third component, the passive force is the smallest and often ignored component. [1, pp. 58]

Cutting forces can have both a dynamic and a static character. Static forces, which is of focus in this study, can be treated as the average cutting forces over time. Momentarily the forces vary as a result of local variations in cutting resistance which is caused by variations in the workpiece material. [2, pp. 103]

The force required to form a chip is dependent on two major factors. The shear strength of the material under cutting conditions and the area of the shear plane. Provided that the latter remains constant, the force is then increased by any heat treatment or alloying that increases the yield and shear strength, more on this in

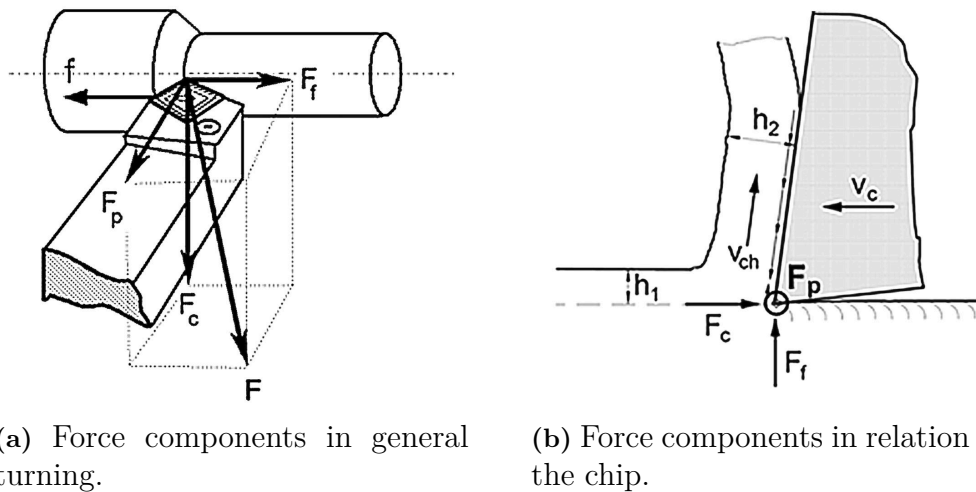


**Figure 2.1:** Forces in turning. a) [2, pp. 105], Figure 3.4, b) [2, p. 56], Figure 3.2.

*Chapter 2.5.* In practice the area of the shear plane varies and is explained to be the most significant influence on the main cutting force often outweighing the influence of shear strength. During orthogonal cutting this area is geometrically related to the undeformed chip thickness, the width of cut and the shear plane angle,  $\phi$ . The forces are directly affected by an increase in these parameters since they all affect the area. The shear plane angle can however not be controlled by the operator and is found to vary greatly under different conditions. When using a rake angle of zero degrees, it has been found that the shear plane angle may vary from a maximum of approximately 45 degrees to a minimum of five degrees. Subsequently, when the angle is very small the shearing force becomes large, and as shown in the literature, up to five times larger than the minimum which occurs at 45 degrees. Thus, much of the research has been focused on predicting this parameter. [1, pp. 58-60]

The other region where forces arise is in the flow zone which is on the rake face of the tool. In a case where the rake angle is zero degrees the feed force is simply the drag force which the chip exerts on tool as it flows away. The contribution to the feed force caused by friction in the non seized areas is believed to be relatively small during most cutting conditions. Thus, the feed force can be considered dependent on the product of the workpiece material shear strength and the area of seized contact on the rake face. The latter parameter is explained to be very difficult to determine though, mainly since it is impossible to observe this area during engagement. [1, pp. 60-62]

As explained [1, pp. 40], it is important to understand that during seizure in metal cutting, relative movement continues. This is said to be possible because the area of seizure is small in combination with a sufficient force to shear the work material near the seized interface. The relative movement does not take place at the interface between the rake face and the workpiece material. This is because the force required

to overcome seizure is typically greater than the force needed to shear the material adjacent to it.

It is debated whether or not the shear strength of the material at the rake face is of much significance due to several reasons. One of which being inaccuracies in the measurement of contact length in combination with the extreme conditions present in this region. Thus, the values of shear strength at the rake face are unlikely to be the same as those present in the shear plane.

### 2.1.1 Analytical approach to forces

To further understand the influence of the shear plane angle it is relevant to study the theories that attempt to describe this. These models are noted as *Analytical*, although *Semi-Analytical* would be more an accurate term since they still rely on experimental data for certain parameters. The first model which is considered one of the milestones in metal cutting theory is Merchant's force circle. However, this model to predict forces is considered inadequately accurate, mainly due to the inappropriate use of friction relationships which are only relevant to sliding conditions. Another model, later developed by Oxley and colleagues, accounts for parameters such as work hardening and treats the frictional problem as shear within a layer of the chip adjacent to the rake face of the tool. In this layer, near seizure conditions are said to exist with the velocity of the workpiece material approaching zero at the interface. [1, pp. 62-65]

However, two major challenges or limitations are presented for Oxley's model. Mainly, there is no good data available for the stress-strain relations near the interface between the chip and the tool. In particular not for the amounts of strain, extreme strain rates, time and temperatures at which material is deformed in the flow zone at the interface. Another issue is, while the importance of the contact area is recognized, the estimations of this area rely on calculations of a mean contact length and the basis for this calculation are deemed to be inadequate. No alternative to experimental measurement of this area has been found and thus it presents difficulties for the model. [1, pp. 67]

### 2.1.2 Empirical approach to forces

As is evident, there are several difficulties attempting to determine the cutting forces with the semi-analytical approach. An alternative to that, employed by the industry, is predicting the forces with an empirical approach. This method is based on the use of constants and curve fitting. All the unknowns are covered by constants and coefficients that relies on experimental data.

The static forces, as explained in *Chapter 2.1* above, are mainly a function of chip area, the depth of cut and properties of the material being cut. Less significant,

but not negligible, are geometrical aspects such as rake angle but also cutting speed and the temperature of the process. As mentioned, these complex relationships can be treated as constants in a function depending on the theoretical chip thickness,  $h_1$ , see *Equation 2.1*. In the simplest of cases this can be modelled as a linear relationship. This linear behavior is valid especially for applications with constant rake angle. [2, pp. 105-106]

$$F_c = C_2 + C_1 \cdot h_1 \quad (2.1)$$

In many machining scenarios it is stated that the coefficient  $C_1$  can be expressed as constant. However, several factors contribute to an disproportional behavior. The coefficient may either be increasing or decreasing as a function of  $h_1$  which for example can be a result of deformation hardening of the material or built up edge. Thus, it is more accurate with this approach to express the main cutting force as above but including  $C_1$  as a function of  $h_1$ , *Equation 2.2*. [2, pp. 112-113]

$$F_c = C_2 + C_1(h_1) \cdot h_1 \quad (2.2)$$

The main cutting force can be treated as a function of the *cutting resistance*. It is defined in [2, pp. 142] as *the resistance per total area of chip that the workpiece material shows in a given application involving a particular cutting tool and cutting data*. This means that cutting resistance is dependent on the cutting process and should thereby *not* be viewed as a simple material constant. It can be described as the energy consumption per cut volume of workpiece material, *i.e.* the specific cutting energy. This parameter is directly tied to the force acting on the tool. It is computed by dividing the main cutting force with the chip area, *Equation 2.3*. [2, pp. 142]

$$Cr = \frac{F_c}{h_1 \cdot b_1} \quad (2.3)$$

This simple equation can be extended by expressing *Equation 2.2* introduced earlier in this section. This extended model is presented below in *Equation 2.4*. It consists of two parameters,  $Cr_1$  and  $Cr_2$ , where  $Cr_1$  describes load and energy consumption on the rake face. The parameter  $Cr_1$  is thus linked to the material dependency. Whereas  $Cr_2$  describes load and energy consumption on the clearance face and is dependent on process and the micro geometry of the cutting tool. This means that  $Cr_2$  is dependent on the contact between workpiece material and clearance face. Thus, increased flank wear results in an increase in the  $Cr_2$  parameter. [2, pp. 142-144]

$$Cr = Cr_1 + \frac{Cr_2}{h_1} \quad (2.4)$$

As explained in [2, p. 144], the cutting resistance is preferably determined by use of the method involving incremental feed in a stepwise manner, generally known as *feed step*. Important remark is that the geometry of the tool remains constant during the process. [2, pp. 142-144]

A term that is fundamentally the same as cutting resistance is the *specific cutting force*,  $k_c$  which is introduced by *Kienzle*. The specific cutting force is often described by the exponential curve fitting of experimentally obtained data. As with cutting resistance, it is based on describing the dependence of theoretical chip thickness  $h_1$  by the use of two constants  $k_{c1.1}$  and  $m_c$ , see *Equation 2.5*. It is pointed out that the *specific cutting force* cannot be assigned a physical attribute since it is a combination of effects from both the rake face and clearance face of the tool. [2, pp. 145]

$$k_c = k_{c1.1} \cdot h_1^{m_c} \quad (2.5)$$

The way of determining the cutting resistance or specific cutting force is by experimentally measuring the main cutting force. Approximate result can also be obtained by measuring the power consumption of the motor in the process. [2, pp. 146]

It is pointed out that from a research perspective the empirical models are flawed in the sense that they all rely on original testing data. This is problematic since that data would be obtained under a certain condition which may not translate well to slightly different conditions. Even though the empirical model, as all other models, can be criticized, they can still be useful in the industry. Keeping in mind that they may not be perfectly accurate, they can be utilized as “starting points” for operation. [1, pp. 374]

### 2.1.2.1 Empirical models describing cutting resistance

This study considers three models for describing the specific cutting force or cutting resistance that are commonly used in the industry. The two first models are presented earlier in *Chapter 2.1.2* although here an extended version is also introduced. This chapter provides some comparison between these models based on the literature study. [3]

The specific cutting force, or the pressure, in the cutting zone can be expressed as either the specific cutting force  $k_c$  or the cutting resistance  $Cr$ . Both are defined as the force required per unit area of the chip. *Kienzle*, which is traditionally the most common model uses the specific cutting force  $k_c$ . The models introduced more recently are the *Woxén-Johansson* model, *Equation 2.6*, and the extension of this model proposed by *Hägglund*, *Equation 2.7*, referred to as the *Hägglund* model or simply *Woxén-Johansson extended* model.

$$Cr = \frac{F_c}{A} = Cr_1 + \frac{Cr_2}{h_e} \quad (2.6)$$

$$Cr_e = \frac{F_c}{A} = Cr_1 + Cr_2 \cdot h_e^{Cr_3} \quad (2.7)$$

In order to obtain the constants needed for *Equation 2.6 and 2.7*, a feed step procedure can be used. This procedure is termed SIFT (stepwise increased feed-rate test) and is explained in *Chapter 3.6*. By using this procedure it is possible to determine the constants  $Cr_1$ ,  $Cr_2$ ,  $Cr_3$ ,  $k_{c1.1}$  and  $m_c$ .

There are some differences between the three models presented here. One difference that can be noted is mainly what occurs when the equivalent chip thickness  $h_e$  is equal to 1.0. What happens is that neither the  $m_c$  constant in the Kienzle model, nor the  $Cr_3$  constant in the Hägglund model, have any effect. The specific cutting force or cutting resistance becomes equal to the value  $k_{c1.1}$  in the Kienzle model and  $Cr_1 + Cr_2$  in the Woxén-Johansson and Hägglund model. A way to further analyze the differences between the models is to multiply each model with the chip area. The result from this multiplication can be expected to be the main cutting force  $F_c$ . Performing this multiplication while the equivalent chip thickness approaches 0 shows some distinct differences between the models. The Kienzle model would show that no energy is consumed when  $h_e = 0$ , which can not be true in either fact or theory, since the deformation of the surface consumes energy. This can be considered the main limitation of the Kienzle model. [3]

According to [3], the error rates between the different models relatively complex. Kienzle model is shown to provide good curve fitting for some ISO-P materials that are brittle and have a strong tendency to strain hardening. The study also showed favourable curve fitting for some ISO-M, ISO-N materials, and for the difficult materials Alloy 718 and Ti6Al4V. However, for the majority materials analyzed in the study, the Hägglund model was shown to be the most favourable for curve fitting.

## 2.2 Process recommendations

In order to support the customer, tool suppliers typically offer a so called *working range* model. This is a process window for suitable ranges of depths of cut and feeds for a specific tool insert. Such model considers several parameters with one being the fact that different materials generates different mechanical loads. Generally, as is explained in [4, pp. 129], such model is difficult to develop. Therefore the aim of such model is to provide, perhaps not the best, but recommendations that are "good enough". The working range model is intended to provide a window of operation where the process works relatively good, but outside the boundaries the result may

be sub-optimal and in some cases even catastrophic. An example of such window is presented below in *Figure 2.2*.

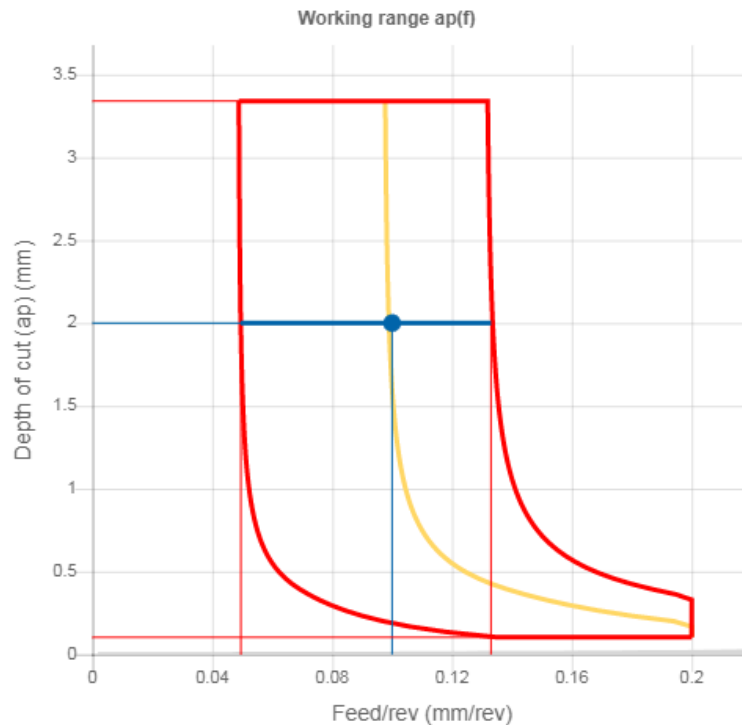


**Figure 2.2:** Example of a process window. This particular window generated by Seco’s web page for a specific insert geometry combined with 316L as material choice.

The boundaries in the working range have different explanations. As presented in [4, pp. 129], the left most boundary is defined by the minimum orthogonal distance,  $h_{0min}$ , from the cutting edge which defines the minimum allowable feed with changing the depth of cut. The right boundary, declining with feed, is defined by the maximum allowed equivalent chip thickness  $h_{emax}$  while changing feed and depth of cut. The upper boundary is defined by  $b_{max}$  as a function of the insert geometry maximizing the depth of cut  $a_p$ . The bottom limit is then instead the minimum depth of cut considering the nose radius. The right boundary is the maximum feed as function of the nose radius which then abruptly limits the right sloped boundary.

Presented in [4, pp. 48], the main logical way of optimizing cutting data is considered in three steps whilst considering physical constraints:

- Maximizing the depth of cut.
- Maximizing the feed.
- Optimizing the cutting speed.

An example of constraints that must be accounted for is force restrictions. Accounting for such constraint may involve balancing the depth of cut with feed. There

are however some constraints as to how much the feed can be increased. Provided that the *absolute feed limit* is not exceeded and the *surface finish* constraint is met, the main concern is the models based on chip thickness  $h_e$ . One of which being the model for *main cutting force* which is directly affected by the value of  $h_e$ .

The maximum cutting force that corresponds to a maximum equivalent chip thickness can be related to the term *breaking feed*. As explained in [4, pp. 132] the maximum value of the chip thickness needs to be within the breaking feed since if exceeded, catastrophic failure will occur.

### 2.3 Cutting tool geometry

Cutting tool geometry refers to the form and dimensions that characterize a tool. There are essentially two aspects for the term, namely *macro* and *micro* geometry. The latter refers primarily to the form of the cutting edge. It is essential for the process to have a favourable cutting geometry since it directly affects the results. [2, pp. 44]

It should be mentioned that various sets of standards are used in the field of metal cutting. However, for this work the terminology presented in [2, pp. 46] is mainly used.

The rake angle and the clearance angle,  $\gamma$  and  $\alpha$ , which are commonly mentioned, depend on the cutting tool's position in relation the workpiece. The rake angle affects chip radius so that by decreasing the rake angle the radius of the chip is also decreased. Regarding how the rake angle affects the forces, it affect the size and direction of the main cutting force. For example, increasing the rake angle will reduce the force on the insert but in the process also weakens the cutting edge. This parameter has a very direct effect on the dynamics of the process. The other angle, the clearance angle, is what provides the tool access to the surface of the workpiece and as a result gives it freedom to move to the new surface being generated in the process. This angle is affected by whether or not the engagement is internal or external. It is also affected by the feed since, if increased, the effective clearance angle decreases. It should be noted that in order to provide clearance, the feed angle needs to be smaller than the clearance angle. [2, pp. 46]

The major and minor cutting edge angles,  $\kappa$  and  $\kappa_b$ , are also dependent on the positioning of the tool. As explained in [2, pp. 46] the theoretical chip thickness,  $h_1$ , together with the theoretical chip width,  $b_1$ , both are depending on this. In the case of orthogonal engagement  $\kappa$  is set to  $90^\circ$ , more on this in *Chapter 2.3.1*.

The inclination angle,  $\lambda$ , also has an effect on the main cutting force as well as the chip removal process. As explained in [2, pp. 47], the most beneficial loading scenario is obtained if this angle is negative. However, it should be noted that this also leads to chips being directed onto the workpiece.

The edge radius  $r_e$  is commonly described as an ideal radius. However, in reality it frequently deviates from the true radius along the edge line as presented in [2, pp. 45]. The exact form of the edge line is what the term micro geometry often refers to. The other radius, introduced in [2, pp. 47], is the nose radius,  $r_n$  which is the rounded point of the insert. In essence, this feature together with the feed, determines the theoretical surface roughness as well as the strength of the nose area.

### 2.3.1 Orthogonal cutting

Even though *Orthogonal cutting* is not used in this study it is still relevant to understand the fundamental requirements and benefits of this. This is intended to provide insight into how that can alter the results and why it is generally the method of choice when setting up experiments.

Orthogonal cutting is the basic process variant that is commonly used for research in the field of metal cutting. The conditions that are required for orthogonal cutting can be expressed in the following way according to [5, pp. 46]:

- The cutting edge angle  $\kappa$  is  $90^\circ$ .
- The inclination angle  $\lambda$  is  $0^\circ$ .
- Only the major cutting edge is being engaged, *i.e.* the nose and the minor cutting edge is not in contact.

Orthogonal cutting is also described in [1, pp. 24]. According to [1, pp. 24] orthogonal cutting entails simplified conditions that is beneficial for laboratory investigations. To achieve orthogonal cutting, the cutting edge must be straight, *i.e.* normal to both the cutting and feed direction. If the workpiece is in the form of a tube and the wall thickness is the depth of cut, only the major cutting edge will be in contact with the workpiece. In this scenario the cutting speed varies along the edge of the cutting tool. Although, if the diameter of the tube is large enough the variation in speed is considered negligible. Orthogonal cutting can also be achieved on a planing or shaping machine where the material is in the form of a plate. The edge of the plate is machined in an orthogonal manner. However, a shaper or planer has limited cutting speed and time of continuous machining. Due to this, the lathe based method is more convenient.

Three methods for orthogonal cutting are mentioned in [6, pp. 24] as the following.

- *Orthogonal plate machining* (OPM), *i.e.* machining a plate in a milling machine.
- *Orthogonal tube turning* (OTT), *i.e.* end-cutting a tube wall in a turning setup.
- *Orthogonal disc machining* (ODM), *i.e.* end-cutting a plate with a tool feeding in facing direction.

### 2.3.2 Chip geometry

The most important aspect of the chip is the *mean chip thickness*,  $h_2$ , which can also be described as  $t_2$ . This parameter can for example be determined, as explained in [1, pp. 26], by measuring the length and weight of a chip. The other factors such as a width are assumed equal to the depth of cut,  $a_p$ . The density of the workpiece material is also assumed to be unchanged during chip formation. Inserting these values into the equation provides an estimation of the mean chip thickness. As is further pointed out, the chip thickness can never be smaller than the *theoretical chip thickness*  $h_1$ . This can also be described as  $t_1$  and is in the case of orthogonal cutting equal to the feed. The ratio between  $h_1$  and  $h_2$  is called the *chip thickness ratio*, which is commonly occurring in the literature. As is presented in [1, pp. 27], a low value relates to a low *shear plane angle*, something that is briefly explained in *Chapter 2.1* above.

#### 2.3.2.1 Equivalent chip thickness

The equivalent chip thickness is a parameter used to approximate the chip area. This parameter is of greater significance when the depth of cut,  $a_p$ , is in the same order or smaller than the nose radius of the insert. It can, as presented in [2, pp. 69], to a lesser degree of accuracy be described by the following basic relation, where  $h_1$  is the *theoretical chip thickness*.

$$A \approx a_p \cdot f \approx b_1 \cdot h_1 \quad (2.8)$$

However, as further discussed in [2, pp. 69] this relationship often yields too large errors. In order to obtain a more accurate representation of the chip area Woxén introduced the *equivalent chip thickness*. This parameter is aimed to describe a theoretical average chip thickness for the length of the active part of the edge line. Since the active part of the edge line is never straight, unless orthogonal conditions apply, this length is curved in one end due to the nose radius. Fundamentally, what is done by this model is straightening out the nose radius which is allowing the chip area to be treated as a rectangle, see *Figure 2.3*. The model, as proposed by Woxén, is presented in *Equation 2.9*. It is noted as  $h_{eW}$  to distinguish it from another way of representing this parameter which is referred to as the *true equivalent chip thickness*.

$$h_{eW} = \frac{A_W}{l_W} = \frac{a_p \cdot f}{\frac{a_p - r(1 - \cos\kappa)}{\sin\kappa} + \kappa \cdot r_\epsilon + \frac{f}{2}} \quad (2.9)$$

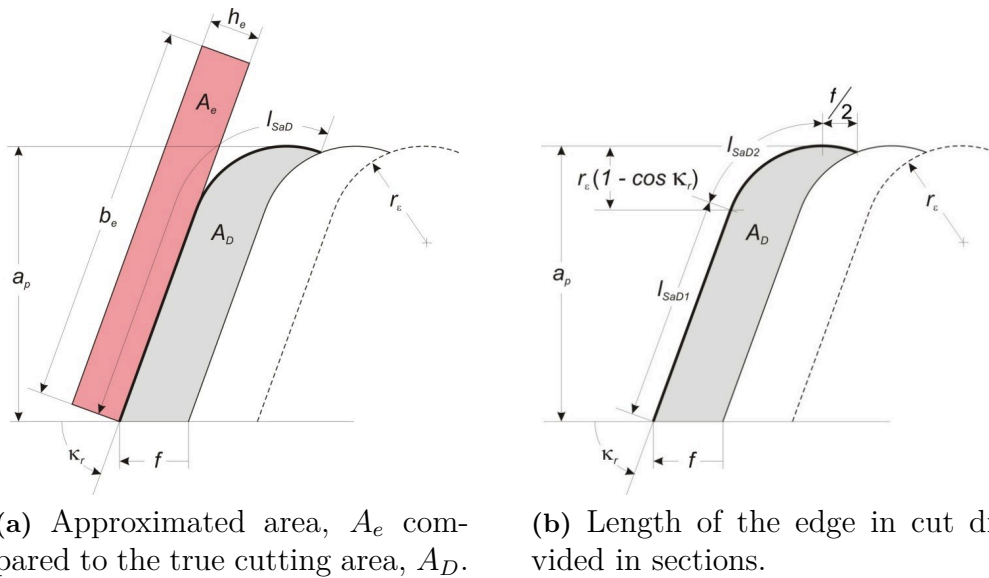


**Figure 2.3:** Model of equivalent chip thickness as proposed by Woxén. [4, pp. 134], Figure 5-10.

As is explained in [2, pp. 82] the *true equivalent chip thickness* accounts for a loss in accuracy that is inherent to Woxén's approximation. The inaccuracy is amplified for large nose radii or small feeds. However, for the purpose of this study Woxén's model is considered sufficient.

## 2.4 Machinability

*Machinability* is a term frequently mentioned in subsequent chapters. Machinability is an ambiguous term that according to [2, pp. 391] can be described as:

*The workpiece materials behaviour in the cutting process and its influence on the machining result.*

The following table lists some process behaviours that are related to the machinability term. The table is derived from [2, pp. 393].

Power and cutting forces	Chip formation	Surface quality	Environmental factors	Tool deterioration
Energy consumption	Chip type and dynamics	Topography	Dust generation	Uniform flank wear
Workpiece deformation	Chip form	Residual stresses	Allergic reactions	Localized wear
Equipment deformation	Hardness	Structure	Process additives	Crater wear
Clamping robustness	Micro geometry properties	Chemical composition	Sound level	Chipping and flaking
Entry and exit damages				Crack formation
Process stability				Plastic deformation
				Diffusion and chemical reactions

**Figure 2.4:** Aspects that affects machinability.

Machinability refers to all the above mentioned aspects of the process. However, those that are most relevant for this study are the ones related to the power and cutting forces. Especially the energy consumption which is directly related the load and thereby the forces the cutting tool is subjected to. [2, p. 142]

## 2.5 Material properties related to metal cutting

As presented in [6, p. 59], the term *work hardening* is described as the phenomenon where a materials strength increases during plastic deformation. This effect is a result of dislocation movement and when the amount of dislocations which in turn increases the encounters and interactions between them. These encounters and interactions impedes movement of the dislocations and thereby increase the resistance to plastic deformation. As is further explained in [2, p. 396], the work hardening of the material affects the properties of the chip and the surface of the material which leads to an increased load on the edge of the cutting tool.

The *adhesion* that takes place between the workpiece and the cutting tool is one aspect that affects machinability and adds complexity to the cutting process. Empirically there is a connection between adhesion and *ductility*, where higher ductility entails greater adhesion. This can cause the removed material fusing to the cutting tool and in doing so, creating a built up edge. This phenomenon can be both beneficial and detrimental. The built up edge can provide protection to the cutting edge

which increases the tool life. However, if the built up edge is removed at a high frequency the tool can suffer increased wear. The built up edge can also result in an increased rake angle,  $\gamma$ , which can lead to an favourable chip formation although it also worsens the surface quality. [2, p. 397]

The *thermal conductivity*,  $k$ , of the workpiece material is important to the temperature of the process. The *Specific heat capacity*,  $C_p$ , of the workpiece material is the particular factor that has the largest relative effect on the process temperature. [2, p. 397]

The *Hardness* of the material is typically directly connected to the *deformation resistance*. Higher deformation resistance increases the main cutting force and thereby the cutting resistance. Thus, increased hardness generally also results in increased main cutting force and cutting resistance. [2, p. 497]

*Multiphase materials* can have an effect on the machinability due to the fact that different phases in a material can have largely varying properties. One phase can be very brittle while the other is more ductile. Achieving exceptional machinability is also greatly dependent on the *structure distribution* of different phases and particles in the material. The distribution of *abrasive* particles is for example something that can have a significant effect on the tool wear. Also, in the structure distribution of the material porosity can contribute to low machinability due to increased material flow in the periphery of the tool. Material porosity can also cause the tool to have varying contact with the material during cutting. [2, pp. 397-398]

*Chemical reactions* between the workpiece material and the cutting tool is also something that can offer limitations to the machinability. *Diffusion* is an example of something that can be considered a chemical reaction. [2, pp. 397-398]

## 2.6 Material structure and composition related to metal cutting

The previously mentioned material properties are governed by the material structure. The previous occurrence of a specific material structure and associated properties is something that is heavily controlled by the constituents of the material. The different alloying elements have a large influence on the process from a machinability point of view. In the subsequent part some alloying elements effects on steel alloys will be described. [2, pp. 412-420]

A low alloyed steel with a low carbon content is characterized by large ductility and thereby adhesion to the cutting tool. Additions of nickel (Ni) and cobalt (Co) increases the risk of material build up on the cutting tool. Additions of elements that are carbide or oxide formers *e.g.* chromium (Cr), vanadium (V), tungsten (W) and aluminum (Al) can increase the wear on the cutting tool. There are also

alloying elements that facilitates machinability by providing a lubricating effect or by favouring chip breaking. Lead (Pb) and sulfur (S) have a lubricating effect on the cutting tool while phosphorus (P) and sulfur (S) can improve chip breaking. The addition of manganese (Mn) can also improve machinability due to the formation of manganese-sulfide (MnS) if sulfur (S) is present, which also have a lubricating effect. Small additions of calcium (Ca) can form soft oxides that offer even better lubrication. [2, pp. 412-420]

Furthermore, as presented in [7, pp. 766], inclusions can play an important role in the process of chip formation as they can serve several functions. Not only can they serve as lubrication for the process but they can as well become diffusion barriers which can isolate the tool from chemical wear. They can also act as localized stress raisers in shear plane and thus can cause a crack formation which will be beneficial for breaking the chips. The inclusions are also playing an active role in the flow zone where they contribute to shearing the material.

In the case of non-metallic inclusions it is further discussed in [7, pp. 756] that the following aspects are deemed relevant for steel materials. The composition, number, size and morphology of the inclusions. Furthermore as presented in [7, pp. 760], the properties as hardness, deformability and distribution are also deemed important.

Thermal conductivity  $k$  is of great importance to machinability. In a material with high  $k$  heat is transported away from the cutting zone into the rest of the workpiece and most importantly into the chips. In a case where a material has lower  $k$ , heat is instead transported into the insert. The balance of the thermal conductivity between the workpiece material and the insert is thereby important to the function of the cutting process. The thermal conductivity of a material is largely a result of the material constituents. Adding alloying elements with low  $k$  like titanium (Ti) will decrease the overall thermal conductivity, while adding copper (Cu) which has high  $k$  will increase the overall thermal conductivity. [2, pp. 412-420]

Inclusions or impurities in the material can be both added by choice or added unintentionally. Inclusions added by choice are often there to improve machinability and steels with these type of inclusions are commonly called free machining steel. These types of steels have higher content of sulphur (S) and lead (Pb). Calcium can also be added to change oxides and sulfides into aluminates which are encapsulated in calcium sulfide. The machinability of stainless steels can also be improved with the addition of sulphur (S), lead (Pb) and calcium (Ca). [2, pp. 412-420]

The cutting process produces lasting deformation and increase of hardness in the surface of the workpiece material due to work hardening. Austenitic steels, duplex stainless steels and steels with a high content of manganese are especially susceptible to work hardening. [2, pp. 412-420]

Hardness is not an indication of a material machinability except within a narrow range of a material group with similar properties and composition. The strength of the material has a more direct effect on its machinability. Generally it can be said that the higher the strength of the material the more energy is required for processing. However, this statement is a basic simplification of a much more complex connection. There is no simple formula to calculate how the machinability is dependent on the strength of the material. The energy that is needed to separate the material is mostly transformed to heat and transported away from the cutting process area by the insert, workpiece material and chips. This means that the relation between the materials strength and thermal conductivity is of importance. Ductility is the property that causes the material to flow while its influenced by shear stress. The materials ductility can be indicated by its elongation at fracture, which can be measured. High ductility in materials can cause problems since the chips might not break in a adequate manner. If the material is also of high strength further difficulties can be experienced. [2, pp. 412-420]

## 2.7 Workpiece materials

Workpiece materials are divided in to six major material groups to support the choice of cutting tool geometry, grade and cutting data. The material groups are in accordance with the ISO standard and all have unique properties in regards to machinability. The two material groups mentioned in the following parts are those that are included in this study.

*ISO-P* is the largest material group and consist of steel alloys of slightly varying types. The types range from low alloy to high alloy together with steel castings, as well as ferritic and martensitic stainless steels. The machinability of ISO-P materials are generally good but may vary depending on material properties. [8]

*ISO-M* consist of stainless steel alloys which have a chromium (Cr) content above 12%. These alloys can also include alloying elements such as nickel (Ni) and molybdenum (Mo) and can exist in several different conditions *e.g.* ferritic, martensitic, austenitic and duplex phase. Common characteristics between all ISO-M materials are that there is significant heat generation, notch wear and that they are prone to built-up edge. [8]

### 2.7.1 Selected workpiece materials

The selected ISO-P material, *100Cr6*, is a through hardening steel which is mostly used for bearings and similar applications with rolling contact and high fatigue. The steel in its hardened condition has high hardness, strength and cleanliness which helps the material to withstand high cycle and high stress fatigue. It can also be used for other machine components requiring high strength and hardness. [9]

The ISO-M material of choice, *316L*, is an austenitic stainless steel. It is less susceptible to corrosion and pitting than more traditional nickel chromium stainless steels. 316L is characterized by high creep resistance, excellent formability as well as corrosion and pitting resistance. It also maintains high rupture and tensile strength at elevated temperatures. Some common applications for 316L varies from structural building components to industrial equipment and even cookware and cutlery. Generally, any component or equipment that require corrosion resistance. 316L has lower carbon content compared to the regular 316 stainless steel. This slightly lowers the strength but makes the material resistant to sensitization during heat treatments and significantly easier to weld. [10]

## 2.8 Previous studies on links between cutting force and materials

In a paper from *Lund University*, [11], the influence of the workpiece material properties on the cutting forces are investigated. It focuses on modelling the *cutting resistance* as a function of the properties of the workpiece material. The aim of that study, as well as for this, is to be able to predict the forces without relying on experimental cutting.

The model proposed by [11] suggests that four different material properties should be used in order to estimate the cutting resistance. These are, *hardness*, *yield strength*, *elongation at rupture*, and *thermal conductivity*.

$$Cr_1 = \alpha' \cdot HV^{\delta'} + \beta' \cdot R_p^{\nu'} + \gamma' \cdot \varepsilon_b^{\eta'} + \xi' \cdot k^{\omega'} \quad (2.10)$$

Where  $HV$  is the Vickers hardness [ $Kp/mm^2$ ],  $R_p$  is yield strength [ $MPa$ ],  $\varepsilon_b$  is the elongation at rupture [%], and finally  $k$  as the thermal conductivity [ $W/mK$ ]. The following,  $\alpha'$ ,  $\beta'$ ,  $\delta'$ ,  $\gamma'$ ,  $\eta'$ ,  $\nu'$ ,  $\xi'$ , and  $\omega'$  are constants. These constants are determined by experimentally obtained values for  $Cr_1$  together with knowledge about the material properties. When the experimental value for  $Cr_1$  is compared to the value generated by the model the constants are determined by minimizing the difference between these values. The presented variation for the results by the model is roughly 13% for all 98 entities used in the study. The coefficient of variation used to evaluate the result in the study, [11], was determined by the following equation:

$$V = \frac{1}{n} \sum_{i=1}^n \left| \frac{Cr_{1,input} - Cr_{1,model}}{Cr_{1,input}} \right| \quad (2.11)$$

The author of the study presented in [11], discuss the possibility of obtaining a better model by modelling  $Cr_1$  for each material ISO-group individually. It is motivated by the fact that all the materials within a group exhibit similar properties in terms of

machinability, even though their mechanical or thermal properties may vary. This was tried and the conclusion from their study is that it seems advantageous with this approach for some ISO-groups, mainly ISO P where the coefficient of variation was roughly 5%. The model was on the contrary worse for determining  $Cr_1$  in ISO-M and ISO-S. However, they further conclude that the general model for all workpiece materials appears to be comparatively good and thus it could be speculated that it might be appropriate for all scenarios. It should be pointed out that some of the error obtained is thought to be due to tribological characteristics on the rake face in combination with potential inconsistency of material properties of the workpiece samples. The final conclusion for this study is that the model are relatively accurate for estimating the cutting resistance. Even though the error is relatively small it is not negligible and the result should thus be viewed as only an estimation.



# 3

## Methods

Presented in this section are the methods used to acquire the results.

### 3.1 Workpiece materials

Described in the following sections is the workpiece materials used for the study. They are as mentioned from two different ISO groups and thus vastly different in properties and morphology. The general description of the materials are presented in *Chapter 2.7.1*.

#### 3.1.1 316L workpieces

The workpiece material selected from the ISO-M group is 316L from two different suppliers, *Supplier A* and *Supplier B*. Even though the workpieces are of the same material they vary slightly in chemical composition and manufacturing process resulting in somewhat different material properties.

Both 316L workpiece materials are, according to their material certificates, hot rolled and annealed. The bars are then peeled for both suppliers, meaning that they are machined to remove surface cracks, cooled layers of "skin", and oxides. From the certificate it also reads that for *Supplier B*, an additional polishing is added after peeling. Since both of them are hot rolled, the process parameters of this method have a direct effect on the grain size. The following annealing step also plays a role, mainly since the time and temperature of this impacts the resulting microstructure.

The differences in alloying content, or chemical composition, also play an important role on the properties. Below in *Table 3.1* the chemical composition as stated in the material certificate of *Supplier A* can be viewed. It can be compared to that of *Supplier B* which is presented in the following table, *Table 3.2*.

C	Si	Mn	Cr	Mo	Cu	Ni	P	S	N
0,015	0,58	1,79	16,69	2,05	0,53	10,14	0,030	0,027	0,072

**Table 3.1:** Chemical composition in *wt%* from *Supplier A* of the 316L workpieces.

C	Si	Mn	P	S	Cr	Ni	Mo	N
0,012	0,29	1,71	0,033	0,025	16,82	10,10	2,04	0,047

**Table 3.2:** Chemical composition in wt% from *Supplier B* of the 316L workpieces.

The alloying content can cause some tendencies for the process behavior as explained in *Chapter 2.6*. In addition to the low amount carbon in this material type, the relatively high amounts of nickel is expected to make the material prone to form a built up edge. Hence a higher cutting speed is preferred for these workpiece materials in order to avoid this.

### 3.1.2 100Cr6 workpieces

The selected workpiece material from the ISO-P group is 100Cr6 which is a high carbon through hardening steel commonly used in bearing applications. The material supplier states the chemical composition as presented in *Table 3.3*. This material is due to the relative high amount of carbon, based on *Chapter 2.6*, expected to have less ductility and adhesion. This causes the process being less prone to suffer from issues related to built up edge.

C	Si	Mn	P	S	Cr	Ni	Mo	Cu	Al	Ti	O
0,98	0,28	0,33	0,014	0,007	1,43	0,14	0,04	0,178	0,022	7ppm	3,6ppm

**Table 3.3:** Chemical composition in wt% for the 100Cr6 workpieces.

In the case of ISO-P, instead of varying the supplier of the material, its condition is varied by different heat treatments. For this study the material are supplied in three different conditions resulting in differences in microstructure and consequently also for properties such as the hardness. The three conditions are designated *Annealed*, *Hardening 1*, and *Hardening 2*. Where *Hardening 2* is the most hardened condition.

## 3.2 Sample preparation

To analyze the workpiece materials, accurate preparation of the samples is necessary. Specifically the sample preparation is performed in order to study the microstructure of the material with microscopy.

Different methods of sectioning and organizing the samples are used between the two ISO groups since the workpieces are of different geometries. The following chapters, *Chapter 3.2.1* and *3.2.2*, describes how the samples are extracted from the different workpieces.

The cut samples are mounted in thermosetting bakelite hot mounting resin with carbon filler. The samples are mounted in such way that the exposed faces are from the circular cross sections of the workpieces. After mounting the samples the surface is ground and polished, creating an even surface suitable for microscopy.

The samples are etched in order to reveal microstructural details that would otherwise not be visible. Features such as porosity, cracks, and inclusions are however visible by only polishing. A properly etched sample reveals properties such as grain size, segregation, as well as the shape, size, and distribution of the phases and inclusions. Other aspects such as mechanical deformation and thermal treatments may also be observed.

The 316L samples are difficult to etch. Due to this the etching is performed electrochemically with Oxalic acid 10% at 10V. Since the 100Cr6 are on the contrary relatively easy to etch, they are simply exposed to Nital 3% by submerging the sample for a short period of time. The time is selected arbitrarily until the surface appears non-reflective, paying close attention that they do not become over etched.

### **3.2.1 316L sample preparation**

The ISO-M materials are supplied in cylindrical bars. Since the total depth of machining for this material group is decided to be a maximum of 30mm, only samples until this radial depths are deemed necessary to analyze. *Figure 3.1*, illustrates how the samples are extracted from the 316L workpieces.

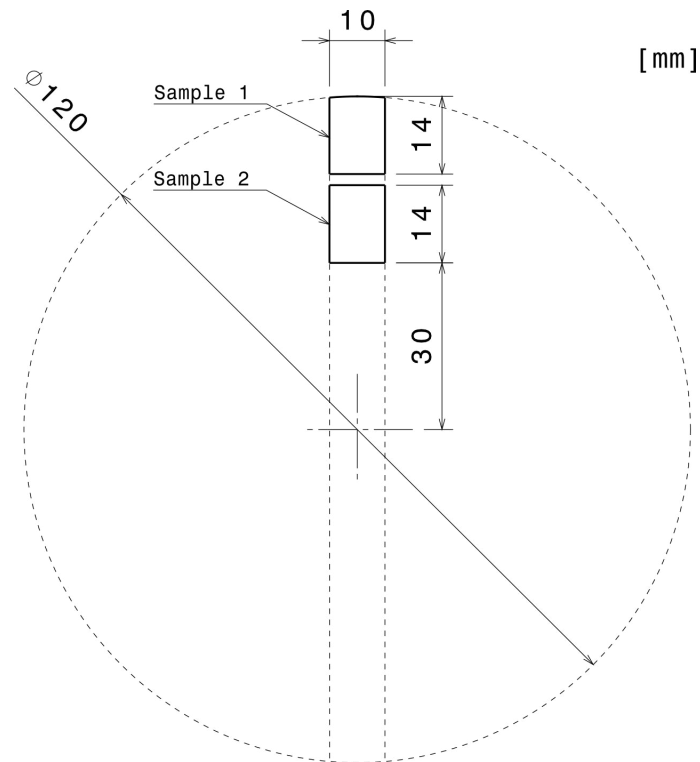


**Figure 3.1:** The figure illustrates the radial cross section and how the 316L samples are cut from the workpiece.

#### 3.2.2 100Cr6 sample preparation

The ISO-P materials are supplied in a slightly different geometry, hollow cylindrical bars, with the reason being that they are hardened. Since the wall thickness is only 20mm the full radial depth can be covered in one sample. In *Figure 3.2*, it is illustrated how the samples are cut for all three workpieces of 100Cr6.

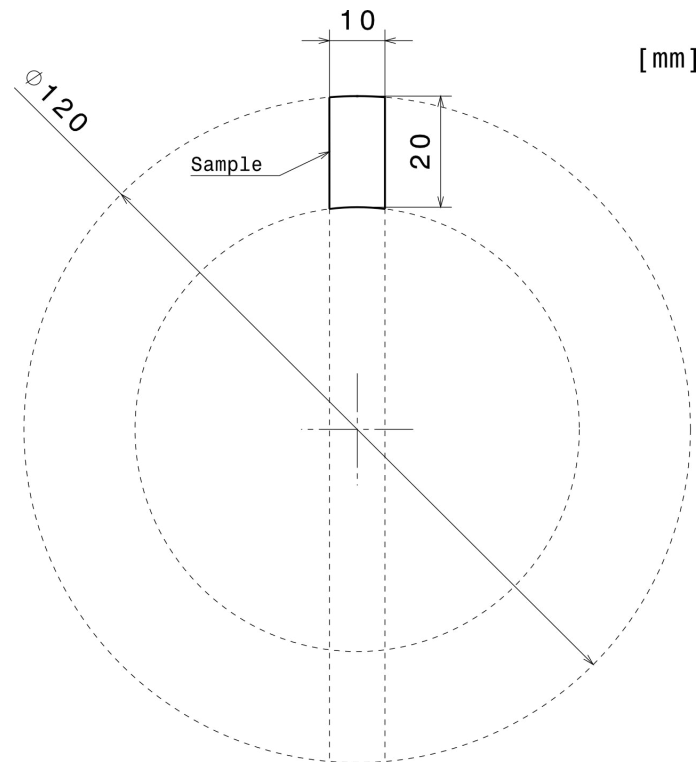


**Figure 3.2:** The figure illustrates the radial cross section and how the 100Cr6 samples are cut from the workpiece.

### 3.3 Microscopy

Described in these sections are the methods used for studying the microstructure of the radial cross sections. Different methods are employed depending on the specific features being studied.

#### 3.3.1 Optical microscopy

The *Light Optical Microscope* used is a *LEITZ DMRX* with a *AxioCAM MRc 5* for image acquisition. This equipment is used to capture the microstructure, more specifically the grains. This is described in detail in the following chapter, *Chapter 3.3.1.1*. This is also used as part of the inclusion analysis in order to capture images to complement and verify the result from ESEM, described below in *Chapter 3.3.2.2*. Note that the LOM-images of the inclusions are captured prior to etching.

### 3.3.1.1 Grain size estimation

The grain size estimations are carried out with a method described in *ASTM standard E112 - 12*. The method in this standard is the *intercept method* which involves placing a line over a plane of the microstructure and determining the number of intersections made between the line and the grain boundaries.

Two diagonal lines are placed on each respective image from the LOM where the lines intersect at least 50 grain boundaries. The intersections are manually counted for each line and the average number of intersects for the two lines are determined. The number of intersections made with each line are divided by the length of the line which provides a value for the average grain size.

The areas analyzed are presented in *Figure 3.3*. Each sample is divided into four radial depths, meaning that the increment is  $3,5\text{mm}$  for each area. One image is captured in a random manner within each grid square and two grid squares are analyzed at each increment in radial depth. This means that a total of two images are captured for each step from the surface in order to obtain an average for each level. The average grain sizes are then plotted for the respective radial depth providing an approximation of the radial variation in grain size.

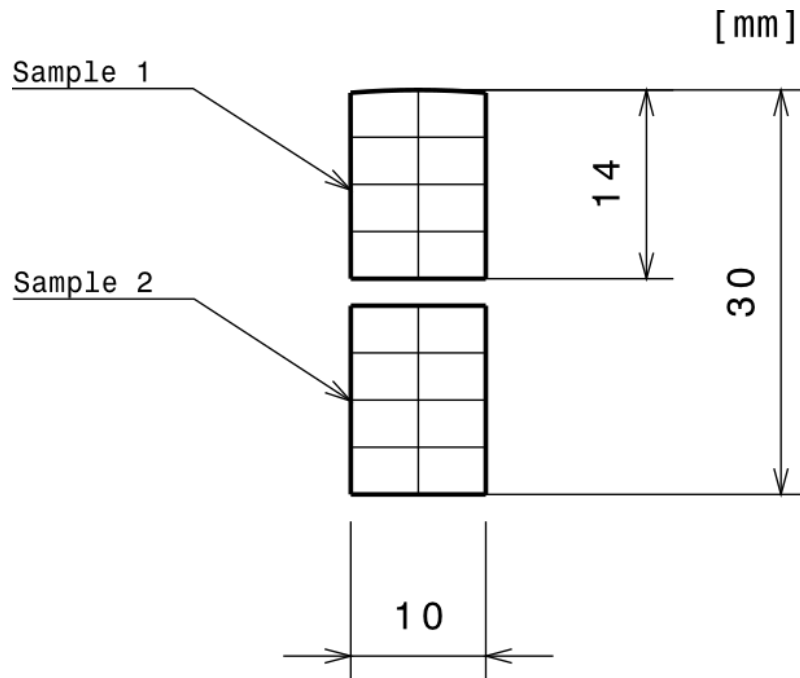


**Figure 3.3:** The figure illustrates how the samples for ISO-M are divided into areas at different radial depths for the grain size characterization.

### 3.3.2 Inclusion analysis

The inclusion analysis is performed with an *Environmental scanning electron microscope, ESEM*. This is carried out before etching since the etchant can alter the result. The equipment used is a *PHILIPS XL 30 ESEM*.

#### 3.3.2.1 Identifying inclusions

The *Energy dispersive spectroscopy, EDS*, is done with an *INCA x-sight* from *Oxford Instruments*. For the analysis, three random areas containing inclusions are studied. The inclusions within each area are identified and the result is a graph with characteristic peaks where the the presence of certain peaks represents the presence of certain elements.

At least three inclusions for a specific morphology are analysed in order to reach some degree of certainty that there is no variation between them. Even though a relatively small amount och inclusions are analyzed with EDS, a large area is visually inspected. Based on the morphology of those inclusions analyzed, the conclusion may be drawn that it is unlikely that there are any unidentified types of inclusions that constitutes a large volume fraction of the material.

#### 3.3.2.2 Quantifying inclusions

The relative amount of inclusions are captured in a systematic manner roughly inspired by the *ASTM E45-18a* standard. This is done for both materials with the aim to observe how the amount and size of the inclusions vary with the radial depth of the workpieces. The inclusions are quantified by image capturing with back scattered electrons and the inclusions can be distinguished by their shape and contrast.

A total of 25 images per sample area are captured at a magnification of  $500x$ . Each sample area is a predetermined  $5x5mm$  square positioned in the center of each sample for the 316L workpieces. The images are evenly spaced with five images captured per row in an alternating right to left manner. The total captured area per square is  $3,6mm^2$  although it is sampled from a total area  $25mm^2$ . The placement of the analyzed areas can be viewed in *Figure 3.4*.

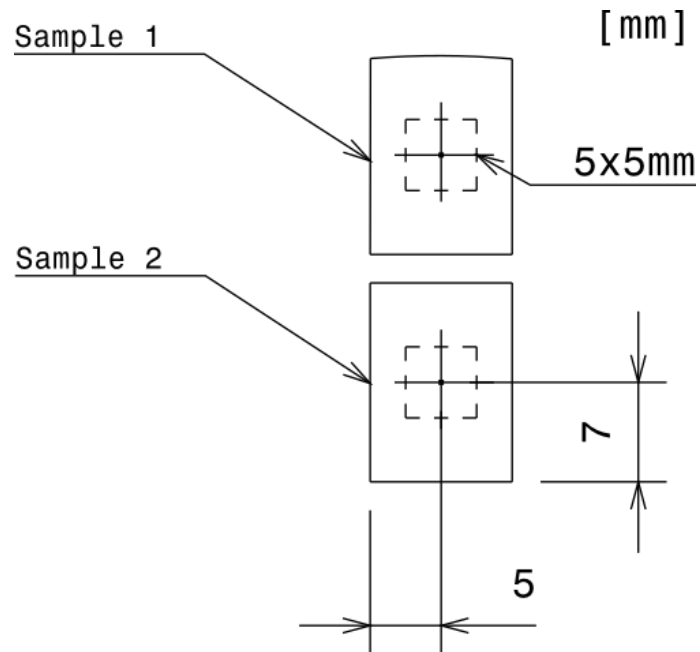


**Figure 3.4:** The figure illustrates the area investigated for inclusions on the 316L samples.

Since the geometry of the 100Cr6 samples are different and because the whole radial cross section can be covered in one sample, two areas are analyzed at different radial depth. The method is the same as for the 316L samples but the placements of the squares are different. This is illustrated in *Figure 3.5*.

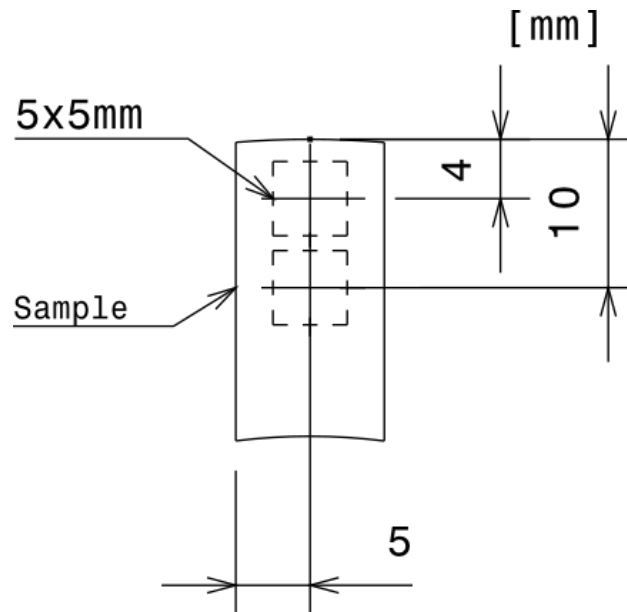


**Figure 3.5:** The figure illustrates the areas investigated for inclusions on the 100Cr6 sample.

The images are analyzed with the open source software *Image-J*. The area covered by inclusions is selected by contrast, utilizing a threshold tool. The software then quantifies the area covered and the size distribution of the particles. Since this is done on both sample areas for the respective material it is thus possible to see if this changes with radial depth.

### 3.4 Monotonic testing

The monotonic testing, *i.e.* the tensile testing, is carried out at Seco's facility in Fagersta for the 100Cr6 workpieces. It is conducted in accordance with *ISO 6892-1:2016* with the exception that the specimens are 60mm in total length together with a gauge length of 22mm. The nominal diameter of the tests are 6mm. Two monotonic are performed for each hardening condition.

### 3.5 Hardness testing

The hardness evaluation is performed with a *Struers DuraScan 70 G5*. The method used is the *Vickers* hardness test which involves creating an indent with a diamond pyramid-shape indenter. The diagonals of the indent is measured optically and based on the lengths of these a value for the hardness is obtained. The indents are made on the polished (and etched) surface of the samples. The specific test method *HV10* is employed which refers to the applied load of 10kgf.

For all samples a total of ten indentations on each are done. In order to detect a variation of hardness with the radial depth of the workpieces, see *chapter 3.2*, the total length of each sample is divided into five depth. Two lines of five equally spaced indentations are made on each sample in order to obtain two values for each depth. By using two indentations for each step it provides an average hardness at each level of radial depth.

The lines are placed manually on the sample using the software meaning that they vary slightly in length. When the lines are drawn, the software distributes the marks for the indentations with equal spacing. Since the length may vary slightly between lines a variation is introduced in spacing as well. In addition to this, the position of the starting point is also manually placed potentially causing a slight offset between the rows of indents. Due to this, the spacing of indents as well the starting points, that together provides the radial depth, is approximated based on averages between lines. The radial starting depth is approximated to  $1,7mm$  and the average step length is calculated to  $2,8mm$ .

The average hardness, from two data points, is plotted against the respective radial depth in order to obtain a graph that approximates the hardness against radial depth.

## 3.6 Machining experiments

The method used for all experiments to gather data about the cutting resistance is the *feed step* method. This method involves a stepwise increment of feed whilst maintaining constant cutting velocity,  $V_c$ , and depth of cut,  $a_p$ . The maximum feed allowed for each material is for this study varied depending on the hardness. In addition to this the cutting speed is also varied between material, with a higher cutting speed for the more ductile workpieces. The cutting data is explained more in detail in the respective section however in *Figure 3.6* the plan over feeds and cutting speeds is presented.

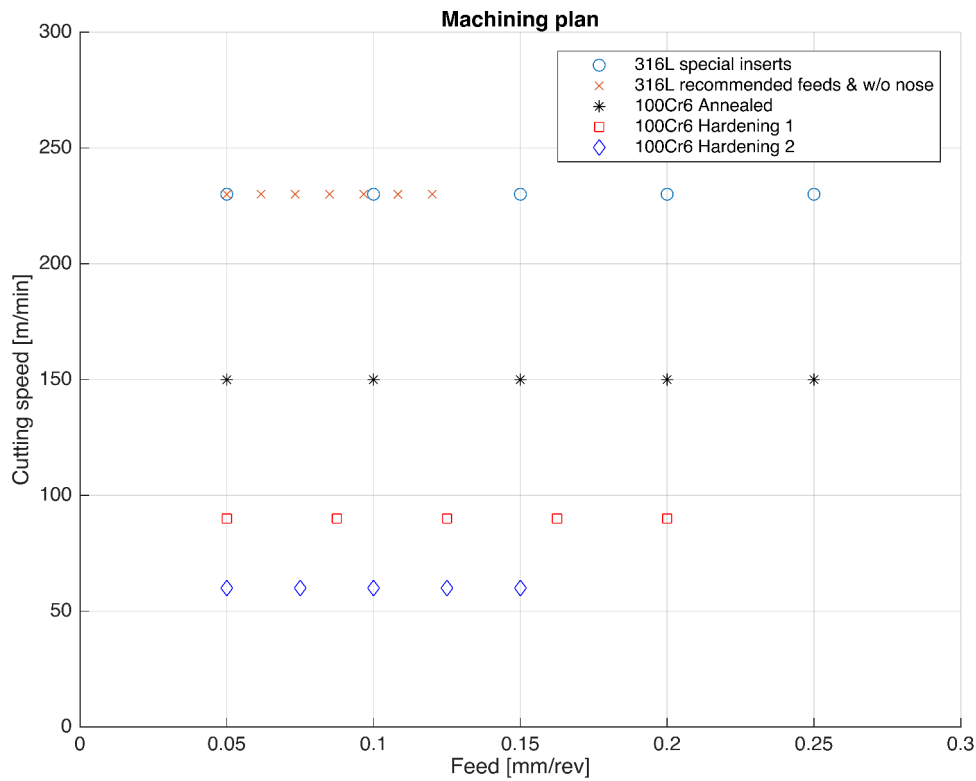


**Figure 3.6:** All feeds and cutting speeds used for the respective machining experiment. (*316L special inserts* refers to the machining of 316L with the special made ISO-P inserts).

All experiments that are carried out to generate the data for the study are done in face turning operation. This mode of turning involves feeding the tool in the radial direction, as is schematically shown in *Figure 3.7*. The machine used for all experiments is an *EMCO Turn 365* which is a conventional three axis CNC-lathe. A *Kistler* force gauge module is used to measure all three force components in their respective direction.

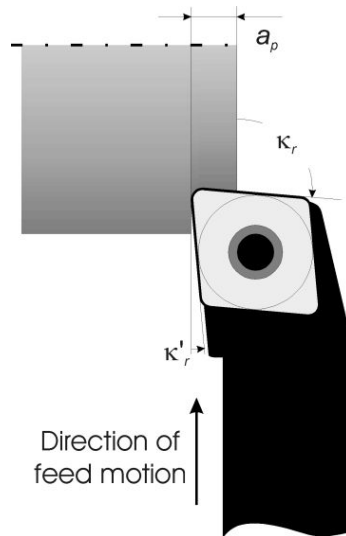


**Figure 3.7:** Schematical representation of face turning operation. [4, pp. 124]

To assure good quality of the data, all measurements are performed with pristine cutting edges which eliminates variations induced by preceding tool wear. All tests are carried out with coolant, emulsion with 6wt% mineral oil (*Castrol CareCut S 600*), measured with a refractometer.

All experiments are repeated at least once in order to show repeatability and thus assure that no significant variation occurs. If the second repetition is within a reasonable tolerance of the previous it is considered good enough.

The values used as data for analysis are the average values of forces obtained at each feed level of the machining experiments. The average value is calculated from the first five seconds of the experiment where the forces stabilize. The reason behind having a fixed time is mainly because the time of engagement is varying between all tests and that this should further reduce influence of tool wear. However, it should be noted that with increased feed a greater distance in radial direction is covered in the time used for the average forces. This means that if microstructural differences depending on radial depth are present in the workpiece, the effect of this can introduce a greater variation with the higher feeds.

The same tool holder is used for all experiments meaning that the geometry of the tool holder is constant. The inserts are of four different variants with varying rake angles and nose radius as well as chip breakers. There are three special made ISO-P inserts which are called *inserts 1*, *inserts 2* and *inserts 3*. There is one commercial ISO-M insert called *inserts 4*. Since the inserts themselves have no clearance angle, all angles except the rake angle is constant and thus carried over from the tool holder. The tool holder has a slight clearance angle together with a negative inclination angle. The cutting edge angle is however  $90^\circ$  meaning that the cutting edge is parallel to the axis of rotation in the case of face turning.

The main cause of the inclination angle for the general process is that orthogonal cutting, as described in *Chapter 2.3.1*, will not take place. Thus the mode of cutting is for all tests is *oblique cutting*.

### 3.6.1 Face turning 316L workpieces

#### 3.6.1.1 Face turning 316L workpieces with recommended feeds

The first experiments in the study are carried out with commercial inserts used within their recommended application and process window. More information about this be found in *Chapter 2.2* where this particular process window is presented in *Figure 2.2*.

The feed steps are selected, with some margin, within the recommended minimum and maximum feed for a certain depth of cut while taking the cutting speed into account. The selected feed steps are presented below in *Table 3.4*. The cutting speed is set to  $230m/min$  which is about the average recommended cutting speed for all feeds selected. The setup is identical to that of turning ISO-P and *Figure 3.9* in *Chapter 3.6.2* is thus representative.

Feed 1	Feed 2	Feed 3	Feed 4	Feed 5	Feed 6	Feed 7
0,06	0,07	0,08	0,09	0,10	0,11	0,12

**Table 3.4:** Table showing the selected feeds for the feed steps for both machining operations for the 316L workpieces using *Insert 4*, in the unit  $[mm/rev]$ .

Three repetitions are performed at each level of feed in order to obtain average values for the force components. For practical reasons this approach is only applied for the first experiments on the 316L workpieces using the commercial ISO-M tool, *Insert 4*.

#### 3.6.1.2 Face turning 316L workpieces without nose engagement

In order to avoid influences from having the nose in engagement, a setup involving equally spaced flanges are used where the width of the flange is the depth of cut. To achieve this setup,  $20mm$  deep grooves are cut into the workpieces, spaced evenly to accommodate sufficient space for the nose in front of the flange being cut. This experiment is considered complementary for the conventional face turning experiments in order to study the effect on the result by not engaging the nose. It can also provide an indication of the degree of inaccuracy possibly introduced by using Woxén's model for equivalent chip thickness.

The same cutting conditions as presented in the previous chapter, *Chapter 3.6.1.1* are used. This is done in order to have the ability to directly compare the results. The setup for this experiment is pictured in *Figure 3.8*.



**Figure 3.8:** The figure illustrates the experimental setup for the face turning of the 316L workpieces without the nose engaged. Note that the insert is censored.

#### 3.6.1.3 Face turning 316L workpieces with special inserts

Tests are performed on the 316L workpieces with the same special made inserts and feeds as for the 100Cr6, described in *Chapter 3.6.2*.

The same levels of feeds are selected for machining the 316L workpieces as for the annealed 100Cr6. The cutting speed is set to the higher value of  $230m/min$  which is used for all experiments on this material. The feeds for this experiment are presented in *Table 3.5* below.

Feed 1	Feed 2	Feed 3	Feed 4	Feed 5
0,05	0,10	0,15	0,20	0,25

**Table 3.5:** Table showing the selected feeds for the feed steps for both machining operations for the 316L workpieces with *Insert 1*, *Insert 2* and *Insert 3*, in the unit [ $mm/rev$ ].

### 3.6.2 Face turning 100Cr6 workpieces

Three special made inserts are used for the machining experiments of mainly the 100Cr6 workpieces from ISO-P. However, they are also used for ISO-M as explained in the previous chapter, *Chapter 3.6.1.3*. The special made inserts are called *Insert 1*, *Insert 2* and *Insert 3*. The reason why these are special made is to have the same grade (coating and substrate) for all inserts. These inserts are based on commercial geometries as well as grade, although they do not exist commercially in these combinations. This is considered important for assuring good quality of the data since tribological effects from the grade would be constant between tests. The intention behind varying the geometry and chip breakers is to observe the effect of this and to calculate an average cutting resistance between the normalized cutting forces. This would further reduce the impact by variations that the normalization does not account for, more in this in *Chapter 3.7.2*.

It should be noted that these inserts have cutting edge reinforcements where the length of which depends on the variant. Since the feeds are always less or equal to the length of these edge reinforcements, limited contact with the insert is assumed where the angle of these effectively acts as the rake angle. For one geometry however the last feed exceeds the length of the edge reinforcement.

In *Figure 3.9*, the setup is shown. The mounted workpiece material is 100Cr6 from ISO-P, however the image is representative for the 316L workpieces from ISO-M as well.

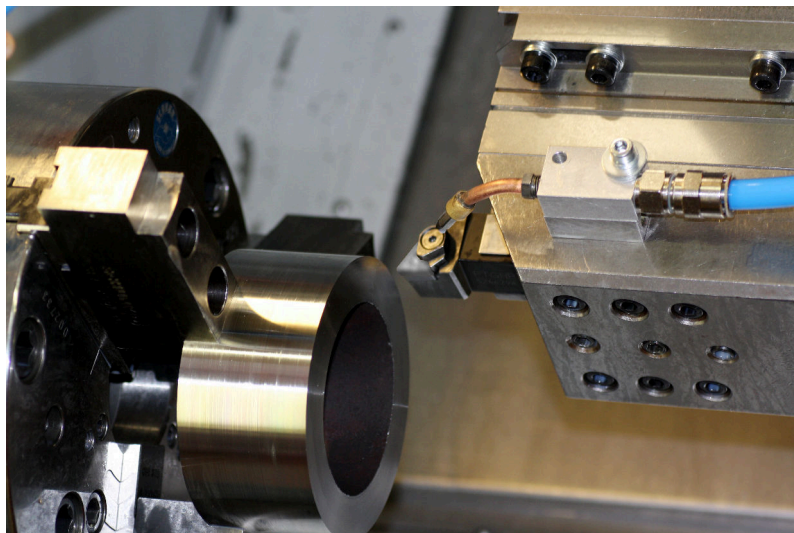


**Figure 3.9:** The figure illustrates the experimental setup for the face turning of the 100Cr6 workpieces as well as the 316L. Note that the insert is censored.

The workpieces are machined in the order of hardening degree and with a different cutting speed and maximum feed depending on the level of hardness. The selected window of feed for each condition is divided into five levels. The reason for subsequently lowering the maximum feed is to avoid problems with vibrations and plastic deformation and excessive wear on the cutting tools since much greater forces are expected for the hardened workpieces. The selected levels for the feeds are presented in *Table 3.6* below. In addition to lowering the maximum level of feed, the cutting speed is also lowered for increasing hardness. The cutting speed is lowered from  $150m/min$  for *100Cr6 Annealed*, down to  $90m/min$  for *Hardening 1* and the lowest value of  $60m/min$  for the hardest condition, *Hardening 2*.

Condition	Feed 1	Feed 2	Feed 3	Feed 4	Feed 5
Annealed:	0,05	0,10	0,15	0,20	0,25
Hardening 1:	0,05	0,09	0,13	0,16	0,20
Hardening 2:	0,05	0,08	0,10	0,13	0,15

**Table 3.6:** Table showing the selected feeds for the feed steps used for the 100Cr6 workpieces, in the unit  $[mm/rev]$ .

## 3.7 Data analysis

### 3.7.1 Obtaining the average forces

The average forces for each combination of workpiece material, insert geometry, and feed level is determined. This is necessary in order to be able to study the static forces generated by said combinations.

The raw data for the force measurements together with time is imported and refined in MATLAB. A script is written that saves the average forces based on a manually selected point in the force-time graph where the forces have stabilized. From the selected point, and five seconds ahead, the average force is calculated and saved. Since two repetitions are carried out, the average between two tests are also calculated. This is saved in a vector and is plotted against the respective feed. The result of this is then normalized to eliminate the effect of insert geometry as explained in the following chapter.

### 3.7.2 Force normalization

To further refine the data and to obtain a result independent of tool geometry, or rather a normalized result that can be transformed for other tool geometries than for those used in the study, a transformation matrix is employed. This method is described in detail in [2, p. 117-127]. By determining the load function from the

measured forces for each cutting tool combination and by knowledge of the geometry of the tools, the forces can be transformed to a value which can be considered a baseline. From this baseline forces can be approximated for another geometry if desired. This method is applied for all cutting force data in the study.

The baseline geometry where all data is normalized to is presented in the following list.

- Rake angle,  $\gamma = 0^\circ$
- Clearance angle,  $\alpha = 0^\circ$
- Inclination angle,  $\lambda = 0^\circ$
- Major cutting edge angle,  $\kappa = 90^\circ$

Load functions are determined from experimental data where the force is plotted against the equivalent (theoretical) chip thickness,  $h_{eW}$ . Ideally the data points fall on a straight line and the forces as a function of theoretical chip thickness is expressed as a linear equation. This is carried out for all three force components,  $F_c$ ,  $F_f$  and  $F_p$ .

Based on the load functions, the force components can be computed in their respective direction for any tool geometry that is defined in terms of clearance angle, rake angle, major cutting edge angle, and the inclination angle. For more details see [2, p. 123].

The illustration presented in *Figure 3.10* indicates the normal planes that the force components are transferred to. This is done by multiplying the force components with transformation matrices that are calculated for each tool geometry. In the end this provides a cutting force component that is in the same plane for all different tools. Some assumptions are being made for the modeling. For example when performing the load transformations, the clearance angle is assumed zero degrees for reasons explained in [2, p. 123].

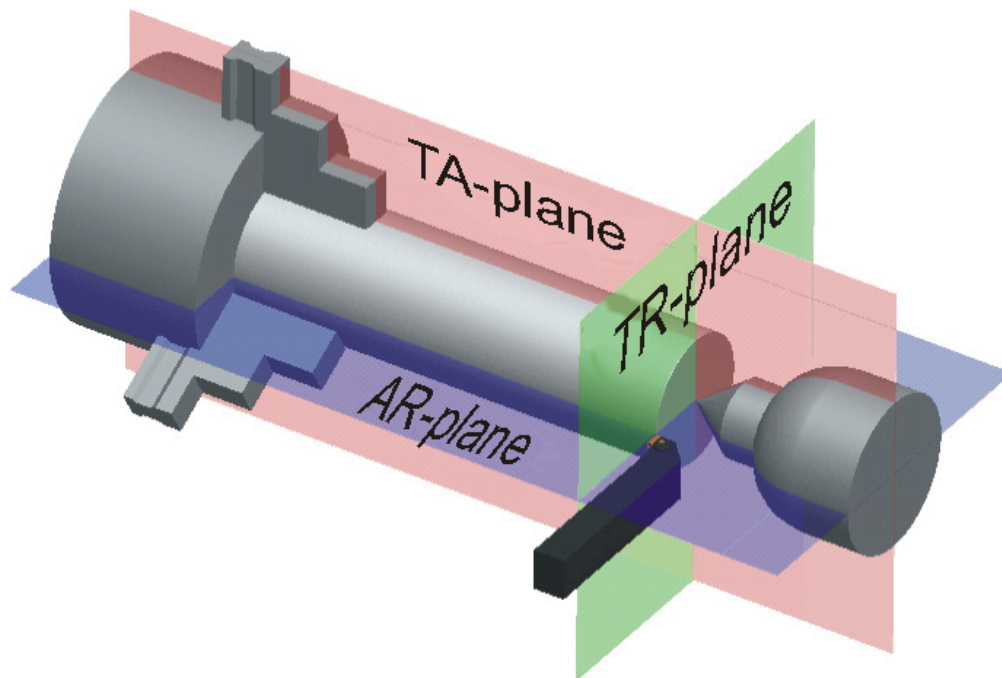


**Figure 3.10:** Model of the plane definitions in turning. [2, p. 41], Figure 2.7.

### 3.7.3 Cutting resistance as a function of equivalent chip thickness

For each insert and material combination the average force response, now independent of insert geometry, can for a certain feed be plotted against the theoretical chip thickness using *Equation 2.1*. Since the nose of the insert is in engagement the equivalent chip thickness,  $h_{eW}$ , is used for a more accurate representation of this parameter. Note that this equation does not account for build up edge or deformation hardening. See *Chapter 2.1.2* for a more detailed description.

The result presented in 4.2 is the *Cutting resistance* as a function of equivalent chip thickness. The cutting resistance is directly dependant on the cutting force since it is defined as the static main cutting force divided by the chip area. The result of this can, as explained in the previous chapter, then be transformed for a specific insert geometry. Since the aim of this study is to analyze how the cutting resistance, and consequently the main cutting force, depends on the material properties, only the average cutting resistance based on the normalized forces as a function of equivalent chip thickness is further used. How the data is treated in this study is schematically shown in *Figure Flowchart special inserts*. The figure illustrates the data for the non commercial inserts used for all workpiece materials. The same approach is applied for the standard inserts used for the 316L workpieces as well, following only one branch.

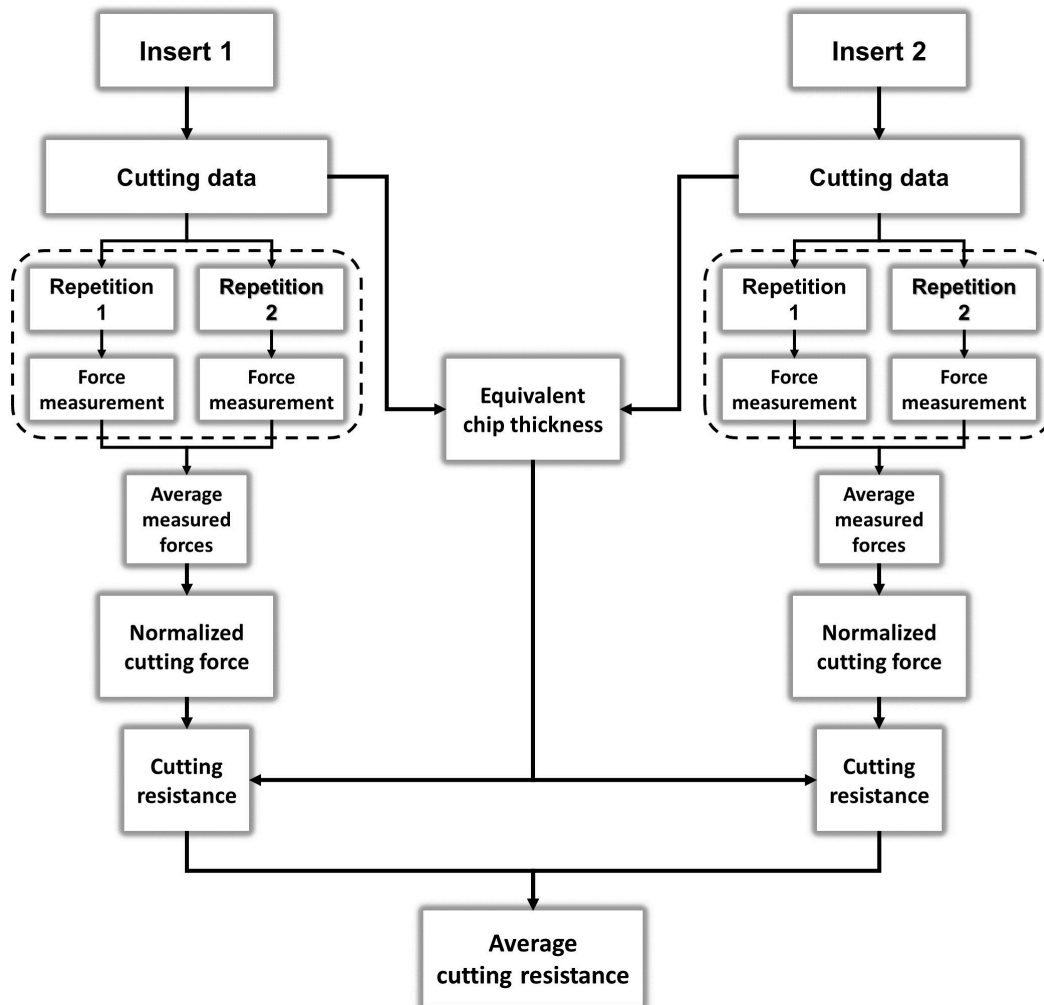


**Figure 3.11:** Flow chart schematically representing how the data for the cutting forces are treated towards calculating the cutting resistance. Note that *Insert 3* is not included due to it not being considered.

### 3.7.4 Investigating connection between material properties and cutting resistance

Since the refined data from the previous steps, normalized for a baseline tool geometry, the cutting resistance is compared between materials. Comparing the cutting resistance with material is however not trivial, mainly since the term material can be divided into several parameters. Thus it is relevant to analyze which parameters have the strongest correlation with the cutting resistance and by that the main cutting force.

## 3.8 Verifying result

### 3.8.1 Machining experiments at Seco Tools

In order to verify the result, a series of experiments are performed at Seco's facility in Fagersta. In this case the operation is changed to longitudinal turning and no cutting fluid is used. Furthermore a different tool holder and different type of inserts are used. In addition to this, a different machine is obviously used, which in this case is more stable. The experiments are carried out for the 100Cr6 workpieces in all three conditions.

The feed step method is carried out in a different manner. A more rapid method is used, instead of making a new cut for each feed level with a pristine edge, the machine is programmed to increase the feed after a set distance meaning that all feeds are covered in one consecutive cut. This has the major benefit of being a faster way of generating data, with the drawback that the tools can wear out during the experiment from one feed step to another..

$$\text{Relative difference} = \frac{Cr_{1,Seco} - Cr_{1,Chalmers}}{Cr_{1,Chalmers}} \quad (3.1)$$

### 3.8.2 Approximating cutting resistance

#### 3.8.2.1 Approximating based on a previous model

To obtain a reference when approximating the cutting resistance a comparison with the more general model from *Lund Univeristy*. This model is presented in *Chapter 2.8*. It is as explained based on four different material properties together with eight constants. The model is presented in *Equation 2.10*.

The constants used in the model depends on ISO group and is presented in [11]. The constants applied for ISO-P are shown in *Table 3.7* below.

By using the material properties determined in this study the cutting resistance is approximated by this method. The relative error between the calculated cutting resistance based on material properties versus the measured values are evaluated with the following equation.

$$\text{Relative difference} = \frac{|Cr_{1,approximated} - Cr_{1,measured}|}{|Cr_{1,measured}|} \quad (3.2)$$

Constant:	Value ISO-P:
$\alpha'$	13,8
$\delta'$	0,80
$\beta'$	-20,7
$\nu'$	0,50
$\gamma'$	679
$\eta'$	0,15
$\xi'$	-2,60
$\omega'$	1,11

**Table 3.7:** Table containing the constants for the approximation. As presented in [11].

### 3.8.2.2 Approximating cutting resistance of 316L with empirical relation determined for 100Cr6

Since this study has well documented data for the 316L workpieces from ISO-M, it is considered relevant to evaluate how "universal" the relationship is between the Vickers hardness and the constant  $Cr_1$ . Since the gradient in the hardness is less significant for *Supplier A* the data for this workpiece material selected. As discussed, the average cutting forces is measured during the first five seconds meaning that the data is based on the first millimeters of radial depth. When studying the hardness profile in *Figure 4.2* the average hardness for the first 10mm of radial depth is about 190HV. The approximated value for  $Cr_1$  is computed based on the relationship in *Equation 4.1* combined with the constants for the hardness presented in *4.9*. The result is shown in *Chapter 4.5.2*.



# 4

## Results

Here in the following sections, all the results of the study are presented.

### 4.1 Material characterization

In this section the result from the material characterization is presented. It is divided into two major sections, one for each material.

#### 4.1.1 316L characterization

##### 4.1.1.1 Inclusions 316L

The volume fraction of inclusions for the 316L workpieces are estimated and presented in *Table 4.4* below. A difference in the amount of inclusions are distinguishable between *Supplier A* and *Supplier B*. The inclusions also tend to be smaller in size for *Supplier B*.

In *Appendix A*, *Figure C.1*, an example image is presented. This particular image is captured on the sample from the workpiece material supplied by *Supplier B* which has the least fraction of the image covered by inclusions out of the two. The image is captured on *Sample 2* which is closer towards the center of the bar.

Radial depth	Supplier A	Supplier B
4,5 – 9,0mm :	0,29%	0,18%
20,5 – 25,0mm :	0,24%	0,17%

**Table 4.1:** Table showing the average area fraction of inclusions on the images within the respective area at different depths comparing the two suppliers.

The types of inclusions are identified with EDS as described in *Chapter 3.3.2.1*. The inclusions can be identified as *Manganese sulfide*, MnS and *Calcium oxide*, CaO for both suppliers. While analyzing the CaO inclusions traces of oxides containing *Aluminum* and *Silicon* are present. Furthermore, the workpiece material from *Supplier A* also contains *Titanium nitride*, TiN.

As mentioned in *Chapter 2.6* the MnS in particular, but also CaO are beneficial for the machining process. The presence of TiN may on the other hand be of more interest when studying tool wear since they, as touched upon in *Chapter 2.5*, can have an abrasive effect on the cutting tool's surface.

### 4.1.1.2 Grain size estimation 316L

The grain size plotted against radial depth of the workpiece is presented in *Figure 4.1*. A clear gradient can be observed where the grains are smaller towards the surface of the workpiece. As shown in the graph the grains are generally larger for *Supplier A* compared to *Supplier B*. The increase in size with depth is however comparable.

Since estimations are based on the the intersects that are counted manually, it should be noted that this is not a perfectly accurate method since it is to some degree subjective whether or not a grain boundary is crossed. This is an issue because not all boundaries are perfectly clear due to the etching process. Furthermore it should be noted that each bar in the chart represents the average grain size within one block on the sample, see *Chapter 3.3.1.1*. All data points are based on two metallographic images with the average value for each image being calculated by two lines. The value presented in the graph is then the average between two images. To provide some statistical relevancy the standard deviation between two images are calculated. For *Supplier A* the average standard deviation between images is  $0,70\mu\text{m}$  and for *Supplier B*  $0,69\mu\text{m}$ . Since the scatter is low, the values in the graph shown in *Figure 4.1* should represent the samples relatively good.

The explanation as to why the grain size varies between workpiece materials can be found in *Chapter 3.1.1*. This should mainly relate to the process of which the materials are manufactured.

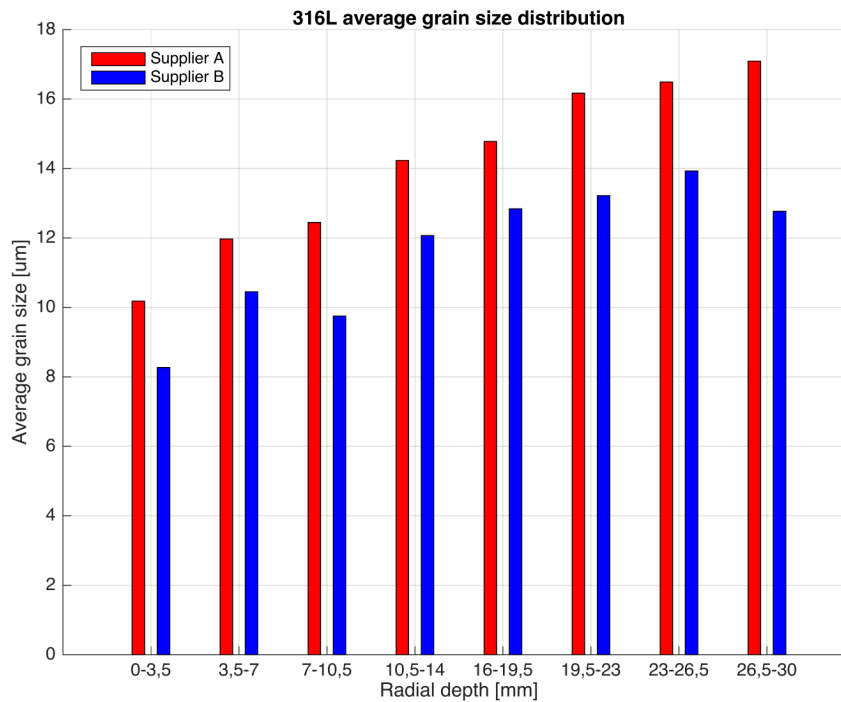


**Figure 4.1:** Graph that shows how the grain size varies with radial depth for the 316L workpieces from the two different suppliers. The average standard deviation over all data points is  $0,70\mu\text{m}$  for *Supplier A* and  $0,69\mu\text{m}$  for *Supplier B*, respectively.

#### 4.1.1.3 Hardness testing 316L

The hardness testing on the ISO-M samples presents a gradient of decreasing hardness with radial depth from the surface. Meaning that the samples are harder closer to the surface of the round workpieces. Since each data point is calculated as the average value from two indents, the average standard deviation between two tests are presented. For *Supplier A* the average standard deviation over all points are  $4,0HV$  and for *Supplier B*  $3,0HV$ . Hence, there is relatively low scatter in the measurements and the plotted values in *Figure 4.2* are representative for the samples.

As can be observed in *Figure 4.2* below the hardness close to the surface is significantly greater for the 316L workpieces of *Supplier B* compared to *Supplier A*. However, after a depth of about  $4\text{mm}$  the hardness drops below that of *Supplier A*.

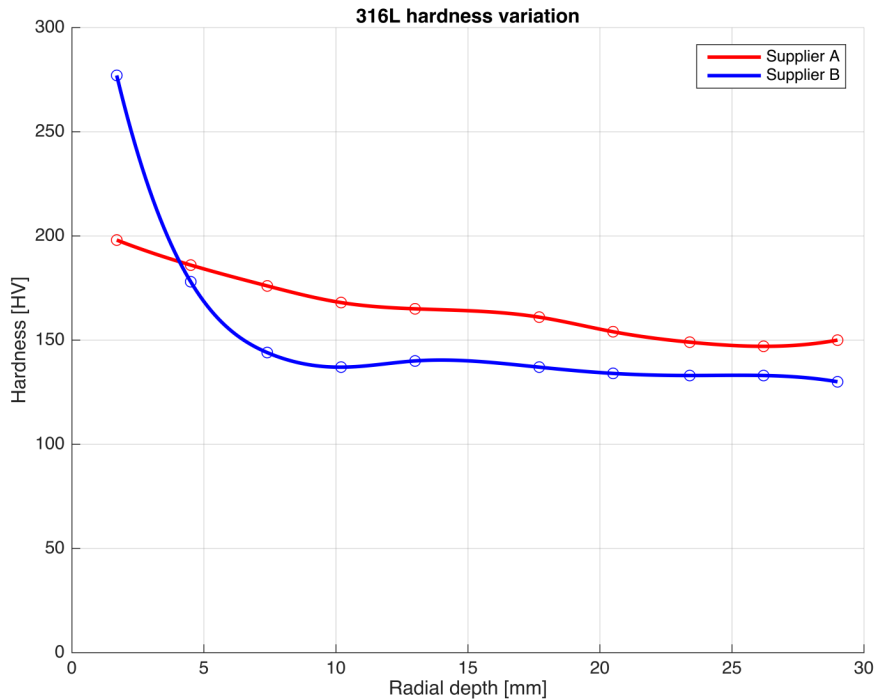


**Figure 4.2:** The hardness variation with radial depth for the 316L workpieces. The average standard deviation over all data points is  $4,0HV$  for *Supplier A* and  $3,0HV$  for *Supplier B*, respectively.

The result of the hardness test coincides with the material certificates where a min and a max value is stated. The hardness of the 316L supplied by *Supplier A* is stated to vary within  $140HB$  to  $215HB$ . For *Supplier B* the hardness is said to vary within  $131HB$  to  $134HB$  at a radial depth of  $30mm$ . When converting the values according to *ASTM E140 - 97e2* for non-austenitic steels it yields about  $140HV$  to  $226HV$  for *Supplier A* and  $131HV$  to  $134$  for *Supplier B*. A more accurate conversion may yield more accurate values, however it is clear that the values of the hardness follow the same trend. That the material of *Supplier A* is generally harder.

## 4.1.2 100Cr6 characterization

### 4.1.2.1 Inclusions 100Cr6

The volume fraction of inclusions for the 100Cr6 sample is relatively low, especially when compared to the 316L samples. Since inclusions should not be affected by heat treatment, it is decided to only analyze a sample from the annealed workpieces. However, when investigating the samples from the hardened workpieces a slight difference can be observed. However, this is likely due to the fact that these are from different lengths of the original untreated bar. Since the amount of inclu-

sions are low it is deemed unnecessary to further study this.

An example image is presented in *Appendix C, Figure C.2*. The image is captured on *Area 2* close to the center of tube wall. Note that there are some issues with contamination on the surface from the polishing step. However, since the inclusions are analyzed with software these particles are counted as inclusions due to their contrast, meaning that a slightly larger value for the amount of inclusions than in reality is obtained. The calculated area fraction, covered by inclusions at each radial depth is presented in *Table 4.2* below. Based on the area fraction it is clear that the amount of inclusions are very low to begin with. Furthermore it is clear that the area fraction becomes smaller with radial depth. This is true at least until the center of the tube wall where *Area 2* is located. Again, since the amount of inclusions is very low in general it is deemed unnecessary to further study this.

Radial depth	Annealed
1,5 – 6,5mm :	0,07%
7,5 – 12,5mm :	0,03%

**Table 4.2:** Table showing the average area fraction of inclusions on the images within each area at different depths on the sample of the annealed 100Cr6 workpieces.

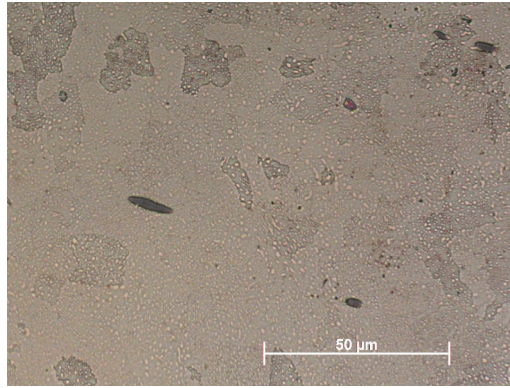
#### 4.1.2.2 Microstructure 100Cr6

Since the grain boundaries in the 100Cr6 material is difficult to observe in the LOM, a qualitative analysis is deemed sufficient. By studying the LOM-images at different radial depth, it is clear that there is no visual variation in microstructure. The difference between the annealed and the hardened conditions is significant. However in between *Hardening 1* and *Hardening 2* it is less distinct, although the structure appears slightly finer for the latter.

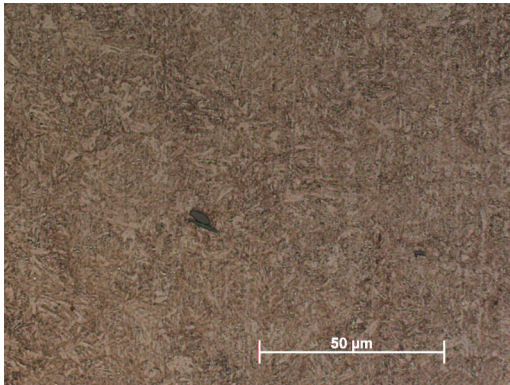
In *Figure 4.3*, the microstructure can be compared for the 100Cr6 samples in the three different conditions. The images are captured at approximately the same radial depth, near the center of the sample. The images are cropped, see *Appendix B* for full size. Note that even though only one image from a certain depth is presented, no significant visible difference in microstructure with varying radial depth is discovered. A total of twelve images at six radial depths are analyzed.

#### 4.1.2.3 Hardness testing 100Cr6

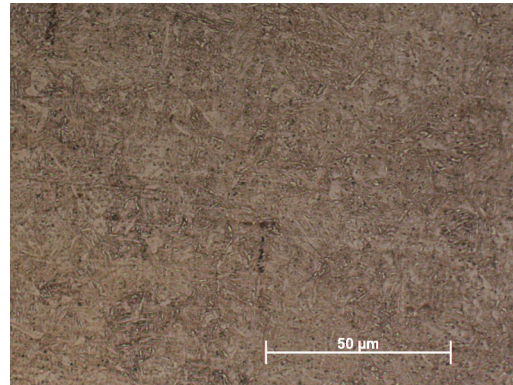
For the 100Cr6 samples the hardness is stable and not significantly dependant on radial depth. This is clear from the very low value of standard deviation as shown in *Table 4.3*. There is however, as expected, a strong difference in hardness depending on the hardening and consequently the microstructure.



(a) Annealed



(b) Hardening 1



(c) Hardening 2

**Figure 4.3:** Comparison of the microstructure of the 100Cr6 samples in three conditions.

Since the hardness does not appear to vary with radial depth, the average hardness per degree of hardening is more relevant. The respective value for each hardening can be viewed in *Table 4.3*.

Condition	Hardness [HV]	Standard deviation [HV]
Annealed	196	4,6
Hardening 1	397	5,0
Hardening 2	492	8,4

**Table 4.3:** Table containing the average hardness for each material condition followed by the respective standard deviation.

#### 4.1.2.4 Monotonic testing 100Cr6

The stress-strain curves plotted from the raw data received from the tensile testing at Seco are presented in *Appendix D*. The strain rate used for all test is  $1\text{mm}/\text{min}$ .

As explained in *Chapter 3.4*, all tensile tests are repeated once to show that there is no significant variation between tests. However, the data contains some flaws that appears to be the result of the extensometer losing its grip. This means that all presented graphs, except the one in *Appendix D, Figure D.3*, are based on two repetitions. The plot representing *Hardening 2* only contains the data from the "good" repetition out of the two. In *Figure 4.4* the engineering stress-strain plots are presented in the same graph. It can clearly be observed that the increase in strength is achieved at the cost of ductility.

Property	Annealed	Hardening 1	Hardening 2
Proof stress [MPa]:	402,14	1159,73	1552,60
UTS [MPa]:	701,40	1259,04	1668,84
Elongation at rupture, $\epsilon_f$ [%]:	44,70	20,37	12,35
Strain hardening exponent, $n$ [-]:	0,278	0,081	0,075
Strength coefficient, $K$ [-]:	1392,06	1672,04	2197,41

**Table 4.4:** Table over the different material parameters obtained through the tensile test for the 100Cr6 workpieces.

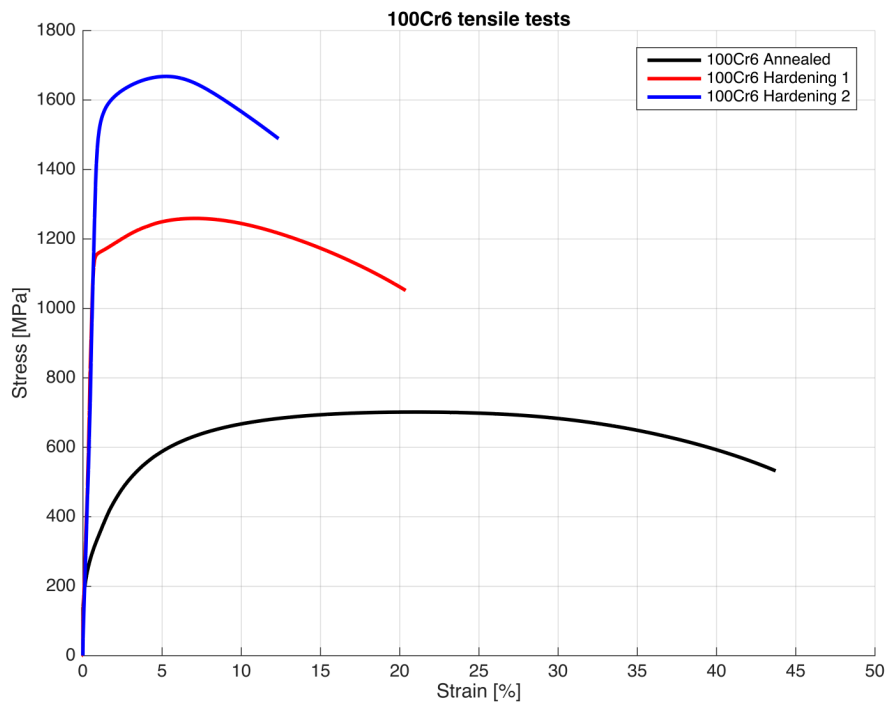


**Figure 4.4:** Engineering stress-strain curves for the 100Cr6 workpieces.

## 4.2 Machining result

Below in *Chapter 3.6.1* to *3.6.2* the results from the machining experiments are presented. As explained in *Chapter 3.6* all test are repeated at least once to show reproducibility. The first experiments on the 316L workpieces with standard tools and recommended process window, as is further explained in *Chapter 3.6.1* show very low scatter between repetitions. Since the scatter in the force measurements is small for all three repetitions on each feed level it leads to the decision to only repeat tests once moving on. In *Appendix I* the scatter can be observed where the difference between repetitions in the measured cutting forces are presented. As is shown, the scatter is relatively low for the most part.

When setting up experiments the percentage by weight of mineral oil in the emulsion is measured to about 6wt%. However, mid way through the experiments visual changes to the cutting fluid is observed and new measurements show that the emulsion by then is only containing about 1wt% oil. After replacing the fluid in the system and mixing the emulsion back to approximately 6wt% the tests are continued. Repetitions made on previous experiments show that this issue has no apparent effect on the force measurements.

In the two following sections, *Chapter 4.2.1* and *4.2.2* the result is presented as the average cutting resistance plotted against the equivalent chip thickness. As explained in *Chapter 3.6*, a number of insert geometries are used, all with a different force response. The following result is presented as the average of the cutting resistance, normalized to a baseline geometry.

As discussed in 2.1.2 and 2.1.2.1, there are three models used to describe how the cutting resistance varies with the theoretical, or equivalent, chip thickness. The model that is best adapted to the data obtained in this study is the *Woxén-Johansson* and thus this model is used to present the results below.

### 4.2.1 Face turning 316L result

Presented in *Figure 4.5* is the normalized cutting resistance as a function of the equivalent chip thickness. The figure compares the result obtained from machining 316L workpieces from two different suppliers while maintaining all parameters constant, only varying the feeds in steps. As can be seen in the figure, there are a number of plots presented, all obtained under slightly different conditions. All plots are based on the average forces over five seconds as soon as the forces have stabilized. The following plots, *316L Supplier A/B* are based on data obtained with the special inserts. As is presented in *Chapter 3.6.1.3*, these plots are based on the largest feed window. The plots named *316L Supplier A/B (recommended feeds)* are data based on the early tests with a recommended type of insert for the application in combination with operating within the recommended process window. This described in more detail in *Chapter 3.6.1*. The last plots, noted as *316L Supplier A/B (without*

*nose contact*) are, as the name suggest, plots based on the data from machining without engaging the nose of the insert. This data is based on the same levels of feed as for the previously described setups. More detail about this in *Chapter 3.6.1.2*.

The measured, and later normalized, cutting forces that these plots are based on are presented in *Appendix E* and *G* respectively. The difference between repetitions divided by the average between them are shown in *Table I.1* and *I.2*. This provides some information about the underlying precision of the data. In *Appendix J* a comparison between the different models are shown, including the normalized cutting forces.

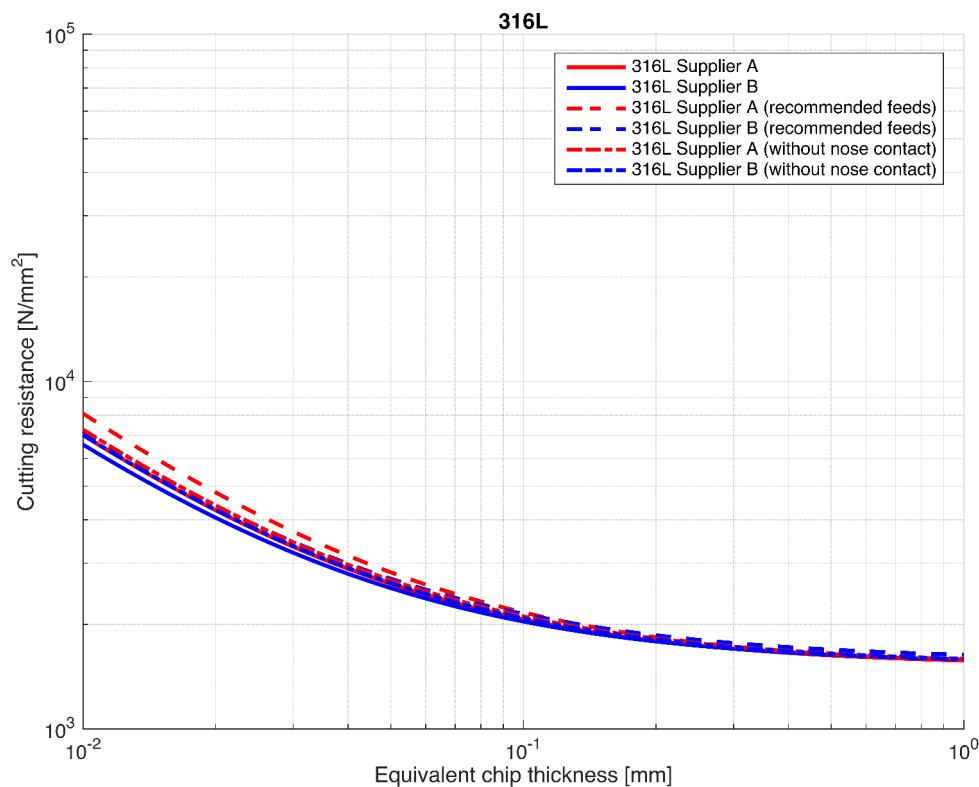


**Figure 4.5:** The cutting resistance for the 316L workpieces, according to the Woxén-Johansson model. Plotted for all machining scenarios against the equivalent chip thickness, in *Log-Log*.

By comparing the constants in presented in the *Table 4.5*, it can be observed that a pattern emerges. The constant  $Cr_1$  is generally slightly higher for *Supplier B*, meanwhile  $Cr_2$  is slightly lower. This coincides with the previous reasoning that the average force is measured while machining close to the surface of the workpiece. That the difference between the suppliers is less when machining without nose contact can to and extent be explained by the fact that the radial starting depth of the workpiece is varying in this setup and thus the effect of the gradient in microstructure is averaged out.

Condition	$Cr_1$ [N/mm <sup>2</sup> ]	$Cr_2$ [N/mm <sup>2</sup> ]
Supplier A rec. feed	1507,49	65,82
Supplier B rec. feed	1579,06	56,41
Supplier A w/o nose	1534,73	57,38
Supplier B w/o nose	1535,06	54,84
Supplier A	1518,42	54,89
Supplier B	1533,36	50,51

**Table 4.5:** Table containing the model parameters, according to the Woxén-Johansson model, for the cutting resistance of the 316L workpieces for all different experiments.

In *Figure 4.6* the plotted main cutting forces based on this cutting resistance is presented. Since this is based on the previous plot no significant difference is expected. All measured forces are presented in *Appendix E* and the normalized forces used as data for the plots are shown in *Appendix G*.

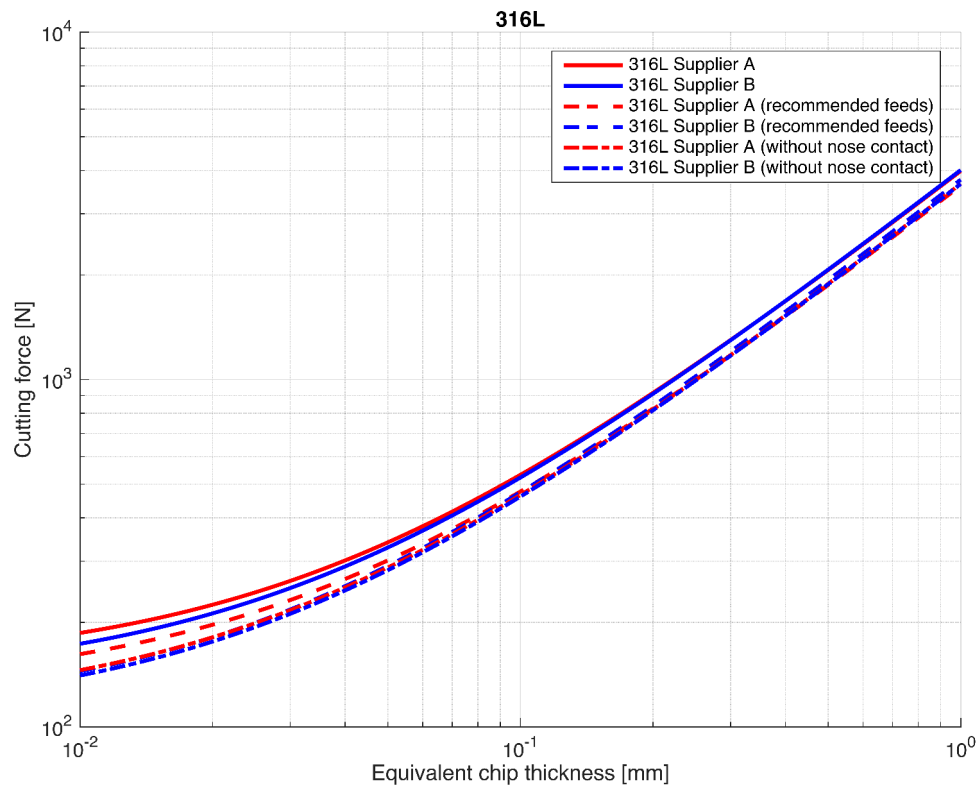


**Figure 4.6:** The main cutting force, according to the Woxén-Johansson model, for the 316L workpieces. Plotted for all machining scenarios against the equivalent chip thickness, in *Log-Log* (derived from the cutting resistance).

### 4.2.2 Face turning 100Cr6 result

As in the previous chapter, the normalized cutting resistance are plotted against their respective feed. This result is presented in *Figure 4.7*. In the case of the 100Cr6 workpieces, the three curves represents the respective force response for a certain hardening condition. The presented plots are based on the average between the normalized data between two out of the three inserts used as illustrated in *Figure 3.11*. The details behind the experimental procedure is *Chapter 3.6.2*. The reason for not including all three inserts is due to issues with heavy vibrations when machining 100Cr6 *Hardening 2*.

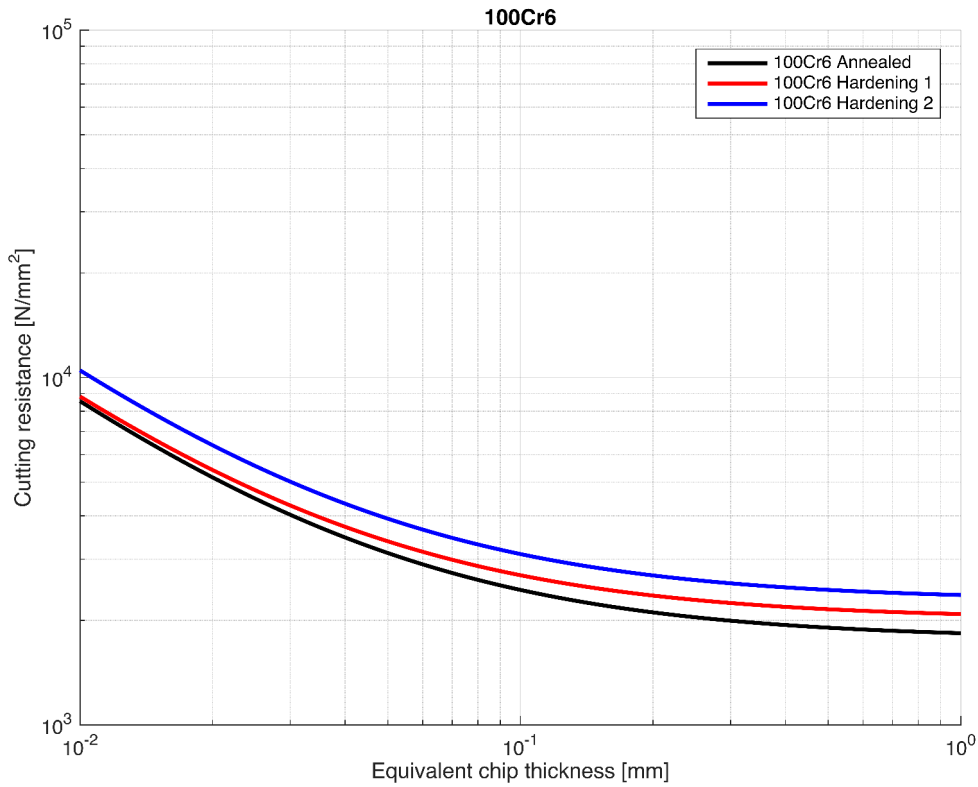


**Figure 4.7:** The cutting resistance for the 100Cr6 workpieces plotted against equivalent chip thickness, in *Log-Log*.

As can be interpreted from the plot, the cutting resistance increases with increased degree of hardening. In *Appendix K* a comparison between the different models are shown including the normalized cutting forces.

Condition	$Cr_1$	$Cr_2$
Annealed	1769,81	67,80
Hardening 1	2017,29	68,06
Hardening 2	2283,83	82,06

**Table 4.6:** Table containing the model parameters, according to the Woxén-Johansson model, for the cutting resistance of the 100Cr6 workpieces.

In figure *Figure 4.10* the plotted main cutting force based on this cutting resistance is presented. The same tendency as for the cutting resistance is shown where in this case the forces increase with degree of hardening. All measured forces are presented in *Appendix F* and the normalized forces used as data for the plots are shown in *Appendix H*.

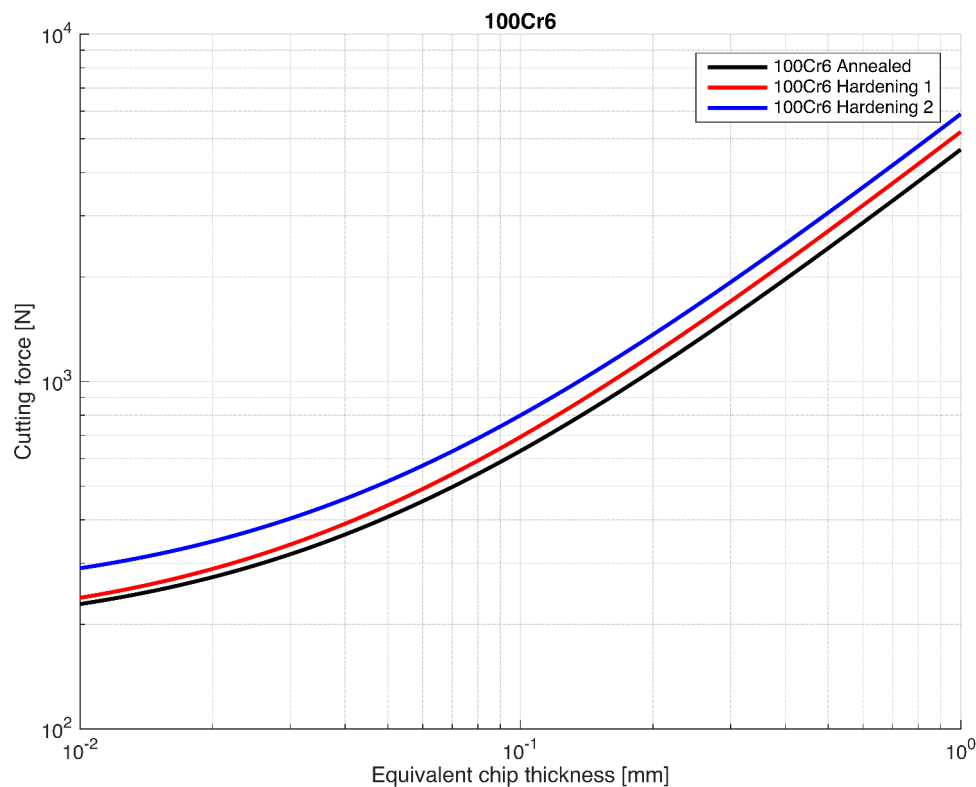


**Figure 4.8:** The main cutting force for the 100Cr6 workpieces plotted against equivalent chip thickness, in *Log-Log* (derived from the cutting resistance).

### 4.3 Verifying cutting resistance

As briefly explained in *Chapter 3.8*, complementary tests are carried out at Seco's facility in Fagersta with the intention of verifying the result obtained at Chalmers.

The normalized results for both plots of the cutting resistance obtained at Seco Tools facility are presented in *Figure 4.9*. A noticeable difference can be observed when comparing these plots with those obtained at Chalmers, *Figure 4.7*. This is clear when looking at the relative difference between the constants of the model. The difference is presented in *Figure 4.8*. It is important to keep in mind when studying the result that the data behind the plots is obtained with a very different method. The most significant differences is as explained in *Chapter 3.8.1* that no cutting fluid is used and that the mode of turning is changed to longitudinal. A further remark is that all feed steps are covered in one cut leading to that potential tool wear from a previous feed level is carried over to the following ones. However no analysis of the effect of this is attempted.

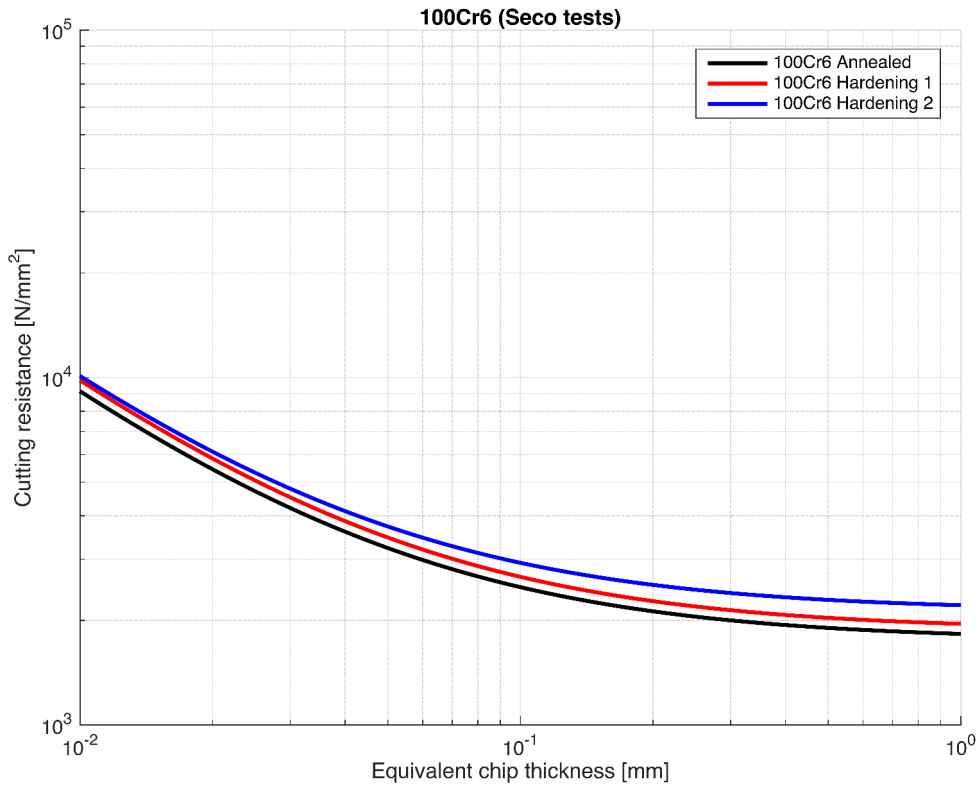


**Figure 4.9:** The cutting resistance of the 100Cr6 workpieces obtained at Seco’s facility plotted against equivalent chip thickness, in *Log-Log*.

Condition	$Cr_1$	$Cr_2$
Annealed	1754,84	73,80
Hardening 1	1875,03	79,45
Hardening 2	2131,95	79,75

**Table 4.7:** Table containing the model parameters for the cutting resistance of the 100Cr6 workpieces obtained at Seco’s facility.

Comparison with Chalmers	$Cr_1$	$Cr_2$
Relative difference	%	%
Annealed	-0,85	8,84
Hardening 1	-7,05	16,73
Hardening 2	-6,65	-2,81

**Table 4.8:** Table containing a comparison for the model parameters between those obtained at Chalmers and at Seco.

In figure *Figure 4.10* the plotted main cutting force based on this cutting resistance is presented. Since the cutting resistance is shown to be lower based on data measured at Seco's facility the plotted main cutting force is consequently also lower in comparison.

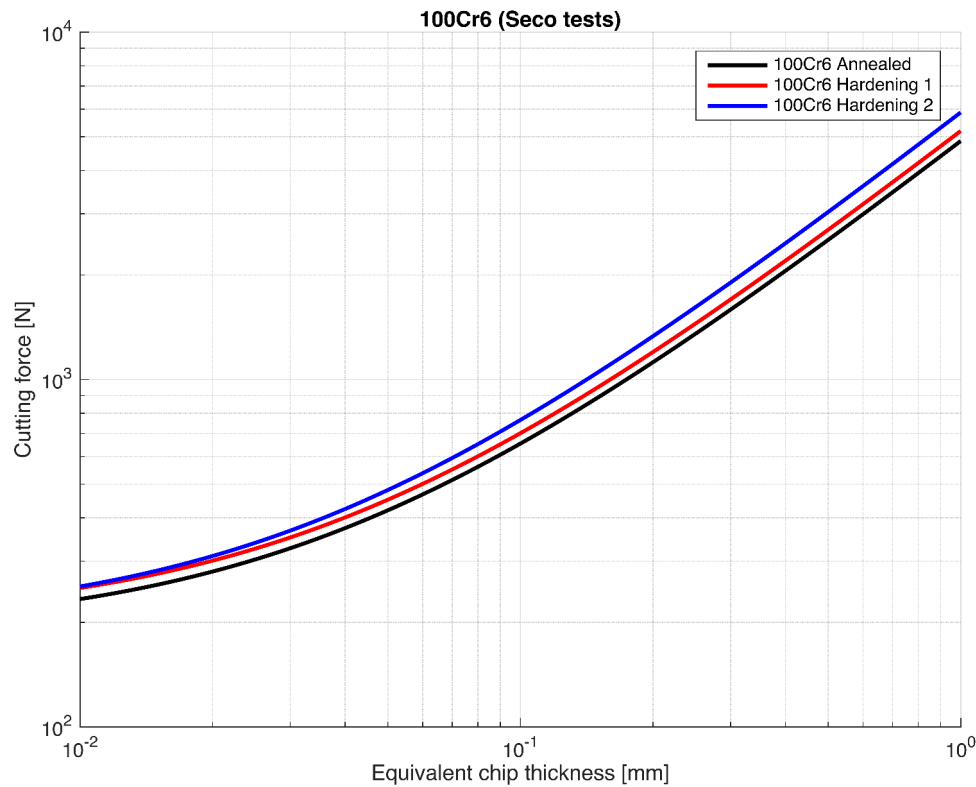


**Figure 4.10:** The main cutting force plotted against equivalent chip thickness, in *Log-Log*. Based on data from measured at Seco's facility.

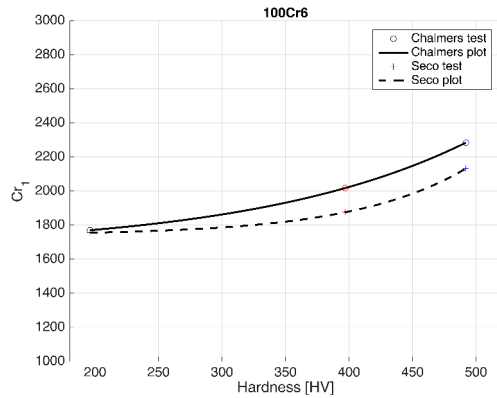
#### 4.4 Empirical relations between material properties and cutting resistance

The result of this study suggest that there indeed appears to be a connection mainly between the constant  $Cr_1$  and the hardness, the tensile and yield strength, as well as the elongation at rupture. This is at least shown to be valid for 100Cr6. In *Figure 4.11a* to *4.11d* these empirical relations are shown. Since the hardness, the yield strength as well as the tensile strength are properties that are obtained through the application of a mechanical load, there is an expected empirical relation in between these as well. As presented in [6, pp. 37-38] there is a relatively strong relationship between hardness and tensile strength and although this depends on material. It is explained to be predictable for plain carbon and low-alloy steels. Based on this already commonly known relation it is not unexpected that a similar relation is

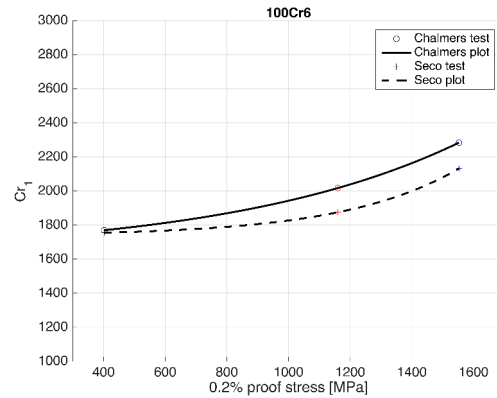
## 4. Results

presented here as well.

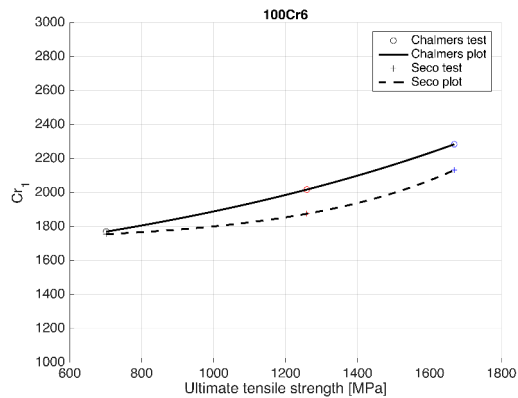
The main issue with this result is that only three data points exist, meaning that no information exists about what happens in between. It is certainly possible that there for example is no increase with say hardness and  $Cr_1$  up until a certain threshold.



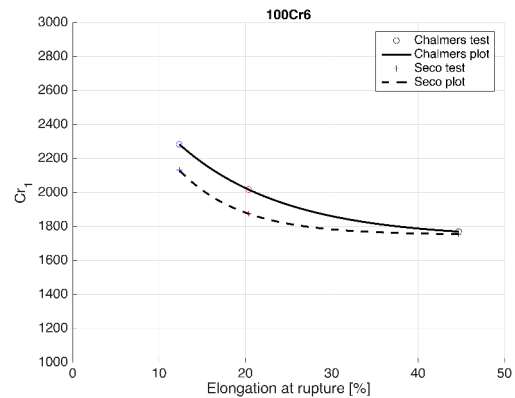
(a)  $Cr_1$  vs Vickers hardness



(b)  $Cr_1$  vs Yield strength



(c)  $Cr_1$  vs Tensile strength



(d)  $Cr_1$  vs Elongation at rupture

**Figure 4.11:** The empirical relations between selected mechanical properties and  $Cr_1$  for 100Cr6.

Comparing the result from the experiments at Chalmers to those obtained at Seco Tools, a difference can be observed. Since the result for cutting resistance is generally lower for the tests carried out at Seco Tools, the same thing is observed here. Although a difference in value, they present more or less the same trend for both setups. This speaks for the fact that even though the process is playing a role here, the relationship connected to the material properties appears to carry over.

All empirical relations in *Figure 4.11* appear to fit a simple exponential function,  $y = a + b \cdot e^{-cx}$ . Expressing this in more familiar terms it yields the following equation.

$$Cr_1 = a + b \cdot e^{-cX} \quad (4.1)$$

Where  $X$  represents the material property in question. The constants for each relationship is presented below in *Table 4.9*.

Constant	a	b	c
Hardness [HV]	1660	34,84	-0,00586
Yield strength [MPa]	1626	84,27	-0,00132
Tensile strength [MPa]	1328	252,2	-0,00080
Elongation at rupture [%]	1731	1522	0,08196

**Table 4.9:** Table containing the constants for the empirical relations shown for 100Cr6.

Studying instead the relation between the  $Cr_2$  constant and the material properties it is evident that for this case the relation is more unstable. Furthermore, since the relationship changes significantly between experiments at Chalmers compared to those at Seco Tools it is evident that this is more dependant on the process rather than the material properties themselves. The constant  $Cr_2$  plotted against each relevant material property is shown in *Figure 4.12*.

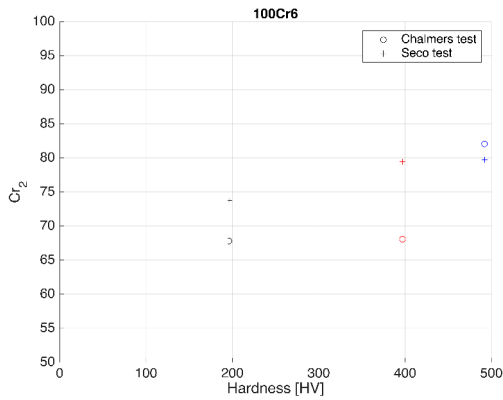
## 4.5 Approximating cutting resistance

### 4.5.1 Approximation of $Cr_1$ for 100Cr6 based on a previous model

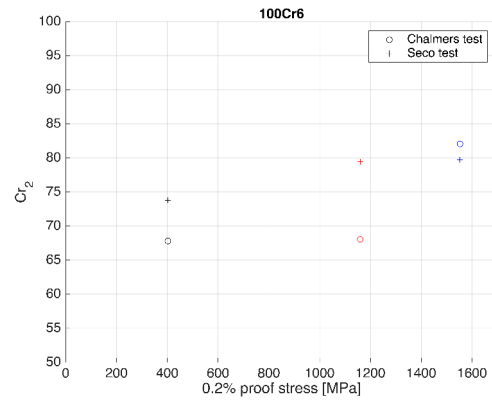
By approximating the constant  $Cr_1$  for 100Cr6 based on the method described in *Chapter 3.8.2.1* further analysis can be made. This model accounts for the hardness, the yield strength, the elongation at rupture, and the thermal conductivity of the material. The first three properties are determined during the course of this study, however the thermal conductivity is obtained from [9]. Based on the assumption that the thermal conductivity does not change with hardening. The following table, *Table 4.10* contains all the inputs in the model for each degree of hardening.

With these parameters as input, together with the constants presented in *Table 3.7*, into *Equation 2.10* generates the result presented in *Table 4.11*.

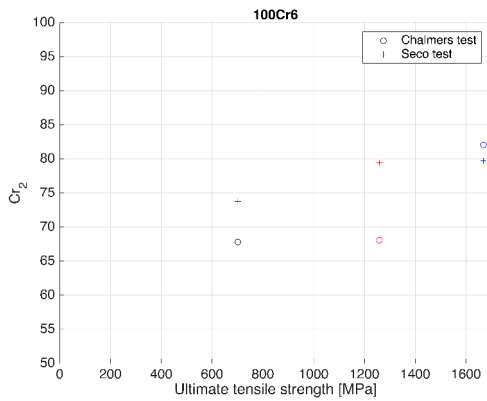
## 4. Results



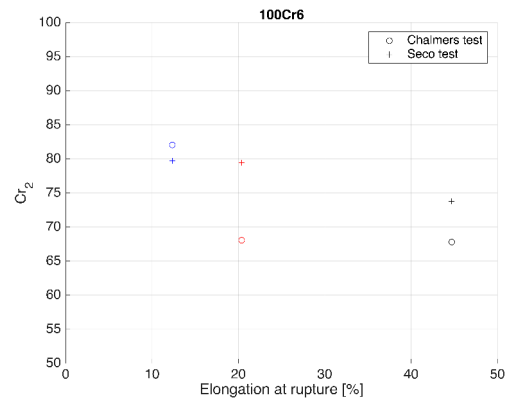
(a)  $Cr_2$  vs Vickers hardness



(b)  $Cr_2$  vs Yield strength



(c)  $Cr_2$  vs Tensile strength



(d)  $Cr_2$  vs Elongation at rupture

**Figure 4.12:** The empirical relations between selected mechanical properties and  $Cr_2$  for 100Cr6, no curve fitting is attempted.

Property	Annealed	Hardening 1	Hardening 2
Hardness [ $HV$ ]:	196	397	492
Yield strength ( $R_{p0,2\%}$ ) [ $MPa$ ]:	402,14	1159,73	1552,60
Elongation at rupture [%]:	44,70	20,37	12,35
Thermal conductivity [ $W/m^{\circ}K$ ]:	40-45	40-45	40-45

**Table 4.10:** Table containing the model parameters of 100Cr6 for the approximation of the cutting resistance.

When instead comparing the cutting resistance calculated from data measured at Seco's facility in Fagersta the error becomes smaller, as shown in *Table 4.12*. Potential reason for this is as discussed in *Chapter 5.3.1.1* that there is no cutting fluid used for those experiments. This may have an effect that is not accounted for.

Condition	$Cr_1$ Approximated	$Cr_1$ Experimental	Error %
Annealed:	1617,20	1769,81	8,62
Hardening 1:	1894,24	2017,29	6,10
Hardening 2:	2008,87	2283,83	12,04

**Table 4.11:** Table containing the result of the approximation. The error is the comparison with the result obtained at Chalmers.

Condition	$Cr_1$ Approximated	$Cr_1$ Experimental	Error %
Annealed:	1617,20	1754,84	7,84
Hardening 1:	1894,24	1875,03	1,02
Hardening 2:	2008,87	2131,95	5,77

**Table 4.12:** Table containing the result of the approximation based on experiments at Seco's facility.

#### 4.5.2 Approximation of $Cr_1$ for 316L with constants based on the relation with hardness obtained from 100Cr6

Since this study has well documented data for 316L from the ISO-M group an attempt is made to approximate its cutting resistance based on the empirical relation between Vickers hardness and  $Cr_1$  determined for 100Cr6. When using the following data as input, presented in *Chapter 3.8.2.2*, it yields the following parameters as input for *Equation 4.1*.

- Vickers hardness  $\simeq 190[HV]$
- $a = 1660$
- $b = 34,84$
- $c = -0,00586$

Based on this, the approximated value for  $Cr_1$  is  $1759,88[N/mm^2]$ . Comparing this to the measured value for 316L *Supplier A* by *Equation 3.2* it yields an error of 15,90%. This is a relatively large error, however comparing this to the errors obtained when approximating based on the previous model presented in *Table 4.11* it is not extreme by comparison. However, it should be considered that this rough approximation is based on an empirical relation derived from a significantly different material using only the hardness. Whereas, the other method for approximation, see *Chapter 4.5.1*, needs information about the yield strength, the elongation at rupture, as well as the thermal conductivity in addition to the hardness.



# 5

## Discussion

### 5.1 Quality of the data

Almost the entire study is based on first hand experimental data that has been generated during the course of this master's thesis. The main reason behind this is the premise that the study should be based on materials from the same batch in order to limit variations that could be introduced in different batches.

Due to limited resources some experimental data from the material characterization may not be perfectly representative of the entire workpieces. This is due to the metallographic samples being extracted from only one cross section of each bar. This yields no information about changes in the material along the longitude of the bar. However, no significant variation is expected to occur. In order to have some statistical relevancy more samples should be extracted and analyzed.

The tensile testing is carried out at Seco Tool's facility and since the method is not done strictly according to a standard, the quality of this can be discussed. When comparing the obtained data to presented data from different suppliers of 100Cr6 the (for this study) important values appears reasonable. However, the values for the Young's modulus are off. This can visually be appreciated in *Appendix D, Figure D.1 to D.3*, paying attention to the scale on the strain axis. The value of the Young's modulus for 100Cr6 should be about  $210\text{GPa}$ , [9], and independent of hardening. The reason behind the variation in this set of data can primarily be that the plot in *Figure D.1, 100Cr6 Annealed*, has no distinct yield point. Furthermore the plot in *Figure D.2* intersects the stress axis, possibly due to issues when zeroing the extensometer. Although, this is of less interest for the study since the values accounted for are the yield and tensile strength together with the elongation at rupture, where the latter may be slightly affected by this.

Some issues are discovered that may slightly compromise parts of the data. One of these emerges when analyzing the inclusions of mainly the 100Cr6 material. The values obtained through image analysis are slightly higher than the real values. This is discussed further in *Chapter 4.1.2.1* and the reason behind this is issues with contamination on the sample surface, as is verified. Since the inclusions are not shown to play a significant role at such low volume fractions this is not further analyzed. There is also a small issue related to the machining, as is briefly commented on in *Chapter 4.2*. This issue is related to the cutting fluid where during machining

the oil content in the emulsion drops as low as to 1wt%, probably due to the oil degradation and filter contamination. This may affect the tribology of the process and thus negatively influence the data by introducing another variation. However, since the repetitions that are done shows that this has no detectable effect on the force measurements this issue is disregarded.

### 5.1.1 Force measurements

To comment briefly on the quality of data presented in *Chapter 4.2* it can be stated that the measurements of the average forces are very stable. Even when relatively heavy vibrations occurs during machining of the hardened workpieces the scatter of average forces are very small. Specifically one insert, *Insert 3*, shows to be more prone to vibrating and due to this it is not used to machine 100Cr6 in the hardest condition.

One further remark is the hypothesis presented in *Chapter 3.6.2* where the edge reinforcements of some of the inserts are discussed. Due to the value of the length of the reinforcements being larger than the feed, the hypothesis is that the angles of the edge reinforcements would effectively be the rake angle of the insert. The final rake angle will also be affected by the angle of the tool holder. For *Insert 1* and *Insert 2* the length of the reinforcements is less than the the value of the maximum feed. By the same logic this would result in the chip thickness exceeding the edge reinforcement and thus entering the actual rake face of the insert. Since the force for highest level of feed for both inserts appears to be slightly off the predicted value, it further strengthens this hypothesis.

The plotted normalized cutting resistance for 316L provides a good testimony to the accuracy of this reasoning. When studying the plots presented in *Figure 4.5* the data for *316L Supplier A/B* and *316L Supplier A/B (recommended feeds)*, it is clear that these fall more or less on top of each other. These plots represent the normalized data as discussed below in *Chapter 5.1.2*. Since the plots representing *316L Supplier A/B*, generated by using the inserts with edge reinforcements, fall very close to the plots based on inserts without edge reinforcements it suggests that this hypothesis is probably plausible.

### 5.1.2 Force normalization

Before normalization, the values of the measured forces show a noteworthy difference between insert types. This is expected and the reason behind this is touched upon in *Chapter 2.3*. By transforming the forces to a common reference plane, the impact of the angular differences between the inserts are minimized. Since the normalized forces becomes much more similar between inserts it is suggested that this normalization is carried out correctly. The residual difference that still exists can be due to factors that the normalization does not account for. In addition to this,

the geometry of the inserts are complex meaning that the rake angles may vary for some inserts along the depth of cut. This is believed to introduce a variation since only one value for the rake angles are accounted for. However, the influence of this is minimized by using several inserts together with using the average normalized value.

The data before and after normalization can be compared by studying *Appendix F* and *H*. Here it is clear that the forces become more even between inserts, especially between *Insert 1* and *Insert 2* which are used to create the plots for the cutting resistance of 100Cr6.

This activity can however be avoided, or greatly simplified, if orthogonal cutting is used in the first place. A simpler normalization is still needed to account for differences in rake angle, although not angles such as inclination angle and/or cutting edge angle.

Orthogonal cutting was initially intended to be used for this study, however the tool holder that ended up being used has an inclination angle. The data becomes processed one extra step by accounting for this, although since the normalization is considered to work as intended this is not deemed a significant issue for the result. All experiments were initially planned to be conducted by machining without the nose of the insert in engagement, as described in *Chapter 3.6.1.2*. Even though not being orthogonal due to the inclination angle this would have eliminated the need of using the *equivalent chip thickness* to calculate the thickness of the chip. This may introduce a slight inaccuracy, although since the depth of cut is large compared to the nose radius this inaccuracy should be relatively small. The reason behind not performing all experiments without the nose engaged is due to problems when machining the grooves necessary for this. Since the tool used to cut the grooves is weak and the machine being prone to vibrate it was decided not perform this operation at all on the 100Cr6 workpieces. Furthermore, the experiments on the 316L workpieces show that the values obtained through using the equivalent chip thickness are more or less indistinguishable to those obtained through machining without the nose.

One remark that is expected to be the reason behind the slight deviation when machining without the nose engaged, is the variation in radial depth where the average forces are obtained. As is mentioned previously, the average is captured at the first five seconds where the forces are stable. In the case of machining without the nose engaged the radial starting depth is varied for practical reasons. This means that the average forces are captured at a varying level of radial depth in the workpiece. That this can alter the result is reinforced by the apparent variation in microstructure and mechanical properties with radial depth as presented in *Chapter 4.1.1*.

## 5.2 Verification

The result for the complementary experiments carried out at Seco's facility presented in *Chapter 4.3* show a not insignificant difference. When comparing the relative difference in *Table 4.8* it is shown that the  $Cr_1$  becomes lower for all workpieces. This constant is as explained in *Chapter 2.1.2* more connected to the energy consumption at the rake face and thus more linked to material dependency. One possible explanation as to why this constant is slightly lower for these experiments could be that the temperature of the process would be higher due to absence of a cutting fluid as coolant. This would need further investigation to determine whether or not this is a reasonable explanation. There are numerous other potential factors that may also be the reason behind this or at least contribute to the difference.

The constant  $Cr_2$  is however larger for these experiments. This constant is more linked to the clearance face and is thus dependant on the contact between insert and workpiece. The same coating is used for these inserts as well as all other test. Due to this it is reasonable to believe that the potentially increased tool wear inherent to the method being used in this case could play a role here. Mainly by the fact that all feeds are covered in one longitudinal cut resulting in the tool being engaged for longer time as well as carrying over any potential wear to the next feed level. Even though the last levels of feeds are not included for the model, clear signs of plastic deformation could be observed for those. Based on this it is not unreasonable to believe that the previous levels may have pushed these inserts far enough to have an impact on the tribology of the process.

## 5.3 Modeling cutting resistance

This study includes, to a degree, some evaluation of the established models describing the cutting resistance. A comparison between the three models on the plotted cutting resistance is presented in *Appendix J* and *Appendix K*. Generally the model error is determined to be smaller for the *Hägglund* model, also referred to as *Woxén-Johansson extended* model. However, due to issues related to the increased degree of freedom introduced by the third constant in combination with the narrow window of feed for the hardened 100Cr6 cutting resistance plots, no good fit is found in these cases. In a case where a wider window of feed could have been used this model would probably have been more preferable. Since the more conventional *Woxén-Johansson* model is easier to approximate with a narrower span of feed this model is selected as a basis for approximation in this study.

### 5.3.1 Approximation of the main cutting force

There are some problems when attempting to approximate the cutting resistance based on material properties. A problem that is fundamentally difficult to overcome is the fact that the cutting resistance is not only dependant on solely the material properties. This is touched upon mainly in *Chapter 4.4* where the process dependency of the constant  $Cr_2$  in the Woxén-Johansson model is presented. Due to the difficulty to predict this part of the cutting resistance model it is inherently difficult to accurately estimate the cutting resistance as a whole. However, this constant is more dominant for small theoretical chip thicknesses and thus becomes less significant for greater feeds.

The question arose whether or not the relation between  $Cr_1$  with yield or tensile strength is better to use as a variable in approximation. It can be argued that the tensile strength is better since some materials having an indistinct yield point making it difficult to define. However, no conclusions are made about this and it should be noted that only yield strength is considered in the previous study discussed.

#### 5.3.1.1 Approximation based on existing model

The method of approximating the forces based on material properties as is presented in *Chapter 2.8* is previously shown to be applicable to a varying degree of accuracy over a large array of materials.

When using the data obtained during this study, with the exception of thermal conductivity, it yields an error that varies with the degree of hardening for 100Cr6. The smallest general error is obtained when comparing the approximated  $Cr_1$  with the measured for 100Cr6 obtained at Seco, with the error for *Hardening 1* being very small.

#### 5.3.1.2 Approximation based on only the Vickers Hardness

An attempt is made to approximate the cutting resistance for 316L based on the empirical relation between  $Cr_1$  and the Vickers hardness shown for 100Cr6. The approximation is compared to the calculated values for *316L Supplier A* presented in *Table 4.5* which is based on exactly the same type of inserts as those used for 100Cr6. The result of this is presented in *Chapter 4.5.2* and the error is relatively large, 15,90%. This is too large to be useful, however it shows the difficulty of approximating the cutting resistance across ISO groups.



# 6

## Conclusion

In this chapter the conclusions of the study are presented. In addition to this some recommendations for further work are suggested.

The study shows that it appears feasible to approximate  $Cr_1$  as a function of mainly hardness or yield/tensile strength. This is shown for 100Cr6 within the selected hardness interval and within the range of cutting data used in the study. However,  $Cr_2$  is shown to be more difficult to predict and, based on these results, exhibits a more volatile behaviour. This parameter is to some degree affected by the material's condition. When only introducing a variation in material properties, while maintaining constant process parameters, the behaviour of this constant appears predictable. However, the tests at Seco Tools in Fagersta show that other aspects of the cutting process have a much stronger impact on this. Due to this no conclusions can be made about this constant other than stating that it is more difficult to predict.

When only varying the degree of hardness for an ISO-P material from the same batch, the cutting resistance is undoubtedly affected significantly. In the case of ISO-M, and specifically 316L from two suppliers, it can be concluded that there exists physical differences between the the workpiece materials. The material characterization show distinct diversity in microstructure and mechanical properties. As suspected, the differences in material properties results in a slight difference in cutting resistance and subsequently the cutting forces. However, since the differences are relatively small this result is not sufficient to draw any real conclusions about relationships with material properties here. Although the differences in mainly the hardness appears to coincide with the theory that cutting resistance, to a degree, scales with hardness. The variation in cutting resistance and thus the cutting forces are shown here to be negligible. However, this may not always be the case, especially not if the production method varies significantly.

Certain inclusions are explained in the literature to have an effect on the cutting resistance, mainly through lubrication, as explained in *Chapter 2.6*. For this study all materials consists of a relatively low volume fraction of inclusions. Furthermore, this is only relevant for the 316L in this case since these workpieces in between themselves contains a varying amount. A significant difference is shown, as presented in *Table 4.4*, although since this parameter is not isolated, no conclusions can be drawn whether or not this has a measurable effect on the cutting resistance.

The significance of tool geometry is clearly shown in this study. The importance of comparing tests to a baseline geometry is stressed. Thus, if a approximation of the cutting resistance is made for a baseline geometry, it is vital to transform this resistance for the tool geometry being used in order to minimize the error. With an accurate representation of the theoretical chip thickness the forces can be more accurately estimated.

### 6.1 Conclusions for the initial research questions

Connecting back to *Chapter 1.4, Specification of issue under investigation.*

- How is the cutting resistance and consequently the cutting force connected to the selected material properties?
- Can the cutting resistance and thereby the cutting force be approximated based on material properties?
- Which material properties have sufficient impact on cutting resistance to be considered in the approximation?
- Which established model for should be used as the base for approximation?

To answer for the main research questions it can be stated that, at least for 100Cr6, there exists empirical relations between the cutting resistance and selected material properties. These empirical relations are presented between the following mechanical properties and the constant  $Cr_1$ . Consequently these are also connected to the cutting resistance itself,  $Cr$ .

- Vickers hardness,  $[HV]$
- Yield strength,  $[MPa]$
- Tensile strength,  $[MPa]$
- Elongation at rupture,  $[\%]$

This is not surprising since most of these properties in between themselves are, to a varying degree, empirically related to begin with. Note that these relationships may not be valid outside the hardness interval studied and outside selected cutting data. The fact that elongation at rupture appears inversely connected to the cutting resistance is likely a consequence following the increased degree of hardening for the material. To observe the effect of this parameter it would be necessary to isolate it possibly by studying two materials with similar hardness and strength but different elongations at rupture.

When attempting to approximate the cutting resistance of 316L based on the empirical relation found for 100Cr6 between simply the Vickers hardness and  $Cr_1$  the error is relatively large. This shows that there are more factors at play and that this approach may not be valid generally, at least not without some factor of compensation that would need to be investigated.

It is not concluded which model for cutting resistance that *should* be used. However, the model that is selected as a basis for the approximation for this study is the *Woxén Johansson* model, *Equation 2.6*. This model is selected due to its simplicity as well as it being a more established model. Furthermore, it is shown to be relatively accurate based on the result in this study. However, it is not concluded whether this is the model most suitable as a basis for approximation.

## 6.2 Emerging questions

Some questions have emerged during the course of this study. The main question would be what happens in between the data points for the empirical relations presented in *Figure 4.11*. Is it for example possible that there exists some kind of threshold where up until that point the cutting resistance is constant? How can the phases that are present play a role in this relationship?

The question arose about what is causing the cutting resistance to be lower for tests at Seco Tools facility, as shown in *Constants relative difference*. There occurred significant vibrations while performing cutting test at Chalmers but to a much lesser extent at the Seco Tools facility. This might be the major cause of the lower cutting resistance at Seco Tools. Other causes might be the effect of not using cutting fluid or it could be related to the structure in the material since the mode of turning was longitudinal at Seco Tools? This would be under the assumption that there is anisotropy in the material.

## 6.3 Further studies

Presented in the following list are some aspects that could be relevant to study further.

- The empirical relation between hardness and tensile strength with  $Cr_1$  should be evaluated for a greater span of hardnesses and materials as well as for a greater window of theoretical chip thicknesses.
- The feasibility of this approach could be evaluated for more materials within ISO-P as well for other material groups.
- Evaluation of the different models for cutting resistance, the Woxén-Johansson model is not necessarily the best, which this study have shown.

## 6. Conclusion

---

The fundamental limitation of this work is the amount of materials being studied. The difference in material properties between the 316L workpieces from the ISO-M group are not significant enough to be used in order to show a relationship. This means that no real conclusions can be drawn about the connection between certain material properties with the cutting resistance within this group. Hence, to be able to draw any conclusions for the ISO-M materials more work should be put into this group, specifically by studying more dissimilar workpieces.

# Bibliography

- [1] E M. Trent and P K. Wright, *Metal Cutting*. 4th ed, Oxford, United Kingdom: Butterworth-Heinemann, 2000.
- [2] J-E. Ståhl, *Metal Cutting: Theories and models*, Lund, Sweden: LTH, Lunds universitet, 2012.
- [3] M. Linde, S. Hägglund, F. Schultheiss. V. Bushlya, J-E. Ståhl, "Machinability analysis of ISO-grouped workpiece material - With focus on cutting force modeling," Lund University, Lund, Sweden, 2016.
- [4] S. Hägglund, "Methods and Models for Cutting Data Optimization," Ph.D. dissertation, Materials and Manufacturing Technology, Chalmers University of Technology, Gothenburg, Sweden, 2013.
- [5] F. Klocke, *Manufacturing Processes 1: Cutting*. RWTH ed, New York City, United States: Springer, 2011.
- [6] J T. Black, R A. Kohser, *Degarmo's Materials and Processes in Manufacturing*. 12th ed, 2007.
- [7] N. Ånmark, A. Karasev, P-G. Jönsson "The Effect of Different Non-Metallic Inclusions on the Machinability of Steels," Department of Materials Science and Engineering, KTH Royal Institute of Technology, Stockholm, Sweden, 2015.
- [8] Sandvik Coromant, "Workpiece materials," [Online]. Available: <https://www.sandvik.coromant.com/sv-se/knowledge/materials/pages/workpiece-materials.aspx>, Accessed on: Feb 01, 2019.
- [9] Ovako, "100Cr6," 2019. [Online]. Available: <https://steelnavigator.ovako.com/steel-grades/100cr6/>, Accessed on: Feb 04, 2019.
- [10] Lenntech, "Stainless Steel 316L," [Online]. Available: <https://www.lenntech.com/stainless-steel-316l.htm>, Accessed on: Feb 04, 2019.
- [11] F. Schultheiss, V. Bushlya, J. Zhou, J.E. Ståhl, "Influence of the workpiece material properties on the cutting forces," Lund University, Lund, Sweden, 2014.



# A

## Microstructure 316L

In this appendix four images extracted from the grain size study is presented. This shows the distinct visual differences between the 316L workpiece materials at two different radial depths. The dark spots on the surface of all images are believed to be the manganese sulfide reacting with the etchant. Note that the samples are etched relatively heavy in order to make the grain boundaries more visible. For the purpose of studying the grain size the samples are etched even further that those presented below.

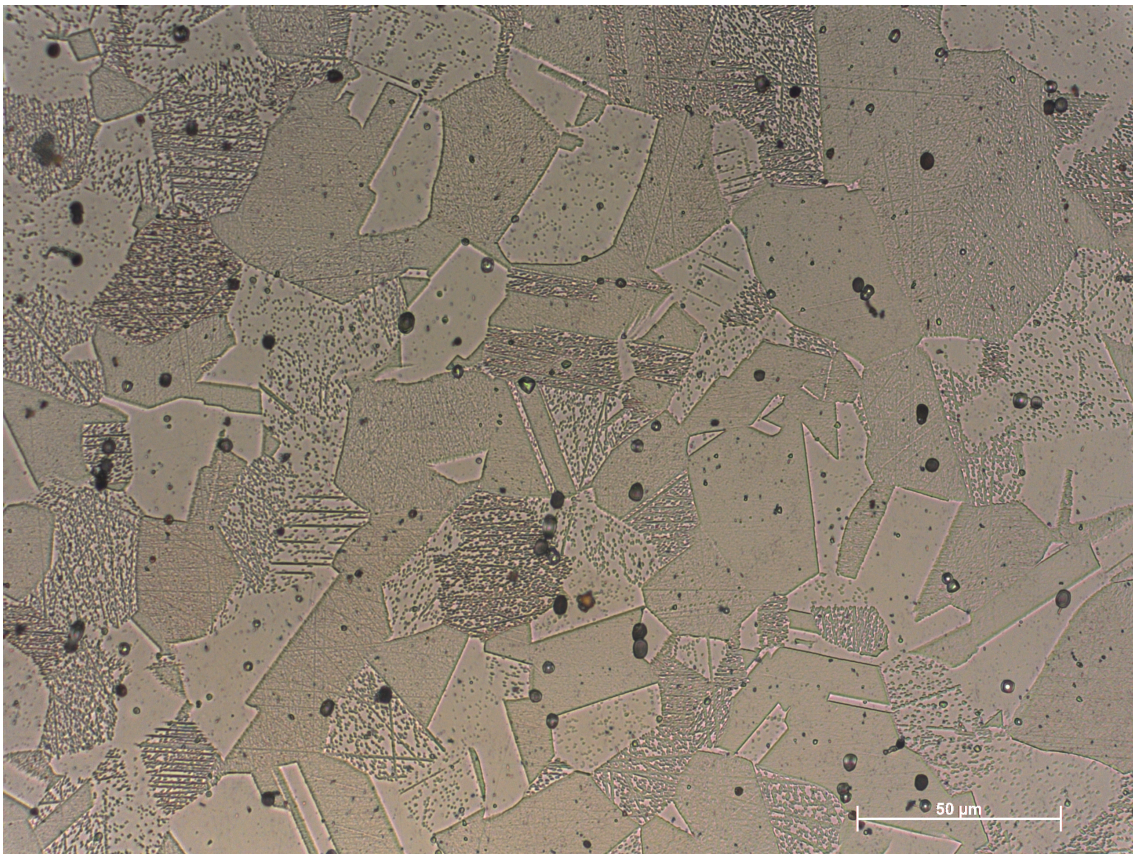


**Figure A.1:** Microscopy image showing microstructure of a 316L sample from *Supplier A*, captured on *Sample 1* from a random spot within the radial depth of 0,0 – 3,5mm.

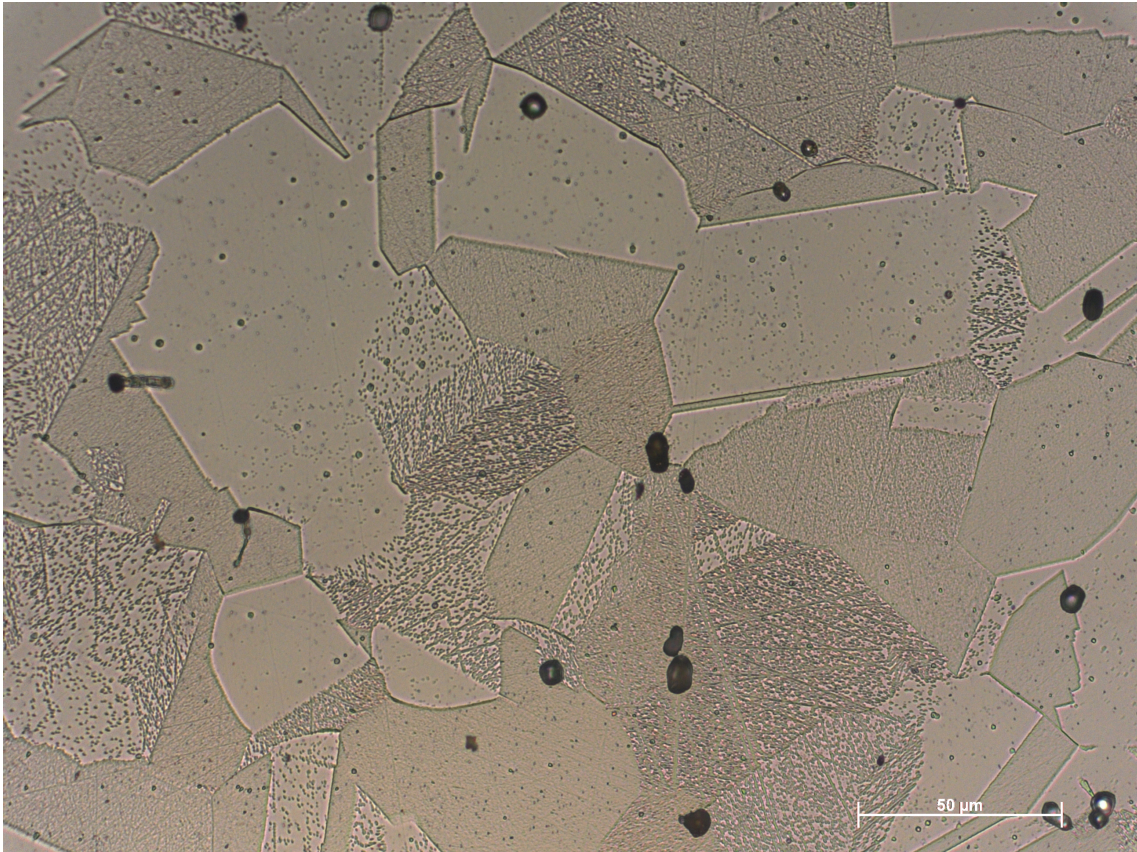


**Figure A.2:** Microscopy image showing microstructure of a 316L sample from *Supplier A*, captured on *Sample 2* from a random spot within the radial depth of 16,0 – 19,5mm.

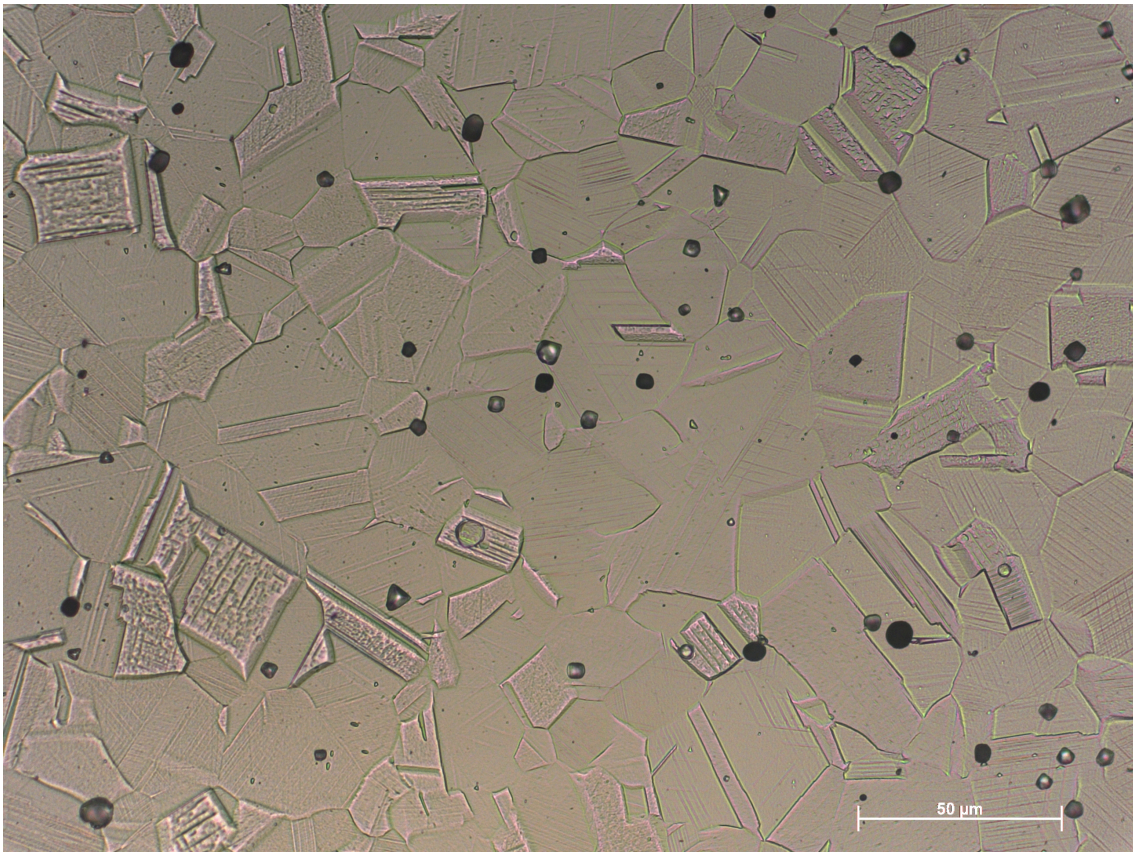


**Figure A.3:** Microscopy image showing microstructure of a 316L sample from *Supplier B*, captured on *Sample 1* from a random spot within the radial depth of  $0,0 - 3,5\text{mm}$ .



**Figure A.4:** Microscopy image showing microstructure of a 316L sample from *Supplier B*, captured on *Sample 2* from a random spot within the radial depth of 16,0 – 19,5mm.

# B

## Microstructure 100Cr6

This appendix contains examples of the microscopy images for the 100Cr6 samples in the three conditions. The presented images are captured at approximately the same position on the samples, near the center.

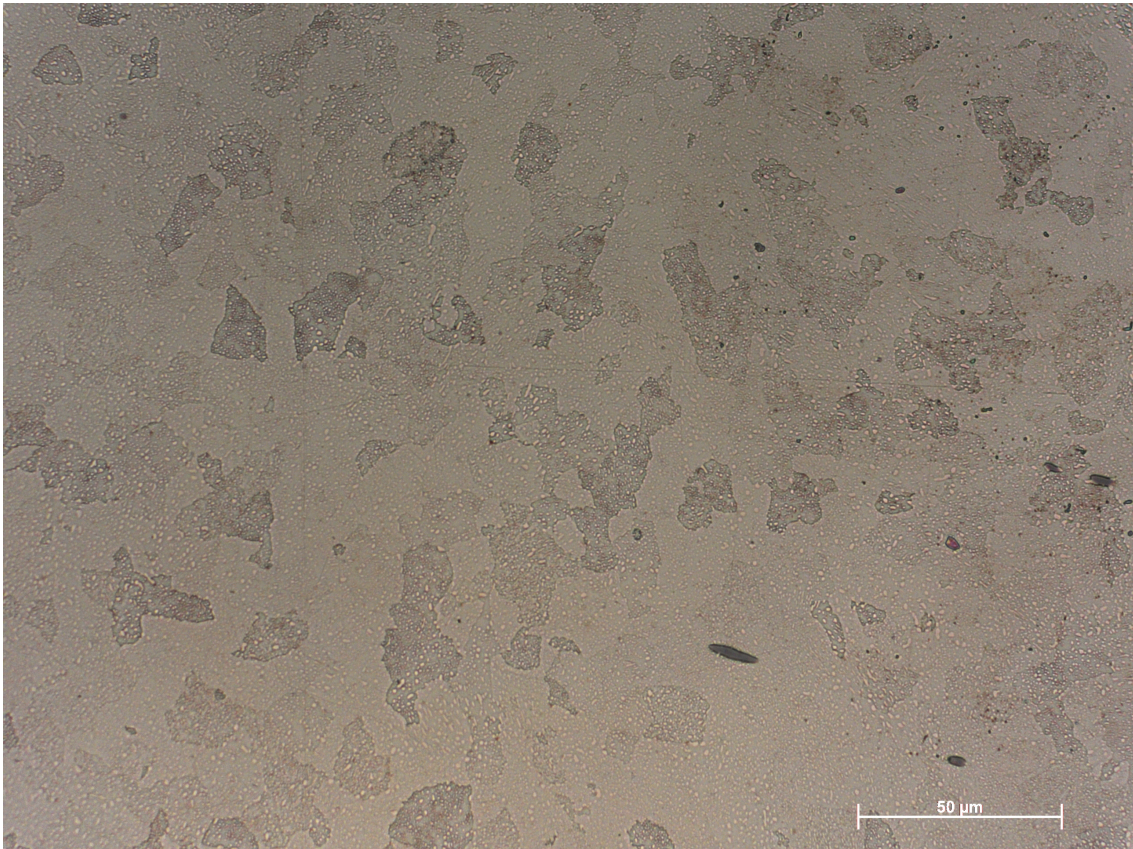


**Figure B.1:** Microstructure of 100Cr6 in *Annealed* condition.



**Figure B.2:** Microstructure of 100Cr6 in *Hardening 1* condition.



**Figure B.3:** Microstructure of 100Cr6 in *Hardening 2* condition.



# C

## Inclusion analysis

This appendix contains a pair of example images from the inclusion study that is performed on images from the ESEM. The presented images are from 316L, *Supplier B*, and from 100Cr6 *Annealed*.

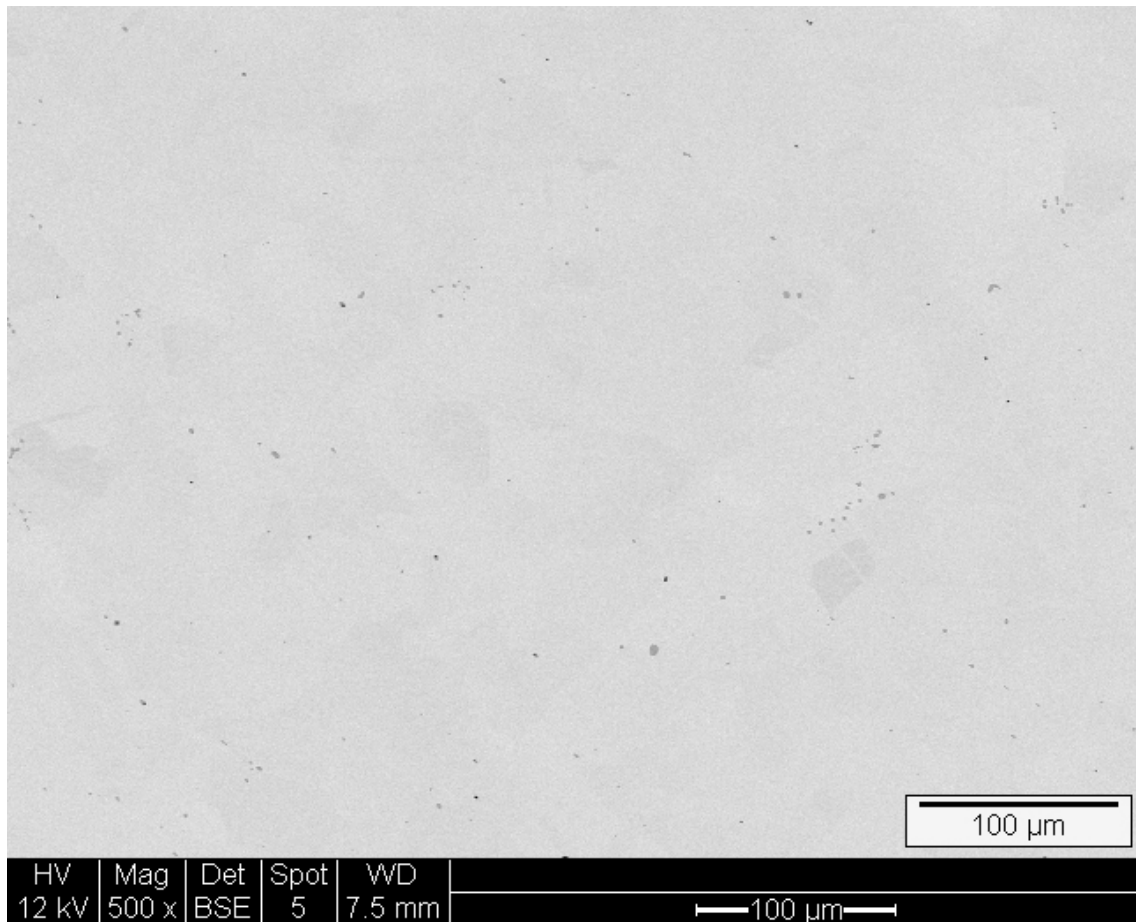


**Figure C.1:** Example image showing inclusions on a 316L sample from *Supplier B*. Captured on *Sample 2*, closer to the center of the workpiece.

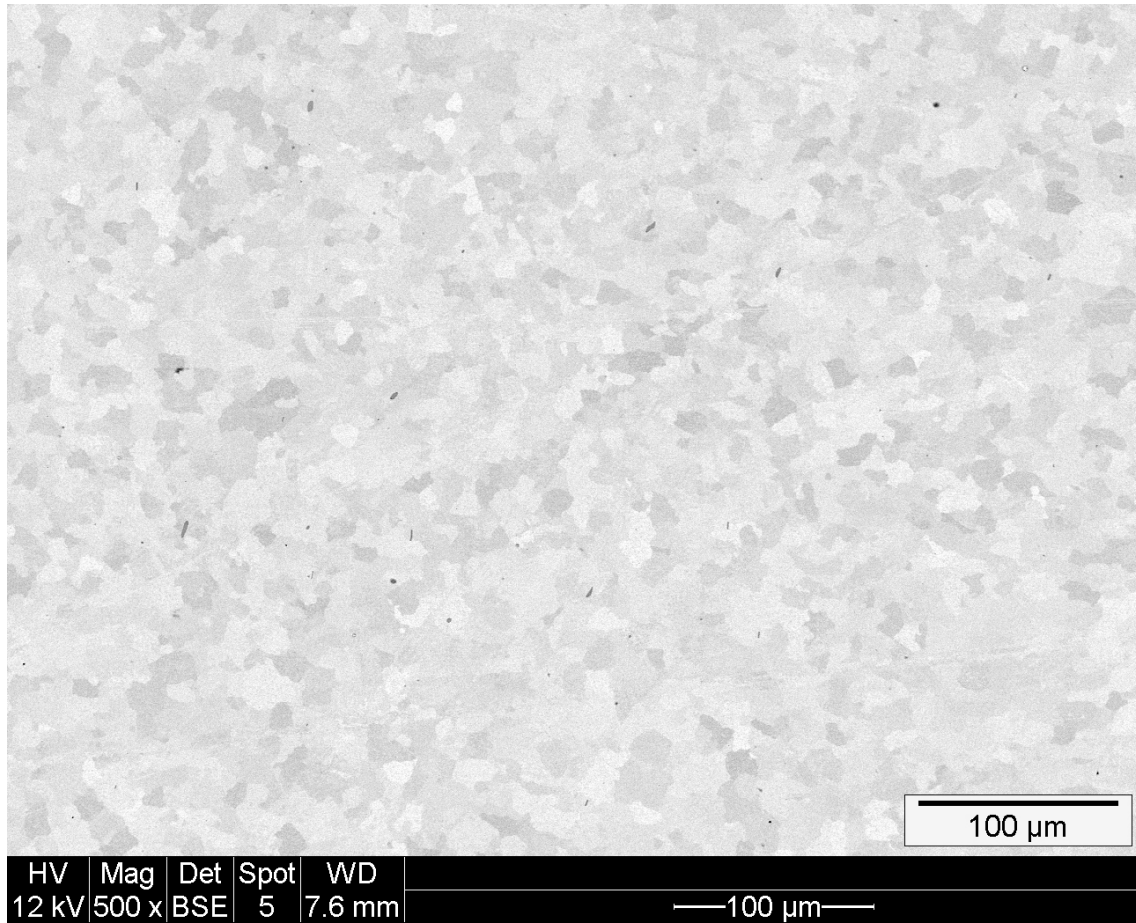


**Figure C.2:** Example image of the sample from the 100Cr6 sample in annealed condition, captured on *Area 2* close to the center of the tube wall.

# D

## Tensile testing 100Cr6

In this appendix the resulting plots from the tensile tests are presented. As is mentioned in *Chapter 4.1.2.4* the graphs are plotted from average data between two repetitions with the exception of *Figure D.3* which is only based on one repetition. The plots below can be compared with each other and it is clear that the strength of the material increases with hardening at the loss of ductility.

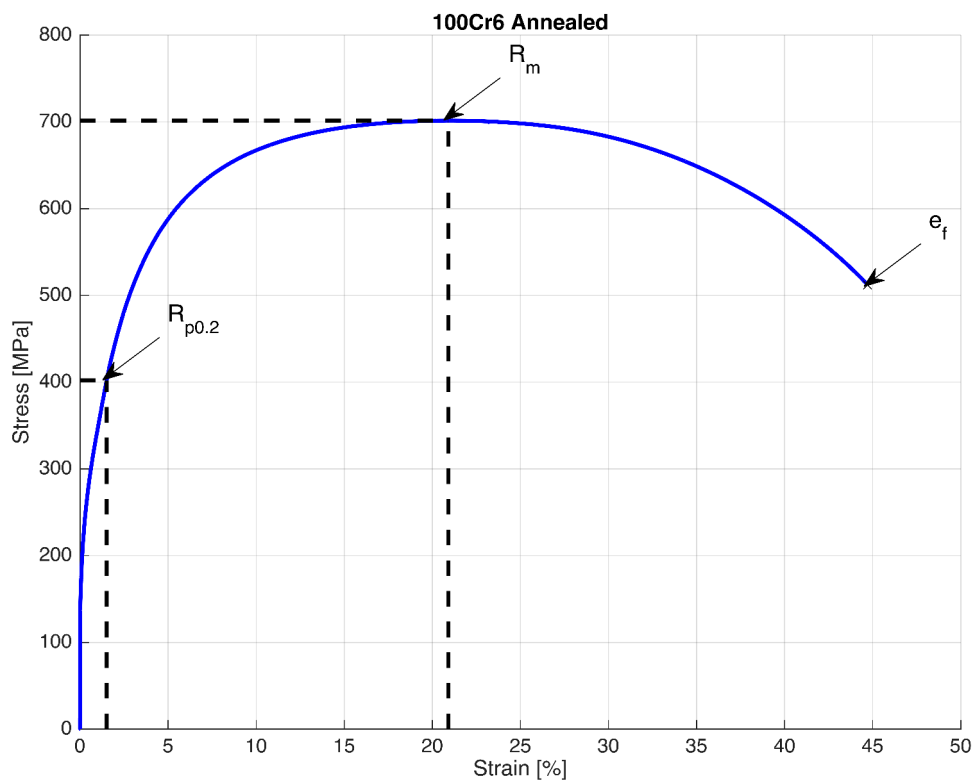


**Figure D.1:** Stress strain curve for 100Cr6 in *Annealed* condition.

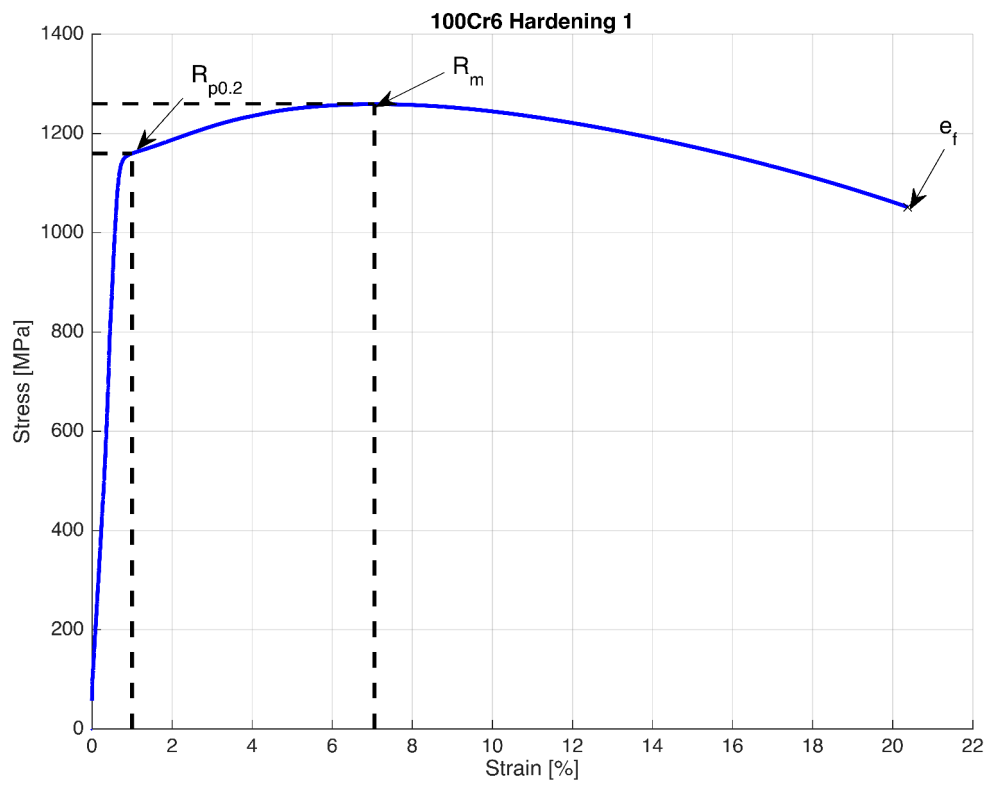


Figure D.2: Stress strain curve for 100Cr6 in *Hardening 1* condition.

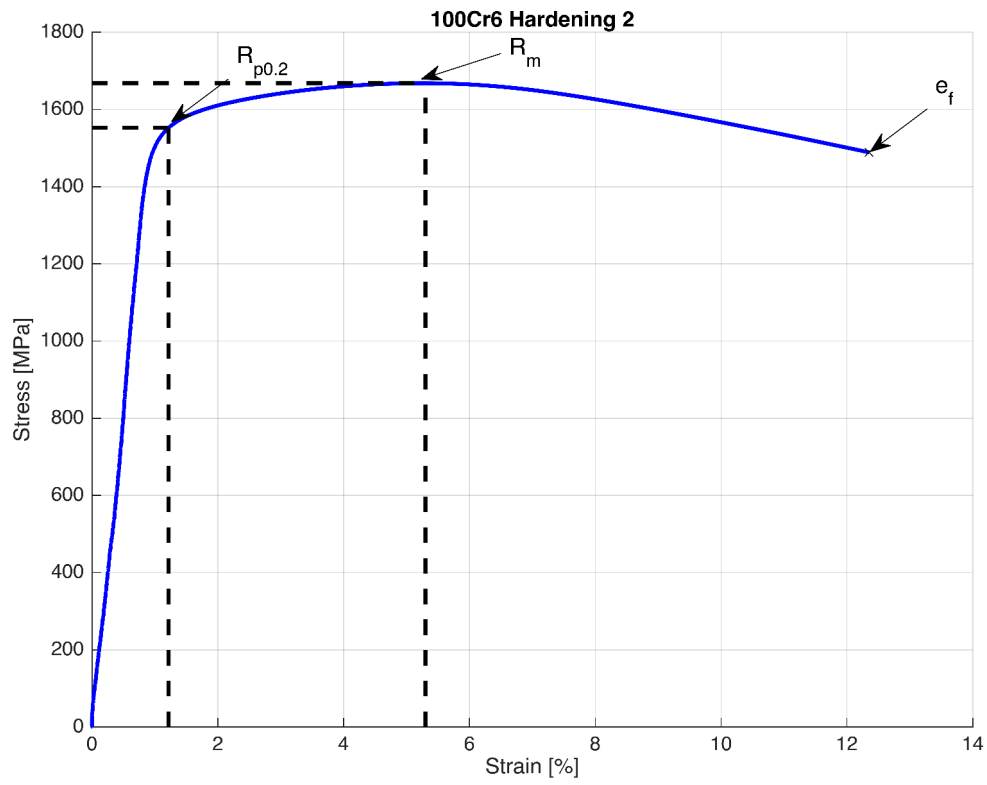


Figure D.3: Stress strain curve for 100Cr6 in *Hardening 2* condition.



# E

## Cutting forces 316L

The measured main cutting forces for the 316L workpieces. The measured value for each repetition is presented and a comparison can be made between the suppliers.

	Rec. feed		W/O nose	
Feed	Supplier A	Supplier B	Supplier A	Supplier B
[ <i>mm/rev</i> ]	Force [ <i>N</i> ]		Force [ <i>N</i> ]	
0,06	317,34	300,39	304,04	282,63
	315,50	304,85	308,27	308,20
	324,52	307,85	NA	NA
0,07	342,74	341,57	339,27	343,42
	354,19	341,32	338,16	341,97
	355,90	325,62	NA	NA
0,08	393,20	383,50	369,57	360,08
	391,01	378,74	368,49	380,42
	390,20	365,23	NA	NA
0,09	422,13	424,27	413,57	410,82
	429,66	412,92	406,08	393,02
	429,84	391,60	NA	NA
0,10	408,13	445,38	438,93	442,01
	454,37	448,14	434,33	425,34
	461,97	443,14	NA	NA
0,11	482,27	469,84	472,27	460,62
	480,76	484,22	476,32	451,37
	491,36	478,61	NA	NA
0,12	530,29	516,57	522,62	531,39
	514,27	515,36	516,50	506,46
	546,08	523,54	NA	NA

**Table E.1:** The measured main cutting forces for the 316L workpieces when machining with recommended feeds and without nose contact respectively, using *Insert 4*, where each repetition is presented.  $V_c = 230m/min$ ,  $a_p = 2mm$ .

		Supplier A			Supplier B		
Feed	Rep	Insert 1	Insert 2	Insert 3	Insert 1	Insert 2	Insert 3
[ <i>mm/rev</i> ]	#	Force [ <i>N</i> ]			Force [ <i>N</i> ]		
0,05	1	281,50	307,27	320,48	288,88	290,50	312,90
	2	295,22	304,44	318,50	286,84	291,72	318,82
0,10	1	476,03	491,09	517,71	468,74	483,21	519,11
	2	483,95	487,72	520,48	481,00	485,67	513,85
0,15	1	638,86	649,18	701,91	639,84	653,90	709,44
	2	634,79	658,75	707,29	620,42	652,46	704,78
0,20	1	781,01	801,31	890,91	787,95	811,62	862,76
	2	796,06	812,44	861,78	765,84	806,60	843,70
0,25	1	952,92	975,00	1021,84	939,38	968,45	1022,87
	2	950,34	997,68	1023,59	969,54	991,64	1027,54

**Table E.2:** The measured main cutting forces for the 316L when machining with special inserts where each repetition is presented.  $V_c = 230m/min$ ,  $a_p = 2mm$ .

# F

## Cutting forces 100Cr6

Here the measured main cutting forces for the 100Cr6 workpieces are presented. The measured value for each repetition is displayed and a comparisons can be made between inserts and hardening conditions. The cutting speed is varied between hardening states and the depth of cut is constant  $2mm$ .

Feed	Rep	Insert 1	Insert 2	Insert 3
[ $mm/rev$ ]	#	Force [ $N$ ]		
0,05	1	353,77	365,19	395,17
	2	360,20	362,98	403,85
0,10	1	561,71	564,47	619,34
	2	549,97	570,40	614,13
0,15	1	745,47	772,39	797,02
	2	743,77	783,50	818,81
0,20	1	910,96	968,27	993,66
	2	924,58	974,96	965,49
0,25	1	1125,30	1203,52	1159,04
	2	1128,51	1221,95	1148,40

**Table F.1:** The measured main cutting forces for the 100Cr6 *Annealed* workpieces where each repetition is presented.  $V_c = 150m/min$ ,  $a_p = 2mm$ .

Feed	Rep	Insert 1	Insert 2	Insert 3
[ <i>mm/rev</i> ]	#	Force [ <i>N</i> ]		
0,05	1	373,61	375,25	431,86
	2	373,89	407,73	432,51
0,09	1	554,44	568,00	607,34
	2	569,20	609,85	611,51
0,13	1	751,23	757,46	846,15
	2	749,76	768,17	812,42
0,16	1	860,21	881,04	971,55
	2	875,91	896,37	925,56
0,20	1	1025,09	1072,33	1131,06
	2	1004,26	1056,63	1190,55

**Table F.2:** The measured main cutting forces for the 100Cr6 *Hardening 1* workpieces where each repetition is presented.  $V_c = 90m/min, a_p = 2mm$ .

Feed	Rep	Insert 1	Insert 2	Insert 3
[ <i>mm/rev</i> ]	#	Force [ <i>N</i> ]		
0,05	1	418,86	455,57	NA
	2	425,46	453,66	NA
0,08	1	612,79	595,09	NA
	2	592,21	606,04	NA
0,10	1	689,55	701,03	NA
	2	707,02	706,30	NA
0,13	1	841,39	847,50	NA
	2	815,33	862,59	NA
0,15	1	930,27	935,04	NA
	2	888,90	943,30	NA

**Table F.3:** The measured main cutting forces for the 100Cr6 *Hardening 2* workpieces where each repetition is presented.  $V_c = 60m/min, a_p = 2mm$ .

# G

## Average normalized forces 316L

This appendix contains tables presenting the normalized cutting forces transformed from the average value of each feed level for 316L.

	Rec. feed		W/O nose	
Feed	Supplier A	Supplier B	Supplier A	Supplier B
[ <i>mm/rev</i> ]	Force [ <i>N</i> ]		Force [ <i>N</i> ]	
0,06	298,86	286,20	283,97	272,44
0,07	332,55	319,39	318,97	322,63
0,08	375,40	360,47	352,15	350,71
0,09	411,72	396,52	392,35	384,79
0,10	427,79	434,82	422,25	418,46
0,11	473,65	468,14	461,37	442,49
0,12	520,26	510,50	508,46	506,30

**Table G.1:** The normalized average cutting force for each feed level for 316L when machining with recommended feeds and without nose contact respectively, using *Insert 4*.  $V_c = 230m/min$ ,  $a_p = 2mm$ .

	Supplier A			Supplier B		
Feed	Insert 1	Insert 2	Insert 3	Insert 1	Insert 2	Insert 3
[ <i>mm/rev</i> ]	Force [ <i>N</i> ]			Force [ <i>N</i> ]		
0,05	273,17	283,97	294,02	271,57	268,43	290,40
0,10	450,21	444,64	455,52	444,41	438,15	452,87
0,15	595,09	588,01	604,09	588,16	585,30	605,87
0,20	735,59	721,33	741,12	723,87	721,11	721,16
0,25	886,32	877,89	857,19	887,71	869,98	858,85

**Table G.2:** The normalized average cutting force for each feed level for 316L when machining with special inserts.  $V_c = 230m/min$ ,  $a_p = 2mm$ .



# H

## Average normalized forces 100Cr6

This appendix contains tables presenting the normalized main cutting forces transformed from the average value of each feed level for the 100Cr6 workpieces.

Feed	Insert 1	Insert 2	Insert 3
[ <i>mm/rev</i> ]	Force [ <i>N</i> ]		
0,05	338,51	335,93	376,94
0,10	521,84	512,47	553,47
0,15	696,33	696,07	706,27
0,20	856,49	864,93	842,53
0,25	1049,94	1075,89	981,42

**Table H.1:** The normalized average main cutting forces for each feed level for the 100Cr6 *Annealed* workpieces.  $V_c = 150m/min$ ,  $a_p = 2mm$ .

Feed	Insert 1	Insert 2	Insert 3
[ <i>mm/rev</i> ]	Force [ <i>N</i> ]		
0,05	350,56	363,86	400,32
0,09	520,94	536,27	541,37
0,13	694,26	687,70	720,10
0,16	797,91	794,76	811,82
0,20	947,23	952,81	983,34

**Table H.2:** The normalized average main cutting forces for each feed level for the 100Cr6 *Hardening 1* workpieces.  $V_c = 90m/min$ ,  $a_p = 2mm$ .

Feed	Insert 1	Insert 2	Insert 3
[ <i>mm/rev</i> ]	Force [ <i>N</i> ]		
0,05	400,86	425,25	NA
0,08	567,79	554,27	NA
0,10	655,82	643,00	NA
0,13	776,71	776,25	NA
0,15	851,70	848,33	NA

**Table H.3:** The normalized average main cutting forces for each feed level for the 100Cr6 *Hardening 2* workpieces.  $V_c = 60m/min$ ,  $a_p = 2mm$ .

# I

## Scatter in force between repetitions

This appendix is intended to provide the reader some overview regarding the quality of the data. Presented in *Table I.1* to *I.5* is the variation in measurements between repetitions divided by the average value.

	Rec. feed		W/O nose	
Feed	Supplier A	Supplier B	Supplier A	Supplier B
[ <i>mm/rev</i> ]	Scatter [%]		Scatter [%]	
0,06	2,83	2,45	1,38	8,66
0,07	3,75	4,75	0,33	0,42
0,08	0,77	4,86	0,29	5,49
0,09	1,81	7,98	1,83	4,43
0,10	12,19	1,12	1,05	3,85
0,11	2,19	3,01	0,85	2,03
0,12	6,00	1,58	1,18	4,80

**Table I.1:** The variation between repetitions divided by the average value presented in percent when machining the 316L workpieces with recommended feeds and without nose contact respectively, using *Insert 4*.  $V_c = 230m/min$ ,  $a_p = 2mm$ .

I. Scatter in force between repetitions

---

	Supplier A			Supplier B		
Feed	Insert 1	Insert 2	Insert 3	Insert 1	Insert 2	Insert 3
[ <i>mm/rev</i> ]	Scatter [%]			Scatter [%]		
0,05	4,76	0,93	0,62	0,71	0,42	1,87
0,10	1,65	0,69	0,53	2,58	0,51	1,02
0,15	0,64	1,46	0,76	3,08	0,22	0,66
0,20	1,91	1,38	3,32	2,85	0,62	2,23
0,25	0,27	2,30	0,17	3,16	2,37	0,46

**Table I.2:** The variation between repetitions divided by the average value presented in percent for machining the 316L workpieces with special inserts.  $V_c = 230m/min, a_p = 2mm$ .

Feed	Insert 1	Insert 2	Insert 3
[ <i>mm/rev</i> ]	Scatter %		
0,05	1,80	0,61	2,17
0,10	2,11	1,05	0,84
0,15	0,23	1,43	2,70
0,20	1,48	0,69	2,88
0,25	0,29	1,52	0,92

**Table I.3:** The variation between repetitions divided by the average value presented in percent for the 100Cr6 *Annealed* workpieces.  $V_c = 150m/min, a_p = 2mm$ .

Feed	Insert 1	Insert 2	Insert 3
[ <i>mm/rev</i> ]	Scatter %		
0,05	0,08	8,30	0,15
0,09	2,63	7,11	0,69
0,13	0,20	1,40	4,07
0,16	1,81	1,72	4,85
0,20	2,05	1,47	5,12

**Table I.4:** The variation between repetitions divided by the average value presented in percent for the 100Cr6 *Hardening 1* workpieces.  $V_c = 90m/min, a_p = 2mm$ .

Feed	Insert 1	Insert 2	Insert 3
[ <i>mm/rev</i> ]	Scatter %		
0,05	1,56	0,42	NA
0,08	3,42	1,82	NA
0,10	2,50	0,75	NA
0,13	3,15	1,76	NA
0,15	4,55	0,88	NA

**Table I.5:** The variation between repetitions divided by the average value presented in percent for the 100Cr6 *Hardening 2* workpieces.  $V_c = 60m/min, a_p = 2mm$ .



# J

## Cutting resistance plots 316L

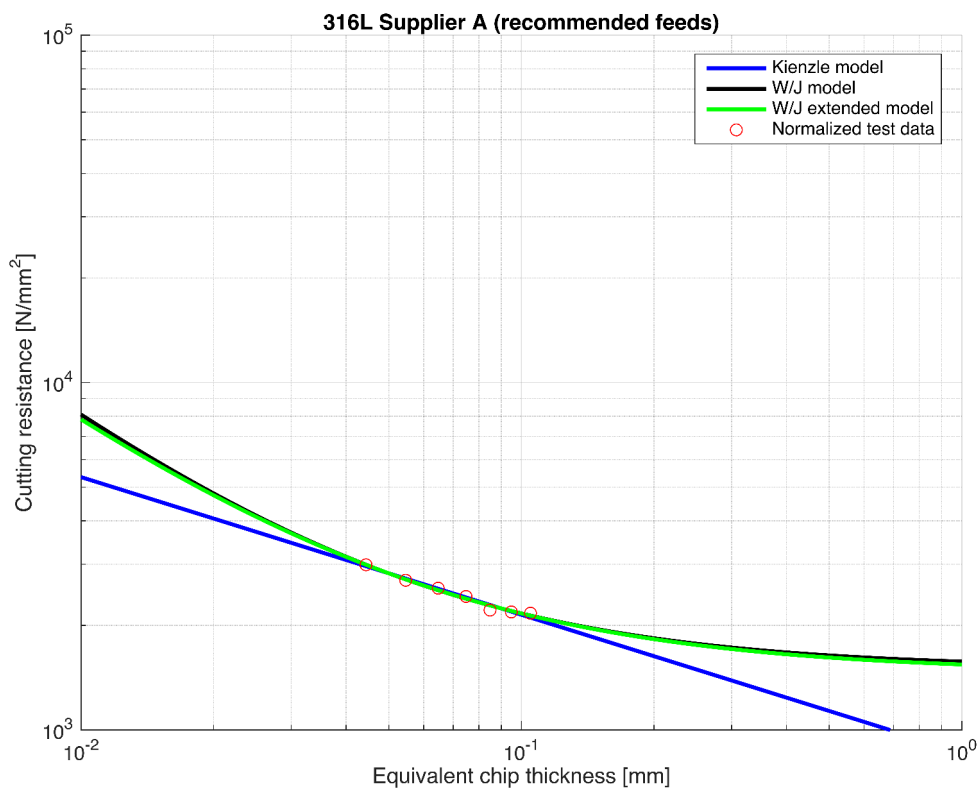


**Figure J.1:** Comparison between the models when machining the 316L workpieces from *Supplier A* within the recommended feed window, plotted in *Log-Log*.

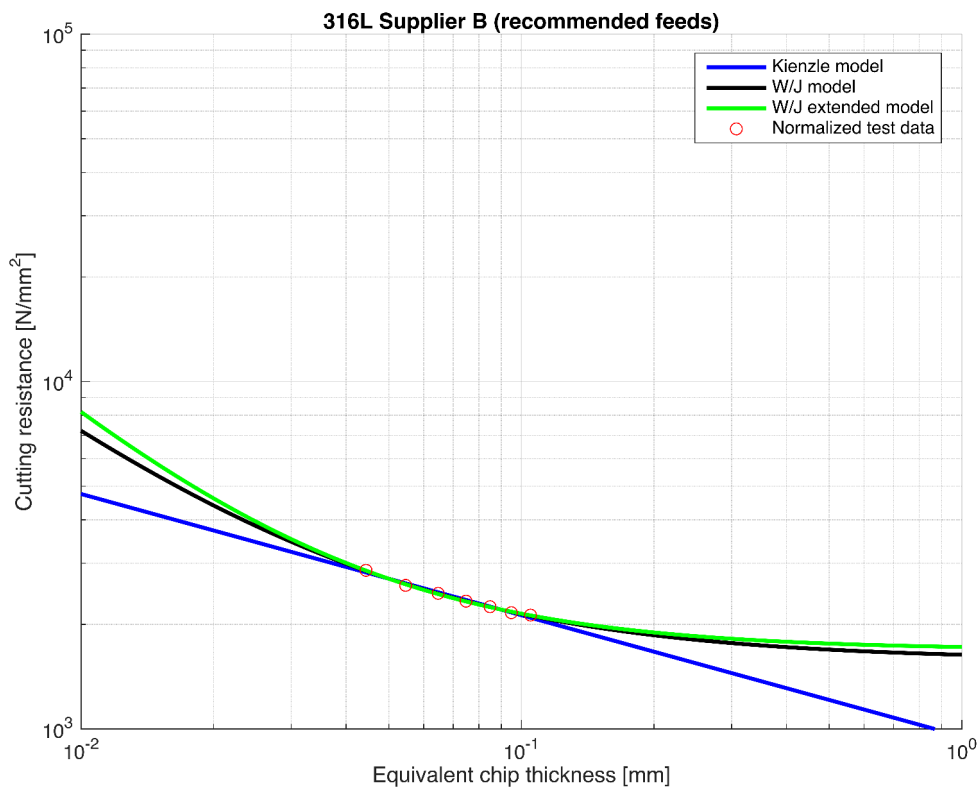


**Figure J.2:** Comparison between the models when machining 316L workpieces from *Supplier B* within the recommended feed window, plotted in *Log-Log*.

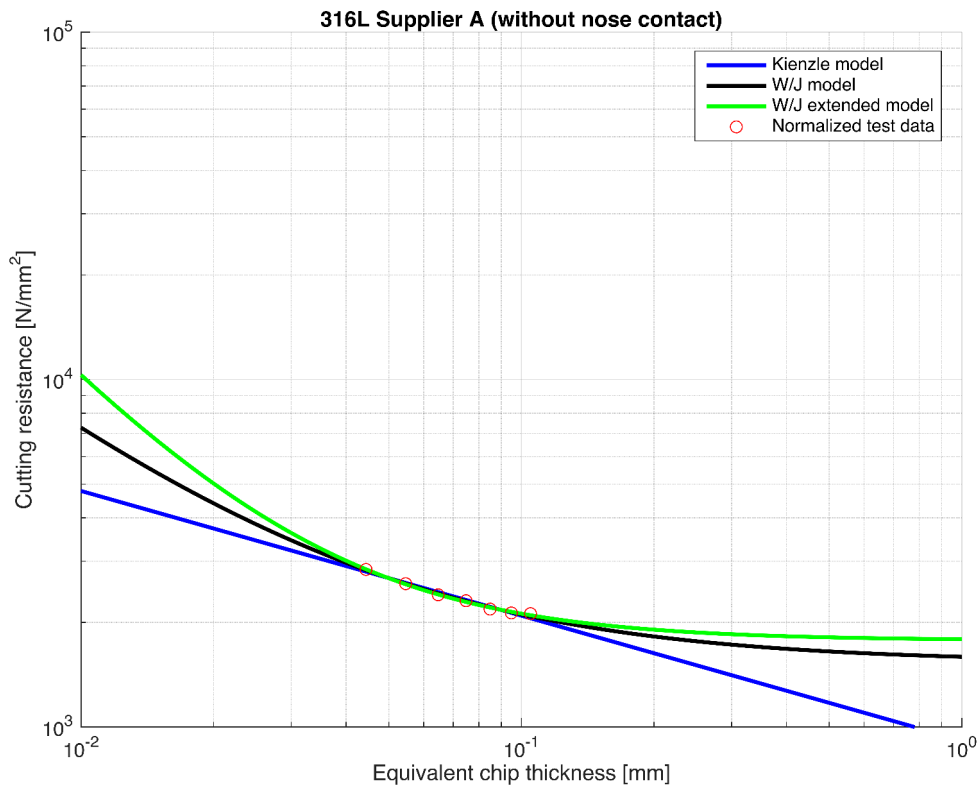


**Figure J.3:** Comparison between the models when machining 316L workpieces from *Supplier A* without nose contact within recommended feeds, plotted in *Log-Log*.

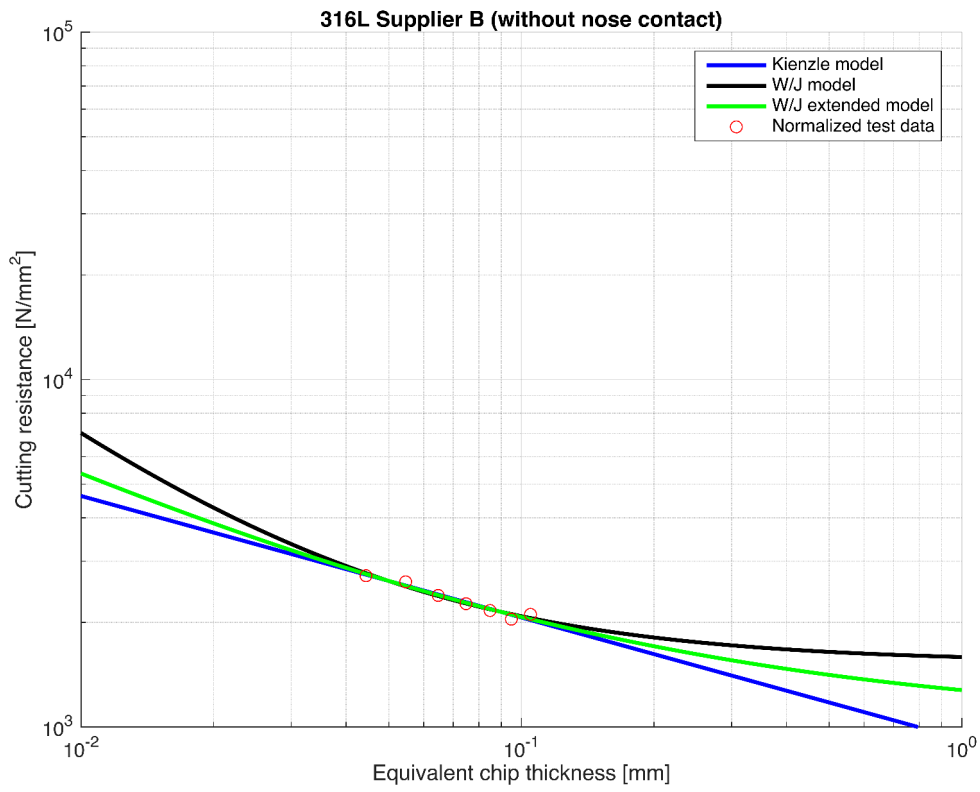


**Figure J.4:** Comparison between the models when machining 316L workpieces from *Supplier B* without nose contact within recommended feeds, plotted in *Log-Log*.

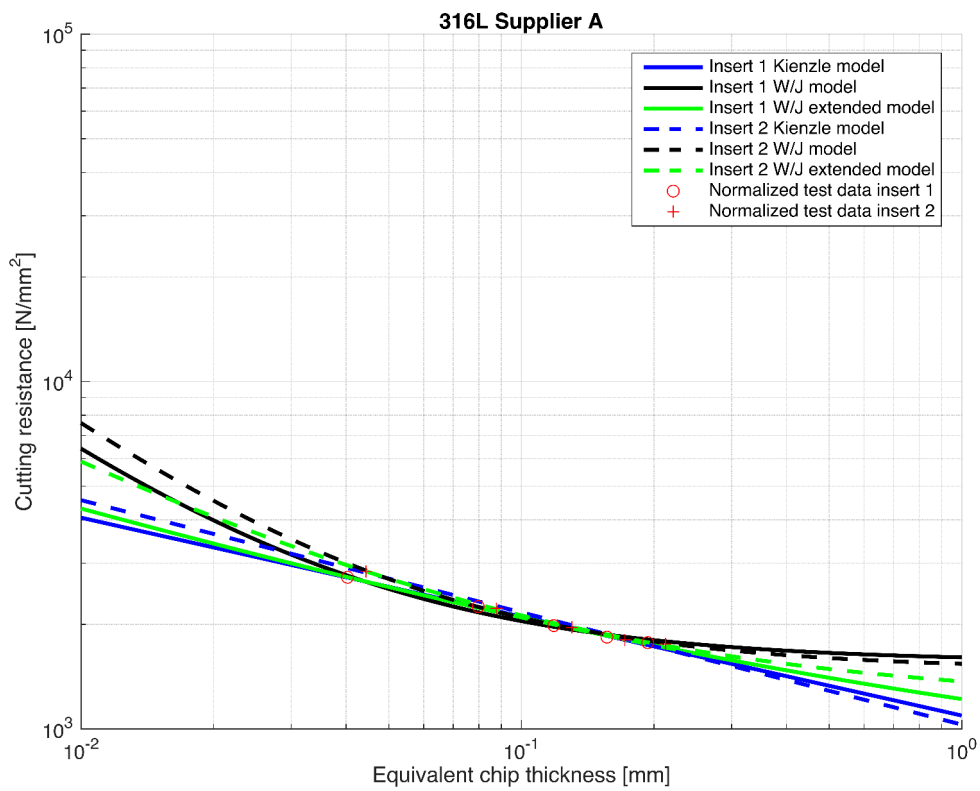


**Figure J.5:** Comparison between the models when machining 316L workpieces from *Supplier A* based on two different types inserts (the same used for 100Cr6), plotted in *Log-Log*.

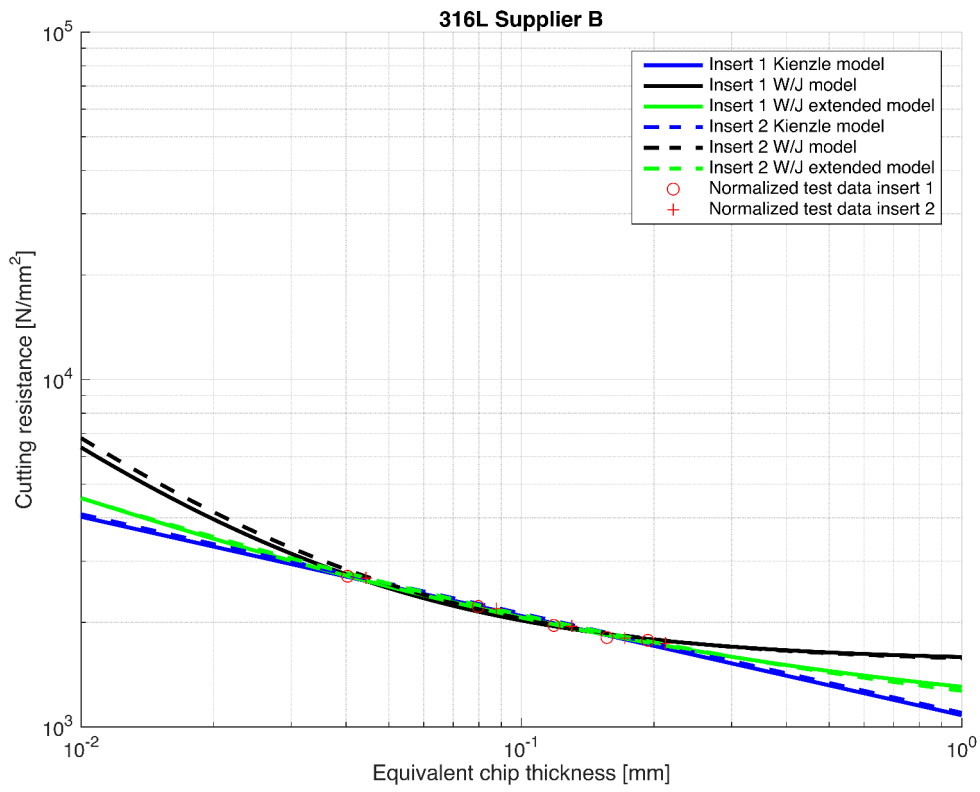


**Figure J.6:** Comparison between the models when machining 316L workpieces from *Supplier A* based on two different types inserts (the same used for 100Cr6), plotted in *Log-Log*.

# K

## Cutting resistance plots 100Cr6

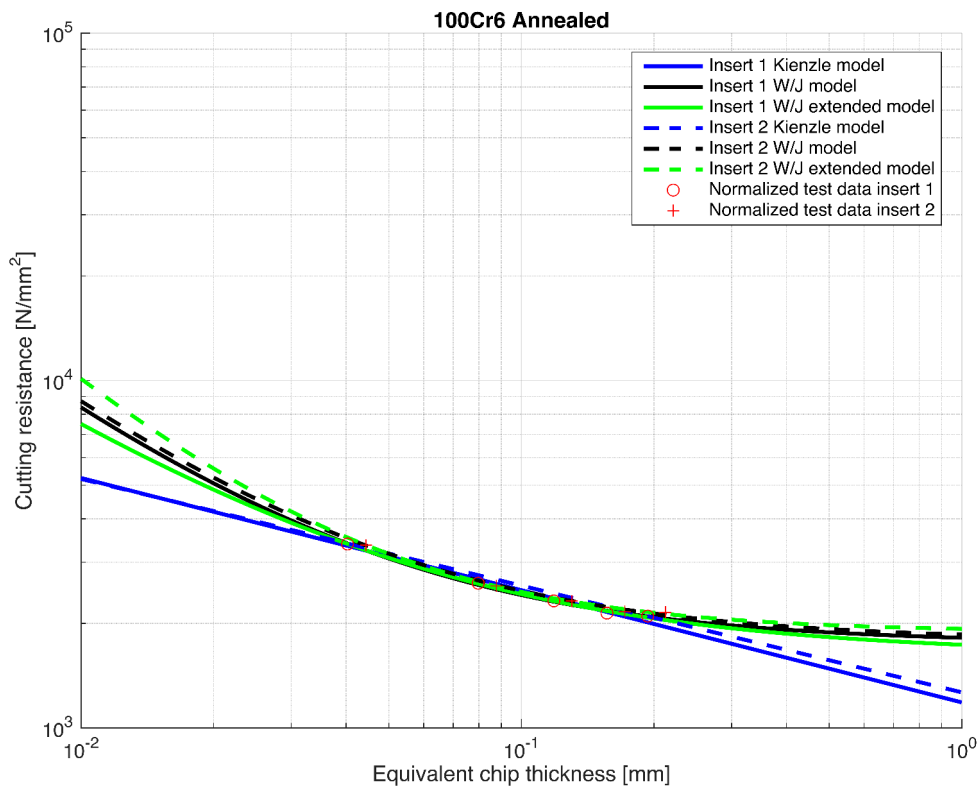


**Figure K.1:** Comparison between the models when machining 100Cr6 *Annealed* workpieces, plotted in *Log-Log*.

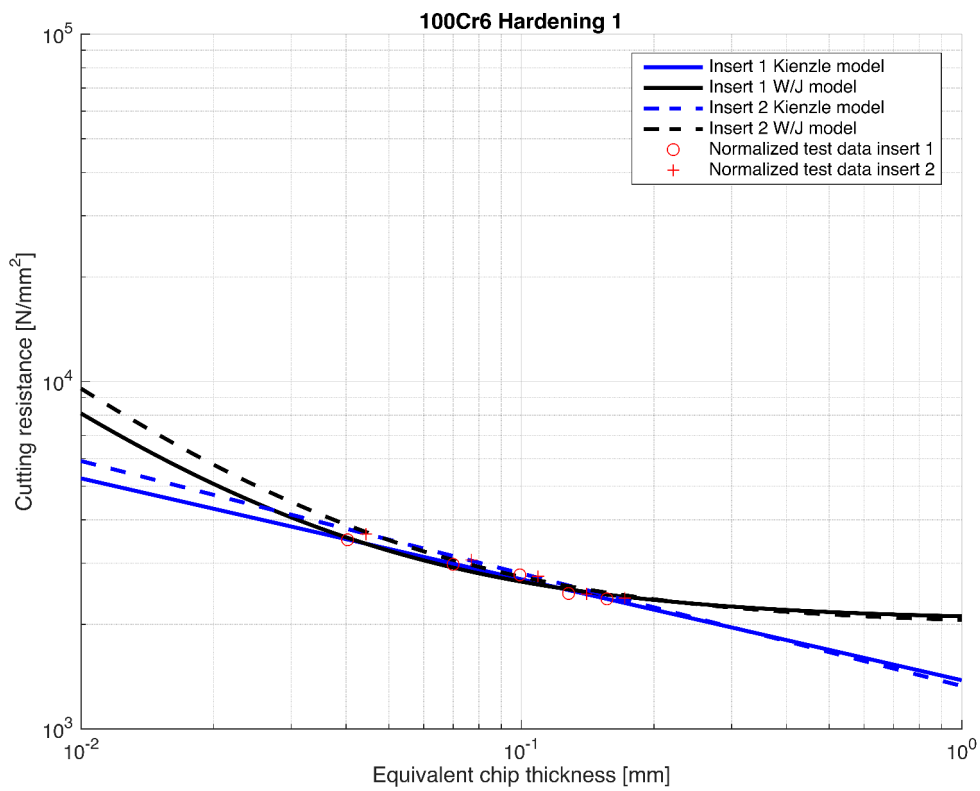


**Figure K.2:** Comparison between the models when machining 100Cr6 *Hardening 1* workpieces, plotted in *Log-Log*. The *W/J extended model* is not included here.

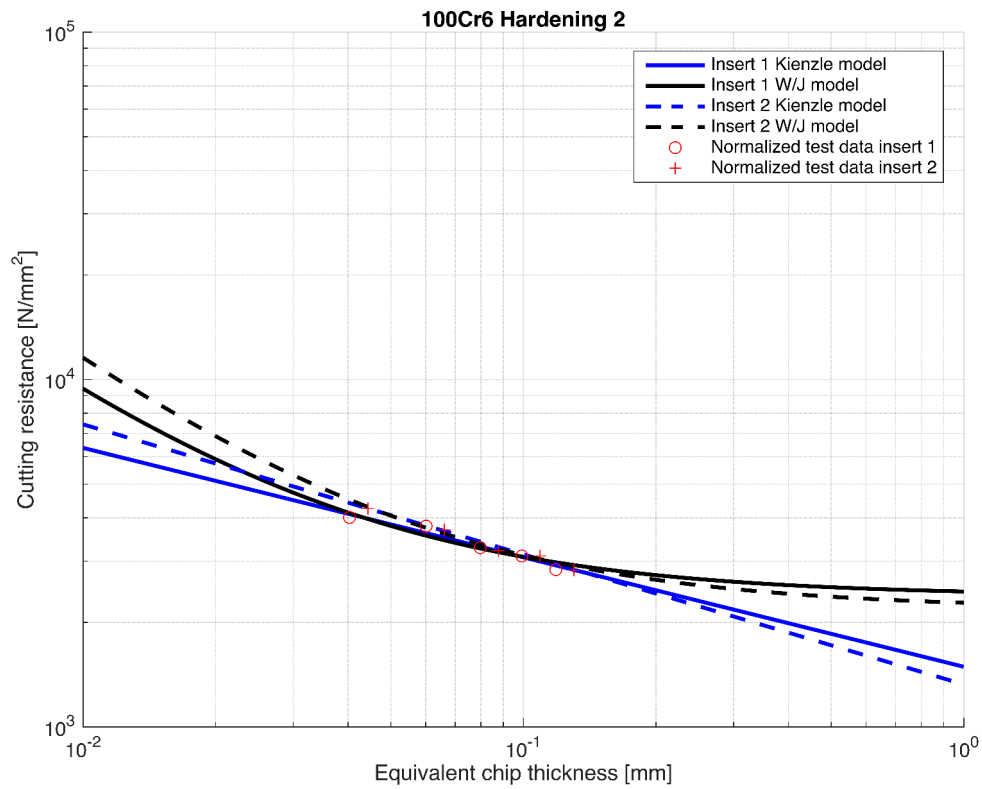


**Figure K.3:** Comparison between the models when machining 100Cr6 *Hardening 2* workpieces, plotted in *Log-Log*. The *W/J extended model* is not included here.